



GRADIENTS OF BRAIN ORGANIZATION

How do gradients change our understanding of brain organization?

Talks on state-of-the-art development and application of gradient approaches



June 22 Saturday 2024

Sungkyunkwan University, Natural Science Campus

Semiconductor Building (330102)

Organizer

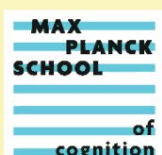


Center for Neuroscience Imaging Research



Montreal Neurological Institute-Hospital

PARTNERS AND SPONSORS





GRADIENTS OF BRAIN ORGANIZATION

8:30 – 9:00

Registration

9:00 – 9:15

Welcome

9:15 – 10:45

Methods and multimodal applications

Chairs: Sofie Valk and Jessica Royer

- Integrated Effective Connectivity Reveals Sensory-Fugal Hierarchy in the Human Brain
Younghyun Oh(Sungkyunkwan University, Korea)
- Multiparametric mapping of superficial white matter architecture using 7T quantitative MRI
Youngeun Hwang and Raul Rodriguez-Cruces (McGill University, Canada)
- Biologically annotated brain connectomes
Vincent Bazinet (McGill University, Canada)
- Uncovering principles of white matter organization in relation to cognition in youth
Joelle Bagautdinova (University of Pennsylvania, USA)
- Panel discussion

11:00 – 12:15

Gradients beyond the neocortex

Chairs: Boris Bernhardt and Shinwon Park

- Striatal connectivity gradients map onto cortico-striatal and dopaminergic projections across health and disease
Marianne Oldehinkel (Radboud University, Netherlands)
- Statistical mapping of cortico-subcortical gradients using geometric eigenmodes
Nikitas Koussis (University of Newcastle, Australia)
- Task-general connectivity model reveals variation in convergence of cortical input to cerebellum
Maedbh King (Massachusetts Institute of Technology, USA)
- Panel discussion

12:15 – 13:15

Lunch break



GRADIENTS OF BRAIN ORGANIZATION

13:15 – 13:30

Flash talks

13:30 – 14:45

Gradients and artificial intelligence

Chairs: Bo-yong Park and Seok-Jun Hong

- GAN-MAT: Generative Adversarial Network-based Microstructural Profile Covariance Analysis Toolbox
Yeong Jun Park (Sungkyunkwan University, Korea)
- Adolescent maturation of cortical excitation-inhibition balance based on individualized and GPU-accelerated biophysical network modeling
Amin Saberi (Max Planck Institute for Human Cognitive and Brain Sciences, Germany)
- Human brain-derived architectural motifs for audiovisual processing
Mashbayar Tugsbayar (Mila - Quebec AI Institute, Canada)
- Panel discussion

15:00 – 16:15

Gradients for individual phenotyping

Chairs: Daniel Margulies and Sara Larivière

- Variability in sensory-association axis, evidence from sex- and individual differences
Bianca Serio (Max Planck Institute for Human Cognitive and Brain Sciences, Germany)
- Using a neural state-space to understand cognition and behaviour
Samyogita Hardikar (Max Planck Institute for Human Cognitive and Brain Sciences, Germany)
- Motion Effects in Procrustes Aligned Individual-Level Gradients
Leonard Sasse (Institute of Neuroscience and Medicine, Brain and Behaviour (INM-7), Germany)
- Panel discussion

16:15 – 16:30

Closing comments

16:30 – 18:00

Poster session

Dual long-axis reorganization of hippocampus in youth

Debin Zeng^{1,2}, Qiongling Li², Deyu Li¹, Yirong He², Xiaoxi Dong², Shaonian Li², Shenghan Bi², Yong He^{2*}, Xi-Nian Zuo^{2*}, Shuyu Li^{2*}

¹*Beijing Advanced Innovation Center for Biomedical Engineering, School of Biological Science & Medical Engineering, Beihang University, Beijing 100083, China*

²*State Key Laboratory of Cognitive Neuroscience and Learning, Beijing Normal University, Beijing, 100875, China*

Keywords: hippocampus, development, reorganization, executive function

Introduction

The reorganization of human hippocampus, especially its interaction with cortex, remains largely undefined in youth. The organization of a single hippocampal long-axis has been predominantly characterized as monotonic(Genon et al. 2021; Strange et al. 2014), despite recent indications of nonmonotonic features in neuron density(Gandolfi et al. 2023) and geometric eigenmodes(Pang et al. 2023). While the human cortical hierarchy has been well recognized for significant developmental and evolutionary advantages(Dong et al. 2021; Tong et al. 2022), hippocampus has been typically considered an evolutionarily conserved brain structure(Strange et al. 2014; Pandya et al. 2015), and overlooked regarding its integrative role of cortical hierarchical processing during development.

Methods

Our study utilized data from the Human Connectome Project Development (HCP-D) with 652 participants (5-21 years) and the Children School Functions and Brain Development Project (CBD, Beijing Cohort) with 300 children (6-13 years). We used the HippUnfold tool(DeKraker et al. 2022) to segment the hippocampus and generate mid-thickness surfaces. Hippocampal-cortical connectomes were created by correlating rs-fMRI time series between hippocampal vertices and cortical regions (defined by the Glasser atlas(Glasser et al. 2016)). A diffusion embedding method yielded the hippocampal functional gradient (Fig. 1a), and cortical projections were computed by taking the dot product between the gradient and the hippocampal functional connectivity for each cortical region. Geometric eigenmodes for each hippocampus were obtained through Laplace–Beltrami operator-based analysis. All developmental effects were studied using generalized additive models. Lastly, transcriptomic association and developmental enrichment analyses were conducted to explore the neurobiological basis of dual long-axis functional gradient development.

Results

Here, we corroborated the presence and significance of a dual long-axis representation of the hippocampal connectome and geometry including both linear and quadratic gradients along its long-axis in youth (Fig. 1b and e). This finding was robust across two independent large-scale developmental cohorts. Projecting the connectome gradients onto the cortex, we clarified how distinct cortical hierarchies allocate

functional connectivity differently along the long-axis, thus coding the hippocampus's intricate and multifaceted role in cortical hierarchical processing (Fig. 1c and d). These discoveries challenge classical views that propose a monotonic gradient of structural and functional differentiation along the hippocampal long-axis, and question the traditional notion of the hippocampus as being evolutionarily conserved in terms of its organization. We observed substantial developmental reorganization of dual long-axis gradients in supporting the maturation of the cortical hierarchy in youth (Fig. 2b). The reorganization further unfolds that the human hippocampus continues to loosen its geometric gradient constraints on functional gradients to support the executive function performance (Fig. 2c and d). Notably, we revealed that neurodevelopmental variability in the functional gradient profiles mirrors a gradient associated with a plasticity-limiting factor (myelin content, estimated by T1w/T2w ratio) (Fig. 2a). At micro-level, we found that neural growth, stress hormone regulation, and neuroactive signaling are involved in this geometry-function-cognition alignment, facilitating such reorganization of the dual hippocampal long-axis gradients in youth (Fig. 2e).

Conclusions

Our findings enrich the understanding of hippocampal-cortical reorganizational principles across structural, functional, and molecular dimensions as well as its maturation, and describe the plasticity distribution within the human hippocampus at systems level, holding potentials to enhance and translate neurodevelopment and neuropsychiatric healthcare.

Figures

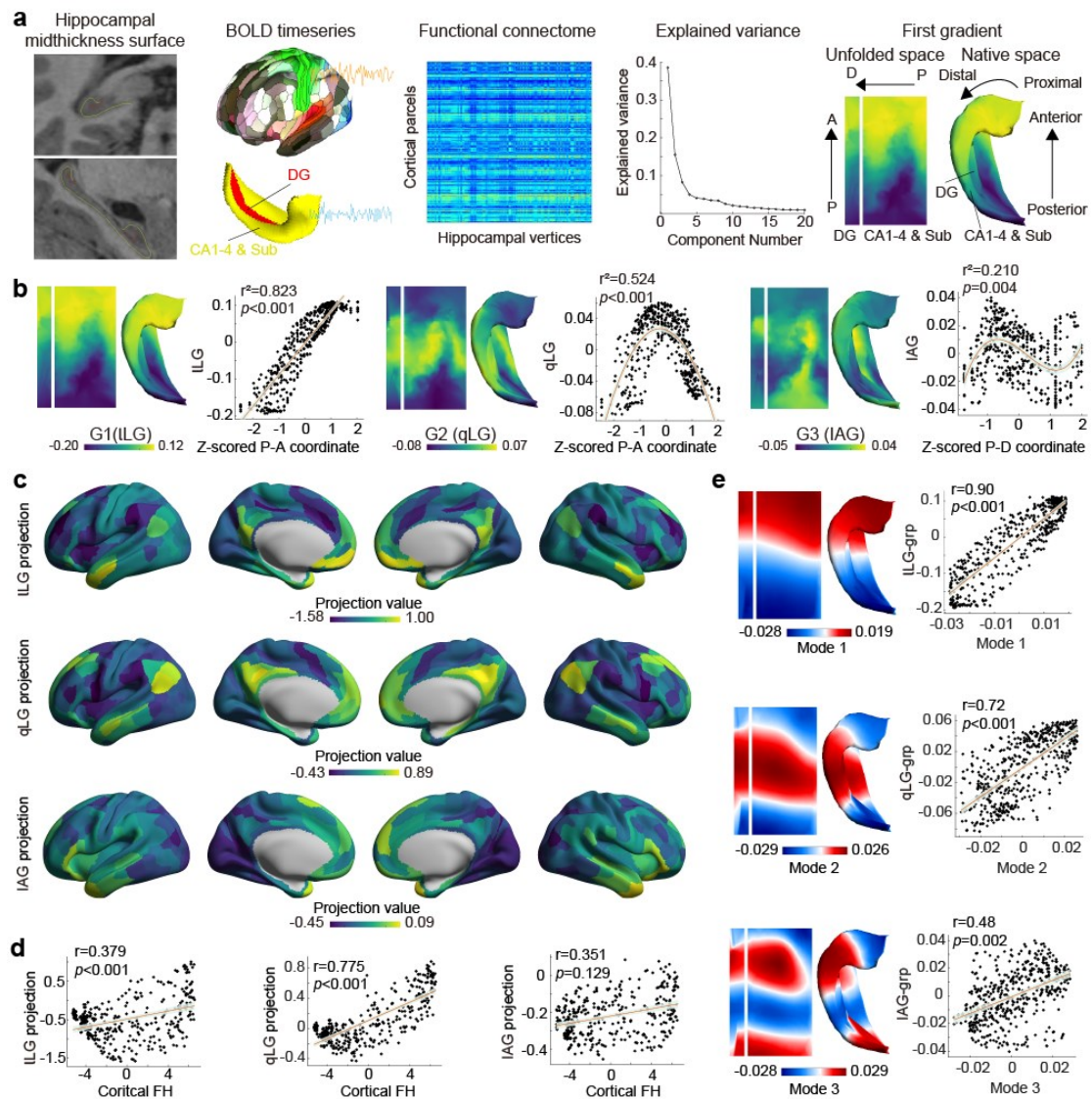


Fig. 1 | Topographic characterization, cortical projection, and geometric constraints of major hippocampal gradients in youth. **a**, Methodological overview for identifying hippocampal gradients. **b**, Topographic characterization of the first three hippocampal gradients at the overall group level and relationships between hippocampal gradients and anatomical positions. **c**, Group-averaged cortical projection of the left hippocampal gradients. **d**, Correlation between the projection pattern of specific gradients in the left hippocampus and cortical functional hierarchy (FH). **e**, Group-averaged first three geometric eigenmodes and relationship between these eigenmodes and hippocampal gradients.

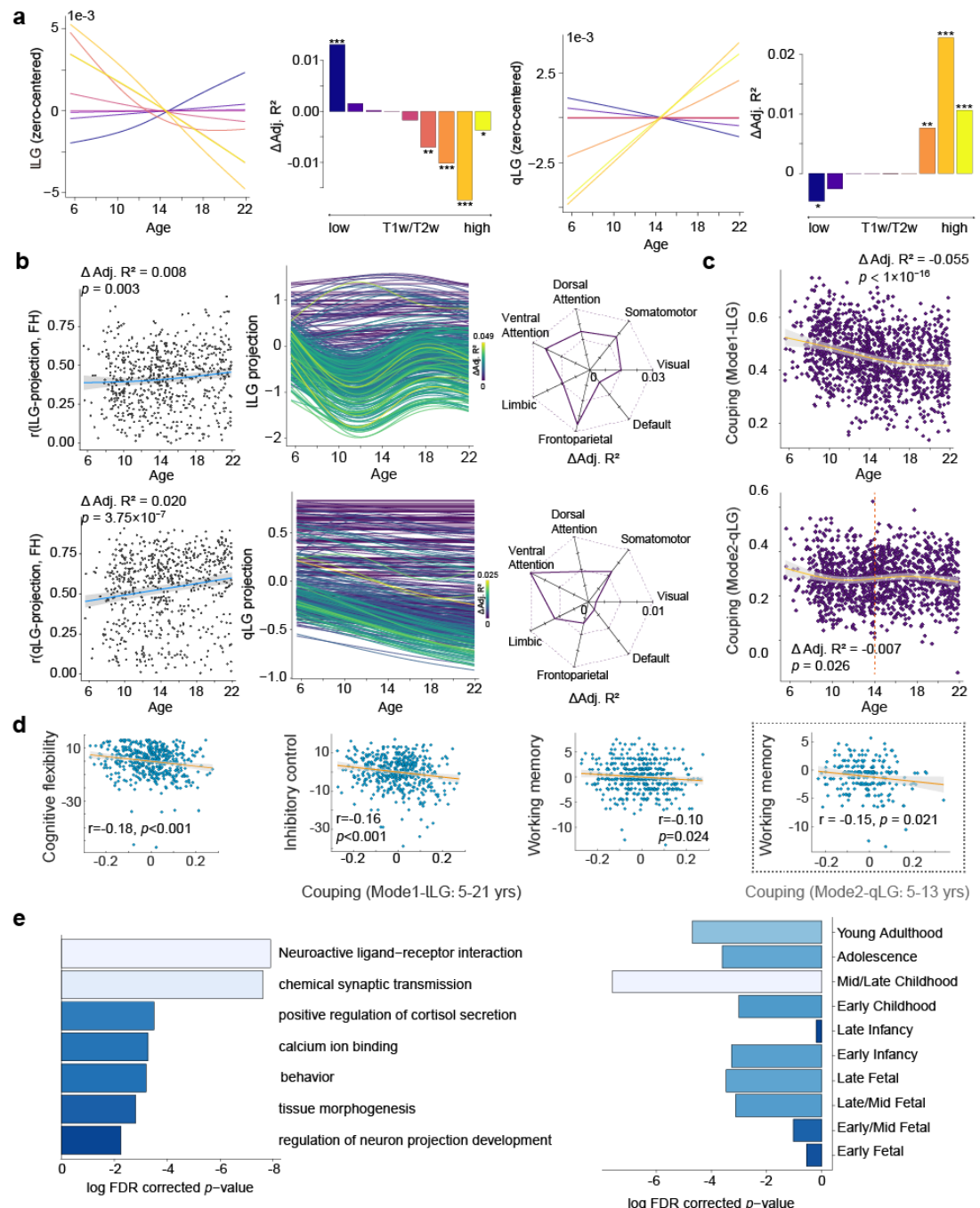


Fig. 2 | Understanding hippocampal-cortical reorganizational principles across structural, functional, and molecular dimensions as well as its maturation. **a**, Development of dual long-axis dimensions of hippocampal gradient parallels myelin maturation. **b**, Cortical projection of the hippocampal gradient links to the maturation of the cortical hierarchy in youth (left) and the cortical region-specific trajectories indicated that the frontoparietal and ventral attention systems play a critical role in this process (middle and right). **c**, Developmental trajectories of geometric-functional coupling of dual long-axis gradients. **d**, Relationship between the geometric-functional coupling and executive function performance. **e**, The enriched biological pathways and gene ontology terms linked to important gene set for ILG (left) and developmental enrichment analysis for this gene set (right).

References

- DeKraker, Jordan, Roy A. M. Haast, Mohamed D. Yousif, Bradley Karat, Jonathan C. Lau, Stefan Köhler, and Ali R. Khan. 2022. 'Automated hippocampal unfolding for morphometry and subfield segmentation with HippUnfold', *eLife*, 11: e77945.
- Dong, Hao-Ming, Daniel S. Margulies, Xi-Nian Zuo, and Avram J. Holmes. 2021.

- 'Shifting gradients of macroscale cortical organization mark the transition from childhood to adolescence', *Proceedings of the National Academy of Sciences*, 118: e2024448118.
- Gandolfi, Daniela, Jonathan Mapelli, Sergio M. G. Solinas, Paul Triebkorn, Egidio D'Angelo, Viktor Jirsa, and Michele Migliore. 2023. 'Full-scale scaffold model of the human hippocampus CA1 area', *Nature Computational Science*, 3: 264-76.
- Genon, Sarah, Boris C. Bernhardt, Renaud La Joie, Katrin Amunts, and Simon B. Eickhoff. 2021. 'The many dimensions of human hippocampal organization and (dys)function', *Trends in Neurosciences*, 44: 977-89.
- Glasser, Matthew F, Timothy S Coalson, Emma C Robinson, Carl D Hacker, John Harwell, Essa Yacoub, Kamil Ugurbil, Jesper Andersson, Christian F Beckmann, and Mark Jenkinson. 2016. 'A multi-modal parcellation of human cerebral cortex', *Nature*, 536: 171-78.
- Pandya, Deepak, Benjamin Seltzer, Michael Petrides, and Patsy Benny Cipolloni. 2015. *Cerebral Cortex: Architecture, Connections, and the Dual Origin Concept* (Oxford University Press).
- Pang, James C., Kevin M. Aquino, Marianne Oldehinkel, Peter A. Robinson, Ben D. Fulcher, Michael Breakspear, and Alex Fornito. 2023. 'Geometric constraints on human brain function', *Nature*, 618: 566-74.
- Strange, Bryan A, Menno P Witter, Ed S Lein, and Edvard I Moser. 2014. 'Functional organization of the hippocampal longitudinal axis', *Nature Reviews Neuroscience*, 15: 655-69.
- Tong, Chuanjun, Cirong Liu, Kaiwei Zhang, Binshi Bo, Ying Xia, Hao Yang, Yanqiu Feng, and Zhifeng Liang. 2022. 'Multimodal analysis demonstrating the shaping of functional gradients in the marmoset brain', *Nature Communications*, 13: 6584.

The ubiquitous gene expression gradient pattern in the human brain

Abstract

Chien-Ming Lo¹, Niall W. Duncan^{1*}

¹. Graduate Institute of Mind, Brain and Consciousness, Taipei Medical University, Taipei, Taiwan

The Allen Human Brain Atlas release has empowered neuroscientists with a powerful tool to unravel the human brain's organization. Gene expression data from the atlas have ignited investigations into fundamental brain principles. Correlated expression patterns of genes tied to microstructural properties have been studied for their relationships with diverse brain features.

This study systematically explores the interplay between the gradient of transcriptomic similarity across brain regions and various gene sets. It also investigates the correlation between this pattern and cortical myelination, as represented by the T1w/T2w map. Surprisingly, even brain 'unspecific' gene sets reveal gradients similar to brain 'specific' sets. The investigation provides evidence that primary gradients in theoretically informed gene sets and the gradients from randomly selected genes are remarkably similar, suggesting a more generalized transcriptomic spatial pattern than previously thought. Additionally, our research highlights unique covariance characteristics within specific functional networks, particularly the Visual, Somatomotor, and Limbic networks, underscoring their relationship between functional networks and spatial transcriptomic patterns in the brain.

The results presented prompt a reevaluation of current methodologies and assumptions in the study of gene-brain associations, raising potential points of caution for researchers who adopt a gradient approach. Moreover, our results suggest a need for a broader awareness of specificity issues in gradient studies across various domains.

Identifying spatiotemporal changes in cortical neurodevelopment using post-mortem and *in vivo* data

Introduction

Despite numerous attempts to model human cortical neurodevelopment, we lack details on spatiotemporal changes occurring within the cortex. Here, we leverage the complementarity of *post-mortem* and *in vivo* approaches to track cortical microstructure throughout early development.

Methods

We assessed age-related changes in cortical cytoarchitecture using photomicrographs of cresyl-stained *post-mortem* human brain tissue (254 cortical patches from 29 Von Economo areas; 0, 1, 3, 15, 24 and 48 months; 6-7 brains per age)¹⁻⁶. We identified the contours of individual cells using a tailored segmentation algorithm⁷ and used a sliding-window approach to extract the number of cells per window and the percentage of area covered by cells in each window (**Fig. 1A**). Measurements were averaged across matching depths (**Fig. 1B**). To examine temporal changes of the cytoarchitectural features, we calculated the product-moment correlation coefficients (*r*) between age and cytoarchitecture for each area and depth.

We characterised cortical microstructure *in vivo* using T1w/T2w scans from the developing Human Connectome Project (dHCP, n=328, 37-44 weeks post-menstrual age)⁸. We sampled T1w/T2w intensities at 14 intracortical depths⁹, producing microstructure profiles at each vertex (**Fig. 2A**). Given these profiles are inherently smoother than the histological profiles, we synopsised their shape using central moments (CMs; mean, centre of gravity, standard deviation). We assessed the influence of age on microstructure via area-specific product-moment correlations with the CMs.

To test whether the CMs can be explained by depth-specific cytoarchitecture changes, we linearly modelled their relationships. Post hoc univariate tests were performed to better interpret how depth-specific changes in cytoarchitecture contribute to *in vivo* changes in microstructure.

Results

Number of cells per window decreases with age at all cortical depths in most brain areas, though the magnitude of the effect varied (**Fig. 1C**). In contrast, the area covered by cells increased or decreased with age depending on cortical depth. Age-related increases were prominent deeper in the cortex, whereas decreases were widespread in superficial cortex. This depth-wise shift was most prominent in association cortex, including prefrontal cortex and temporo-parietal areas that neighbour the occipital lobe.

We observed significant global increases in mean intensity of MRI-derived profiles, but region-specific changes in the balance of microstructure across cortical depths (**Fig. 2B**). Specifically, the centre of gravity increased in areas on the inferior surface of the cortex, suggestive of microstructural increases deeper in the cortex. In contrast, the standard deviation of the profiles decreased with age in the frontal and temporal lobes, signifying increasingly balanced microstructural density across cortical depths.

Multivariate regressions showed more than 60% of variance in CM changes could be explained by depth-specific changes in cytoarchitecture. Effects were more prominent in mid-cortical depths, pointing towards a depth-specific correlation between cytoarchitecture and MRI-derived microstructure.

Discussion

Our study provides novel insights into the cellular basis of intracortical development. We found evidence for selective decreases in cellular density, as well as increases in cell size. Furthermore, by demonstrating the statistical relationship between histology- and MRI-derived changes, our work provides the foundation for further investigations into the multi-scale nature of cortical development, involving microstructure, morphology and connectivity.

Figures

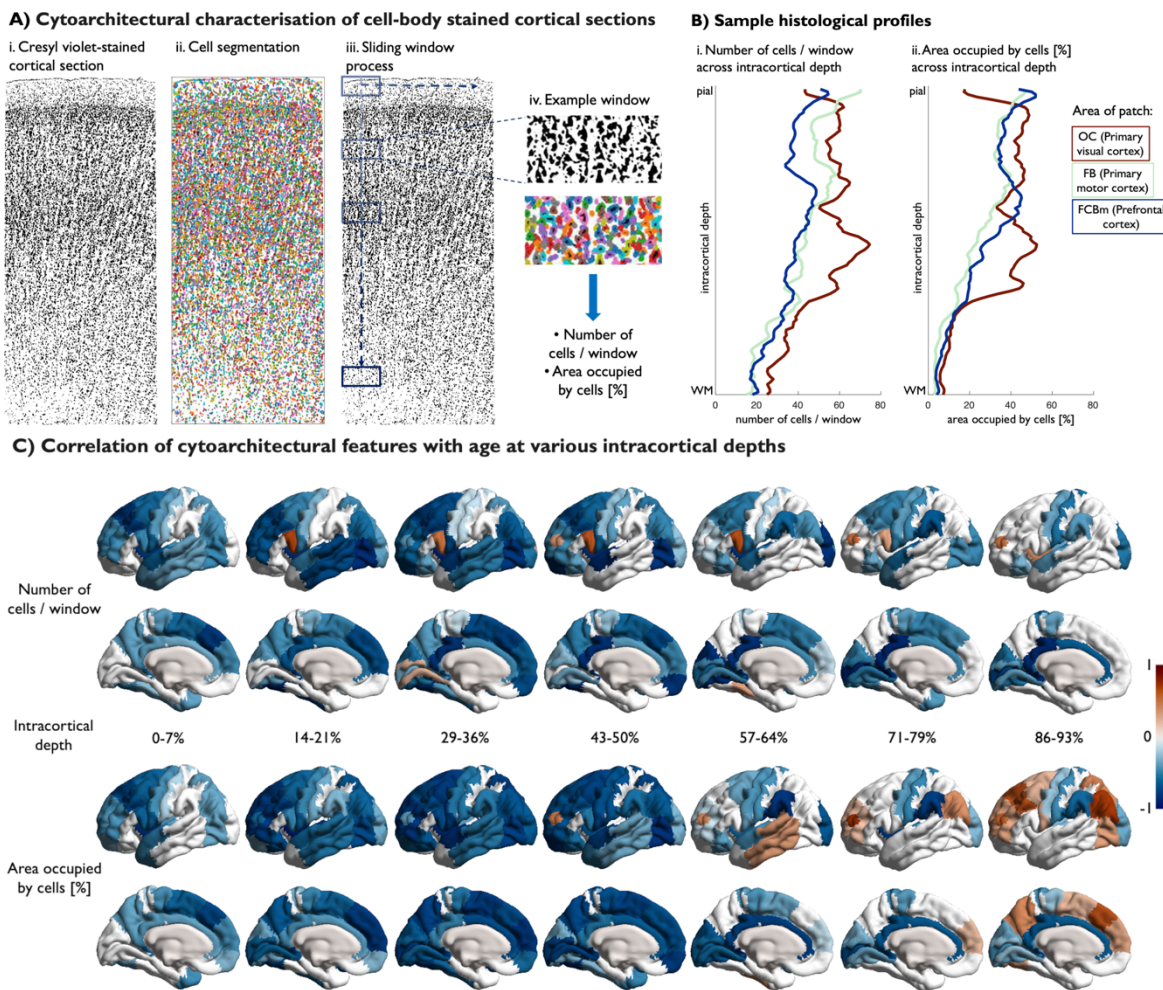


Figure 1: A) Sample cortical patch of a Cresyl-stained brain slice (*left*). A cell-segmentation algorithm was applied (*middle*) and using a sliding-window approach, we extracted the number of cells and the area occupied by cells across cortical depths (*right*). To account for the different cortical thicknesses and improve comparability to the *in vivo* dataset, all profiles were resampled, averaged across duplicate areas, and clustered into 14 depths. **B)** Sample histological profiles of cell number per window and area occupied by cells across cortical depths between the pial and white matter (WM). Each line corresponds to the profile of a different Von Economo's cortical area, OC (red), FB (green) and FCBm (blue). **C)** Statistically significant product-moment correlation coefficients (*r*) of age with number of cells and area occupied by cells at different cortical depths. White regions correspond to areas where no cortical patches were available or to areas with non-significant correlation coefficients. Histological patches were originally labelled using the terminology of Von Economo and Koskinas. We thus used these labels to accurately project the correlation coefficients onto *fsaverage* using the Von Economo parcellation¹⁰.

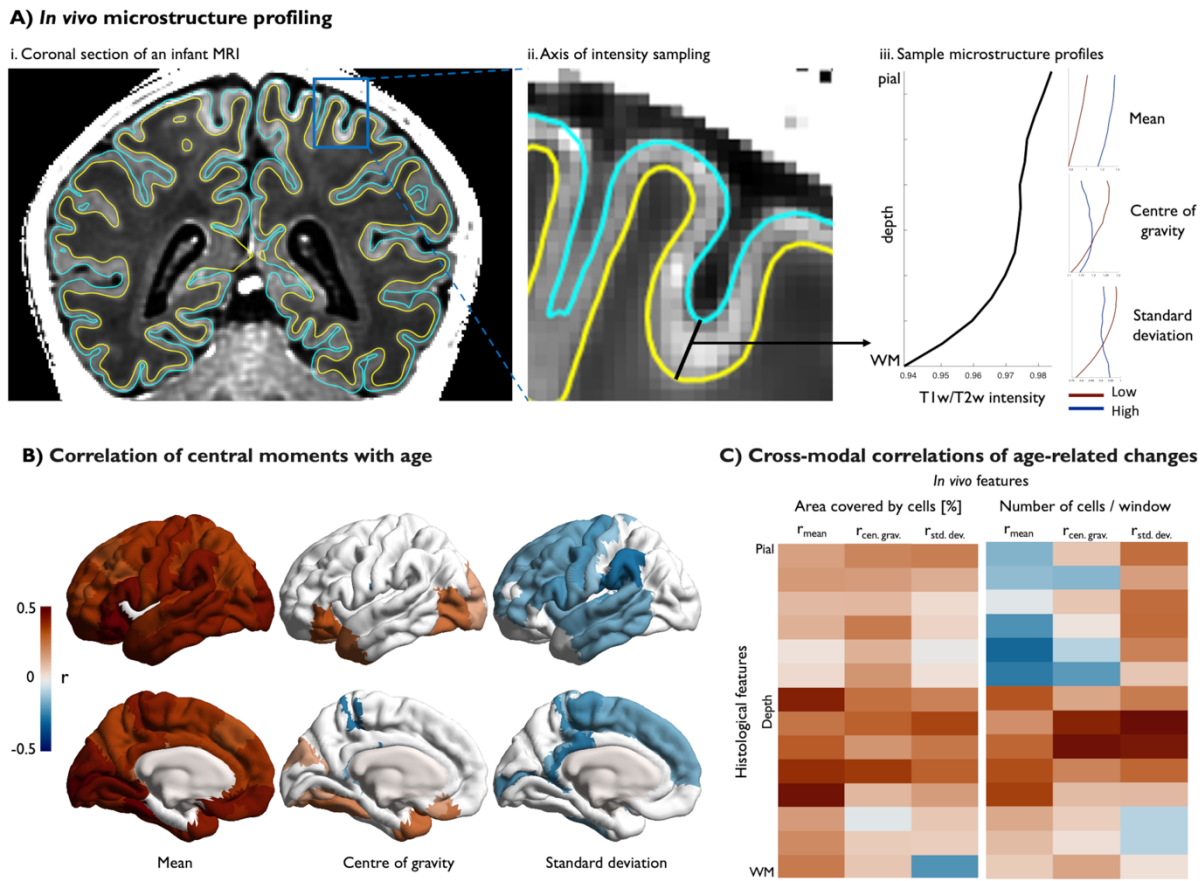


Figure 2: **A)** *In vivo* microstructure profiles were extracted from T1w/T2w images of infant brains. Subsequently, the shape of each microstructure profile was characterised by three central moments (mean, centre of gravity and standard deviation). On the right side of the main sample profile, three graphs show sample profiles with a high and a low value of each corresponding central moment. **B)** Product-moment correlation coefficients (r) of gestational age with each central moment. White regions correspond to areas with non-significant correlation coefficients ($p_{\text{FDR}} > 0.05$). **C)** Interaction of the age-related changes in central moments and the age-related, depth-specific changes in histological features. The correlation matrix shows the product-moment correlation coefficients between each pair of variables. For this analysis, only post-mortem samples with an age overlap to the *in vivo* dataset were used.

References

- Conel J. L. (1939). *The postnatal development of the human cerebral cortex. The cortex of the newborn: Vol. I.* Harvard University Press.
- Conel J. L. (1942). *The postnatal development of the human cerebral cortex. The cortex of the one-month infant: Vol. II.* Harvard University Press.
- Conel J. L. (1947). *The postnatal development of the human cerebral cortex. The cortex of the three-month infant: Vol. III.* Harvard University Press.
- Conel J. L. (1955). *The postnatal development of the human cerebral cortex. The cortex of the fifteen-month infant: Vol. V.* Harvard University Press.
- Conel J. L. (1959). *The postnatal development of the human cerebral cortex. The cortex of the twenty-four-month infant: Vol. VI.* Harvard University Press.
- Conel J. L. (1963). *The postnatal development of the human cerebral cortex. The cortex of the four-year child: Vol. VII.* Harvard University Press.
- Upschulte, E., Harmeling, S., Amunts, K., & Dickscheid, T. (2022). Contour proposal networks for biomedical instance segmentation. *Medical Image Analysis*, 77, 102371. <https://doi.org/10.1016/j.media.2022.102371>
- Makropoulos, A., Robinson, E. C., Schuh, A., Wright, R., Fitzgibbon, S., Bozek, J., Counsell, S. J., Steinweg, J., Vecchiato, K., Passerat-Palmbach, J., Lenz, G., Mortari,

- F., Tenev, T., Duff, E. P., Bastiani, M., Cordero-Grande, L., Hughes, E., Tusor, N., Tournier, J.-D., ... Rueckert, D. (2018). The developing human connectome project: A minimal processing pipeline for neonatal cortical surface reconstruction. *NeuroImage*, 173, 88–112. <https://doi.org/10.1016/j.neuroimage.2018.01.054>
9. Paquola, C., Vos De Wael, R., Wagstyl, K., Bethlehem, R. A. I., Hong, S.-J., Seidlitz, J., Bullmore, E. T., Evans, A. C., Misic, B., Margulies, D. S., Smallwood, J., & Bernhardt, B. C. (2019). Microstructural and functional gradients are increasingly dissociated in transmodal cortices. *PLOS Biology*, 17(5), e3000284. <https://doi.org/10.1371/journal.pbio.3000284>
10. Scholtens, L. H., de Reus, M. A., & van den Heuvel, M. P. (2015). Linking contemporary high resolution magnetic resonance imaging to the von Economo legacy: A study on the comparison of MRI cortical thickness and histological measurements of cortical structure. *Human Brain Mapping*, 36(8), 3038–3046. <https://doi.org/10.1002/hbm.22826>

Functional divergence between the two cerebral hemispheres contributes to human fluid intelligence

Xinyu Liang^{1,2}, Junhao Luo¹, Liyuan Yang¹, Deniz Vatansever², Elizabeth Jefferies³, Gaolang Gong¹

¹*State Key Laboratory of Cognitive Neuroscience and Learning & IDG/McGovern Institute for Brain Research,
Beijing Normal University, Beijing, China*

²*Institute of Science and Technology for Brain-inspired Intelligence, Fudan University, Shanghai, China*

³*Department of Psychology, University of York, York, United Kingdom*

Introduction: Hemispheric lateralization is linked to potential cognitive advantages (1). It is considered a driving force behind the generation of human intelligence (2). However, establishing quantitative links between the degree of lateralization and intelligence in humans remains elusive. Here, we propose a novel framework that utilizes the hyperaligned multidimensional representation space (3) derived from hemispheric functional gradients (4) to compute between-hemisphere distances within this space. We tested whether the hemispheric differences contributed to fluid intelligence in HCP large cohort (5). In addition, we considered brain size as a physical underpinning of cognition based on the evolutionary evidences (6, 7), proposing a possible pathway in which hemispheric differences might mediate the influence of brain size on fluid intelligence.

Methods: The final sample included 777 right-handed young adults (428 females; age = 22-36 years; handedness = 79.55 ± 17.85). Using preprocessed rs-fMRI images (8), we estimated vertexwise hemispheric functional gradients (4). A group-level hemispheric gradient template was generated for subsequent functional alignment with Procrustes rotation. The between-hemisphere functional distance was measured as the Euclidean distance between each pair of homotopic vertices in a 6-dimensional common representation space. Firstly, we examined whether the spatial distribution of between-hemisphere functional distance aligns with the cortical pattern of overall functional lateralization observed in meta-analytic task activations (9). Furthermore, we conducted a topic based meta-analysis along the between-hemisphere functional distance map (10). Secondly, we used a partial correlation controlling age, sex, handedness and head motions to assess the association between global functional distance and fluid cognition composite score (11). Besides, a GLM was applied on each vertex to localize the brain regions that positively contributed to the fluid cognition composite score. Finally, to determine whether between-hemisphere functional distance could play a mediating role in the effect of brain size on fluid intelligence, we conducted a mediation analysis and tested the significance by 10,000 bootstrapping tests.

Results: The between-hemisphere functional divergence varied across the cortex, with greater hemispheric divergence in transmodal regions than in primary and unimodal regions (Fig. 1a). It was significantly correlated with the overall functional lateralization (Fig. 1c) and exhibiting a systematic shift from perception to higher-level cognition (Fig. 1d). We found the global between-hemisphere functional distance was positively correlated with the fluid cognition composite score ($r = 0.125, p < 0.001$), indicating that participants with a greater hemispheric functional distance had slightly greater fluid intelligence. At the vertexwise level, we found that better fluid intelligence was associated with larger between-hemisphere functional distance in the frontal and parietal regions (Fig. 2b). At last, we verified a significant partial mediating effect of between-hemisphere functional distance on the relationship between brain size and fluid intelligence, for both the global level (Fig. 2a) and the regional level (Fig. 2c).

Conclusions: Our findings reveal that the between-hemisphere functional distance partially mediates the impact of brain size on fluid intelligence. Together, these findings illuminate the profound significance of brain lateralization as a fundamental organizational principle of the human brain, providing direct evidence that hemispheric lateralization supports human fluid intelligence.

Figures:

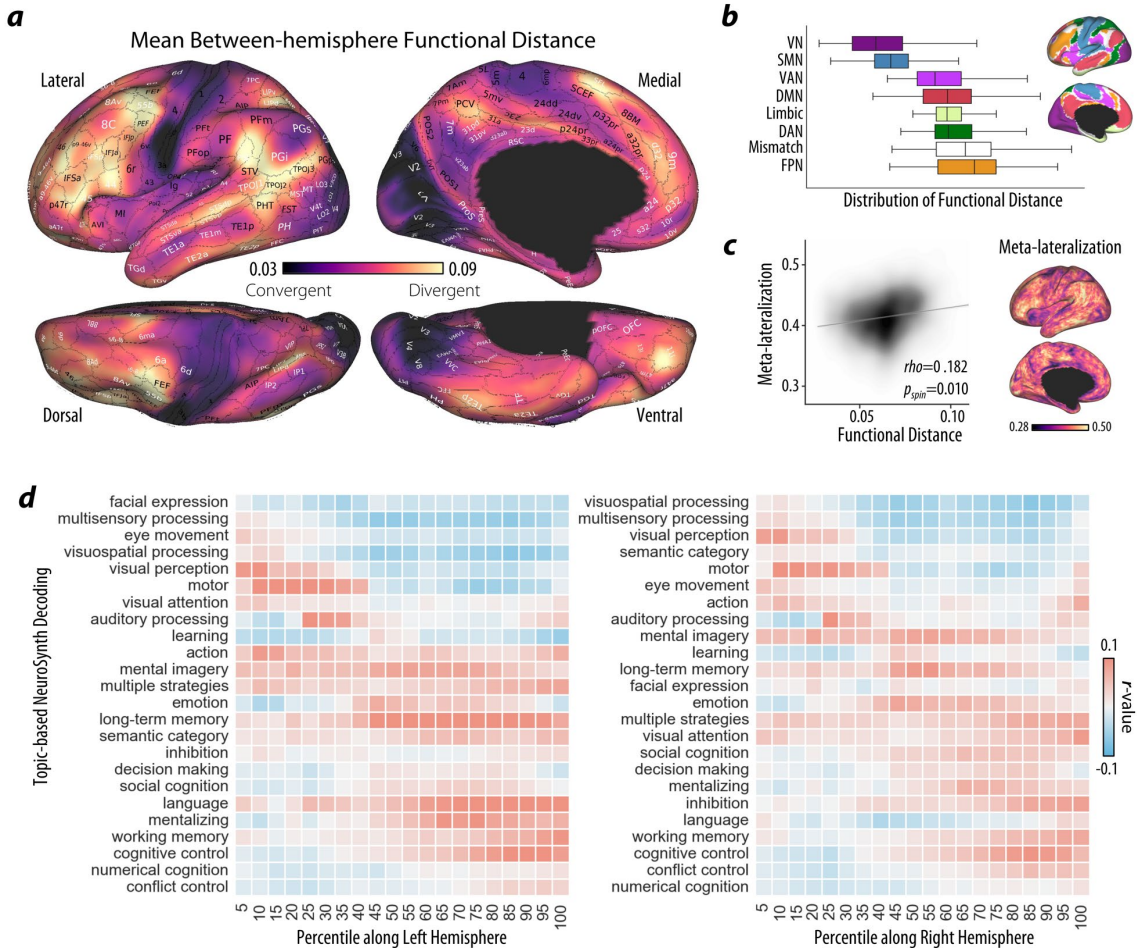


Figure 1. The cortical variation of between-hemisphere functional distance. (a). The group average map of between-hemisphere functional distance in the HCP datasets ($N = 777$). (b). We plotted the distribution of between-hemisphere functional distances within each network in a symmetric version of Yeo's 7 networks. The mismatch zone is defined by mismatch vertices that belong to distinct networks across two hemispheres. (c). We calculated the cortical map of the overall functional lateralization index across all 575 cognitive terms. A significant correlation between the cortical map of overall functional lateralization and the between-hemisphere functional distance map was found by a spin test with 10,000 permutations. (d). Then we used Neurosynth's ROI association approach of regions of interest along the between-hemisphere functional distance map with 24 topic terms. The terms were ordered by the positively weighted mean of their location along the left and right hemisphere.

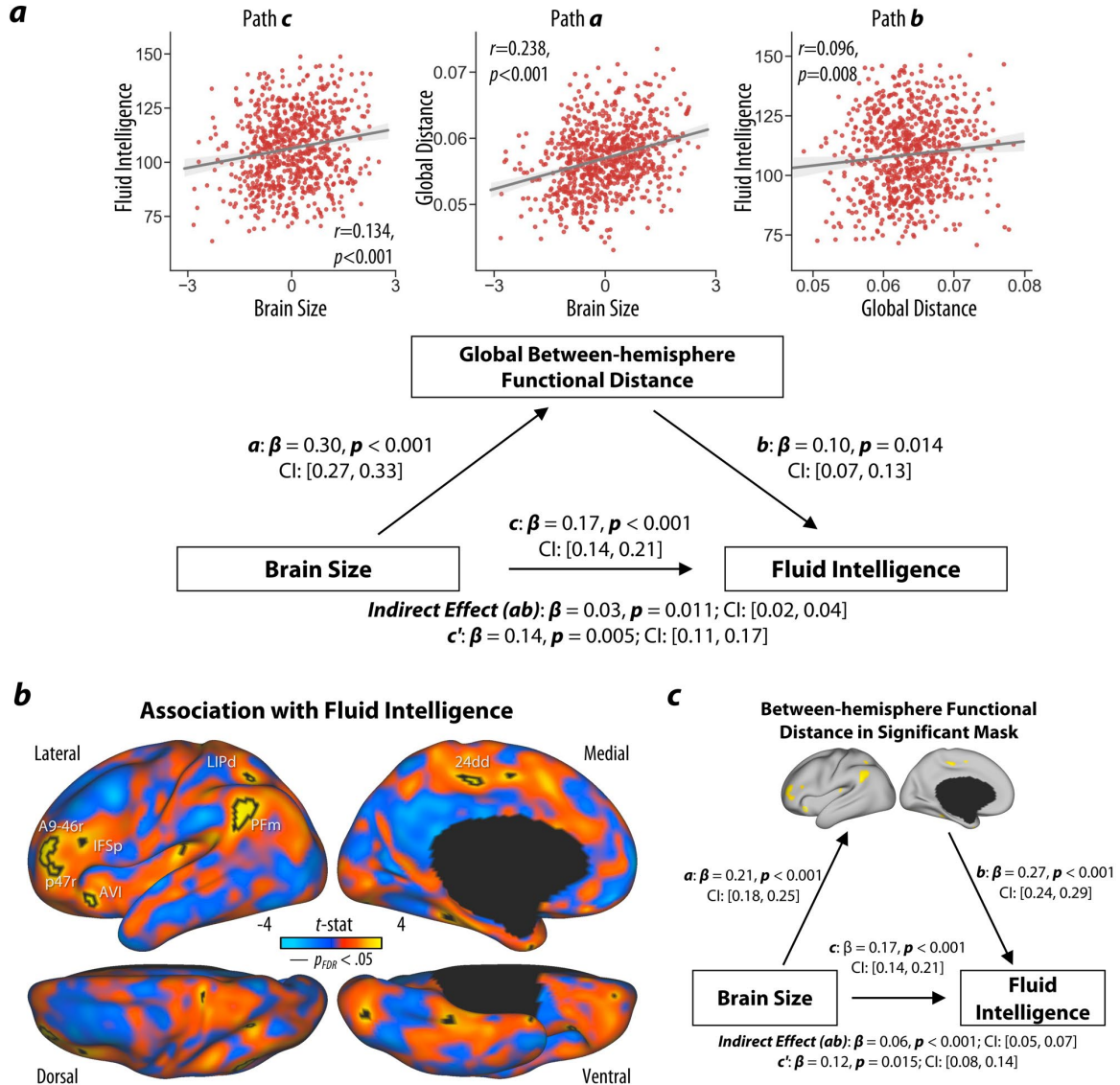


Figure 2. Individual differences in between-hemisphere functional distance mediate the effect of brain size on fluid intelligence. (a). We observed significant correlations between brain size, global between-hemisphere functional distance and fluid intelligence after controlling for age, sex, handedness and mean framewise displacement. We tested the significance of the hypothetical mediation pathway, in which global between-hemisphere functional distance could partially mediate the impact of brain size on fluid intelligence. Significance was tested by bootstrapping (10,000 replacements). (b). A GLM analysis was performed on vertexwise between-hemisphere functional distances to identify regions associated with intelligence, in which age, sex, handedness, brain size and mean FD were included as covariates. The resultant t maps for fluid intelligence are shown. The regions with gray outlines were significant vertices after FDR correction (one-tailed $p_{FDR} < 0.05$). (c). The mean between-hemisphere functional distances within a mask consists of all significant vertices also exhibited a significant mediating effect on the relationship between brain size and fluid intelligence.

References:

1. S. J. Gotts, *et al.*, Two distinct forms of functional lateralization in the human brain. *Proc Natl Acad Sci U S A* **110**, E3435–44 (2013).
2. O. Güntürkün, S. Ocklenburg, Ontogenesis of Lateralization. *Neuron* **94**, 249–263 (2017).
3. J. V. Haxby, J. S. Guntupalli, S. A. Nastase, M. Feilong, Hyperalignment: Modeling shared information encoded in idiosyncratic cortical topographies. *eLife* **9**, e56601 (2020).
4. X. Liang, *et al.*, Sex-related human brain asymmetry in hemispheric functional gradients. *NeuroImage* 117761 (2021). <https://doi.org/10.1016/j.neuroimage.2021.117761>.
5. D. C. Van Essen, *et al.*, The WU-Minn Human Connectome Project: an overview. *Neuroimage* **80**, 62–79 (2013).
6. S. F. Witelson, H. Beresh, D. L. Kigar, Intelligence and brain size in 100 postmortem brains: sex, lateralization and age factors. *Brain* **129**, 386–398 (2006).
7. D. van der Linden, C. S. Dunkel, G. Madison, Sex differences in brain size and general intelligence (g). *Intelligence* **63**, 78–88 (2017).
8. M. F. Glasser, *et al.*, The minimal preprocessing pipelines for the Human Connectome Project. *Neuroimage* **80**, 105–24 (2013).
9. V. R. Karolis, M. Corbetta, M. Thiebaut de Schotten, The architecture of functional lateralisation and its relationship to callosal connectivity in the human brain. *Nat Commun* **10**, 1417 (2019).
10. D. S. Margulies, *et al.*, Situating the default-mode network along a principal gradient of macroscale cortical organization. *Proc Natl Acad Sci USA* **113**, 12574–12579 (2016).
11. N. Akshoomoff, *et al.*, Viii. Nih Toolbox Cognition Battery (cb): Composite Scores of Crystallized, Fluid, and Overall Cognition. *Monographs of the Society for Research in Child Development* **78**, 119–132 (2013).

The differentiation of multiscale structural gradients from children to adolescents correlates with the maturation of cortical macrostructure and function

Yirong He¹, Qiongling Li^{1,2,3}, Debin Zeng⁴, Lei Chu⁴, Xiaoxi Dong¹, Shuyu Li¹

¹*State Key Laboratory of Cognitive Neuroscience and Learning, Beijing Normal University, Beijing, 100875, China*

²*Beijing Key Laboratory of Brain Imaging and Connectomics, Beijing Normal University, Beijing, 100875, China*

³*IDG/McGovern Institute for Brain Research, Beijing Normal University, Beijing, 100875, China*

⁴*Beijing Advanced Innovation Center for Biomedical Engineering, School of Biological Science & Medical Engineering, Beihang University, Beijing 100083, China*

Keywords: structural connectome; gradients; development

Introduction

The brain development of children and adolescents is accompanied by maturation of cortical myelination and white matter network. Many studies have revealed that cortical maturation follows a pattern of spatiotemporal hierarchy(Sydnor, Larsen et al. 2021). Connectome gradient techniques representing brain topological organization in a low-dimensional space can capture the cortical macroscale hierarchy(Margulies, Ghosh et al. 2016). A recently introduced *in vivo* model integrated three features of structural connectivity, including diffusion MRI tractography, geodesic distance, and microstructural similarity(Paquola, Seidlitz et al. 2020). Here, we leveraged this approach to investigate structural connectome development from childhood to adolescence and related it with maturation of cortical morphology and function.

Methods

Dataset. We collected a longitudinal cohort of 276 participants with 437 scans from Children School Functions and Brain Development Project in China.

Compute multiscale structural connectome gradients. Base on T1w, T2w, and diffusion MRI, we computed geodesic distances, microstructural profile covariance (MPC), and tact strength between brain regions. We followed the steps from (Paquola, Seidlitz et al. 2020) to compute multiscale structural connectome gradients. We calculated several global features to measure the gradient transitions during development, including gradient range, explanation ratio, standard deviation, dispersion, and eccentricity. By leveraging a mixed effect linear model, we identified the developmental trajectories.

Association with development of morphometric features. We utilized 5 cortical morphometric measures to investigate the relationships between multiscale structural gradients and morphometric features. We performed principle component analysis (PCA) to summarize these 5 features and related the PC 1 to the multiscale structural gradient 1.

Multiscale structure-function coupling. We conducted an analysis on the coupling between structure and function. Coupling was computed as Spearman rank correlation between connectivity profiles of structure and function.

Results

During development, the first gradient showing differentiation between transmodal and primary regions, and the second gradient separating anterior and posterior regions (Fig 1A). According to the trajectories of global measures, the first gradient increased with development and vice versa for the second gradient. Age-related changes in multiscale structural gradient 1 during development revealed the gradual maturation of the S-A axis (Fig. 1). The first principal component of morphological features was associated with the first gradient, and the age-related patterns of change were also correlated (Fig. 2A-D). The pattern of coupling between multiscale structure and functional connectivity adhered to the S-A axis, and the majority of systems exhibited an increase in coupling with development (Fig. 2E-F).

Conclusions

In conclusion, by applying connectome gradient analysis, we revealed that the organization of structural connectome moves toward a more distributed direction with development, which correlates with maturation of cortical macrostructure and function.

Figures

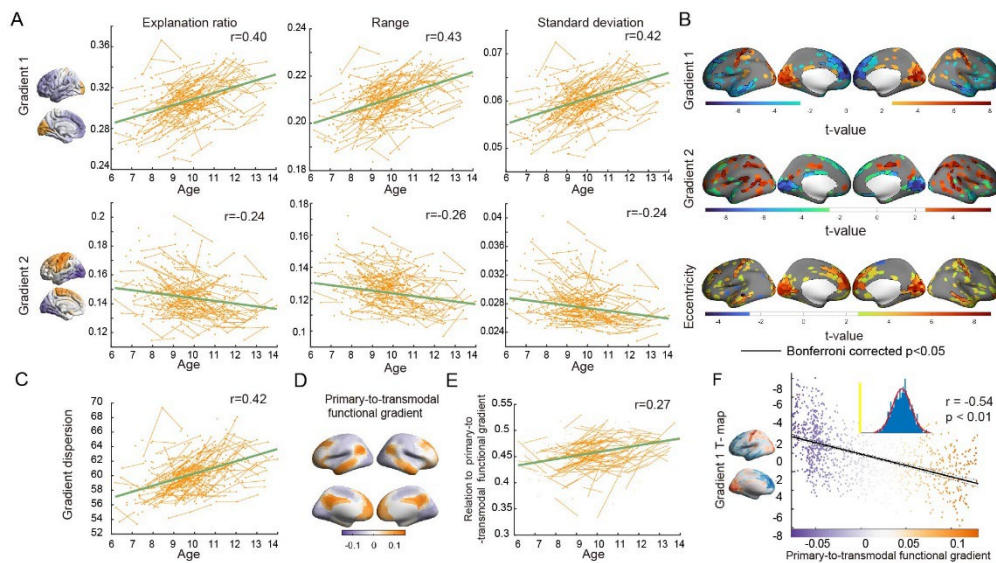


Fig. 1 Age-related changes of gradients at both the global level and the node level.

A. Global measures changed with age ($p < 0.001$). **B.** Node-wise gradients and eccentricity map changed with age ($p < 0.01$). **C.** Global dispersion changed with age. **D.** Primary-to-transmodal functional gradient. **E.** Correlation between **D** and structural gradient 1 changed with age. **F.** Spatial correlation between gradient 1 t-map and functional gradient.

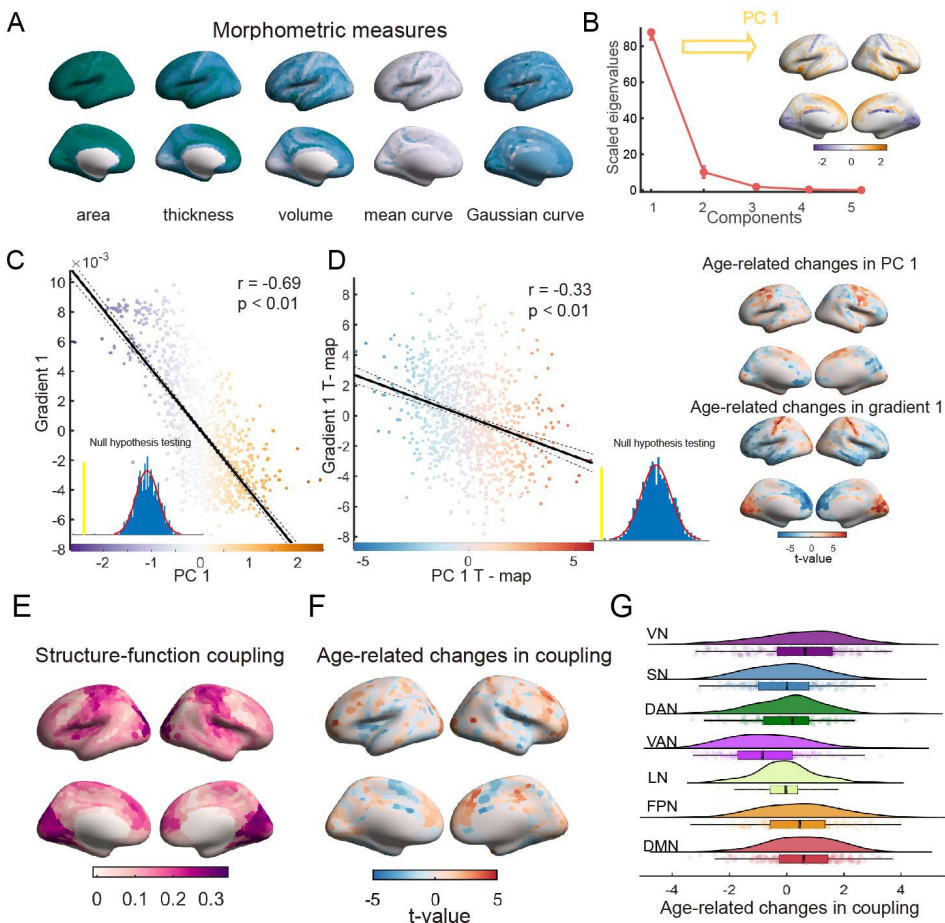


Fig. 2 Relation to cortical macrostructure and function.

References

- Margulies, D. S., S. S. Ghosh, A. Goulas, M. Falkiewicz, J. M. Huntenburg, G. Langs, G. Bezgin, S. B. Eickhoff, F. X. Castellanos, M. Petrides and others (2016). "Situating the default-mode network along a principal gradient of macroscale cortical organization." Proceedings of the National Academy of Sciences **113**(44): 12574-12579.
- Paquola, C., J. Seidlitz, O. Benkarim, J. Royer, P. Klimes, R. A. I. Bethlehem, S. Larivière, R. V. de Wael, R. Rodríguez-Cruces, J. A. Hall, B. Frauscher, J. Smallwood and B. C. Bernhardt (2020). "A multi-scale cortical wiring space links cellular architecture and functional dynamics in the human brain." PLoS Biology **18**(11).
- Sydnor, V. J., B. Larsen, D. S. Bassett, A. Alexander-Bloch, D. A. Fair, C. Liston, A. P. Mackey, M. P. Milham, A. Pines, D. R. Roalf and others (2021). "Neurodevelopment of the association cortices: Patterns, mechanisms, and implications for psychopathology." Neuron **109**(18): 2820-2846.

Exploring sex-specific neuroendocrine influences on the sensorimotor-association axis in single individuals

Bianca Serio^{1, 2, 3, 4*}, Deniz Yilmaz^{5*}, Laura Pritschet⁶, Hannah Grotzinger⁶, Emily G Jacobs⁶, Simon B Eickhoff^{3, 4}, Sofie L Valk^{2, 3, 4}

¹ Max Planck School of Cognition, Leipzig, Germany

² Max Planck Institute for Human Cognitive and Brain Sciences, Leipzig, Germany

³ Institute of Neuroscience and Medicine, Brain & Behavior (INM-7), Research Centre Jülich, Jülich, Germany

⁴ Institute of Systems Neuroscience, Medical Faculty, Heinrich Heine University Düsseldorf, Düsseldorf, Germany

⁵ Palo Alto High School, Palo Alto, CA, USA

⁶ Department of Psychological and Brain Sciences, University of California, Santa Barbara, CA, USA

* Shared first-author

Introduction: Human neuroimaging studies consistently show multimodal patterns of variability along a key principle of macroscale cortical organization – the sensorimotor-association (S-A) axis. However, little is known about day-to-day fluctuations in functional connectivity along this axis within an individual, including sex-specific neuroendocrine factors contributing to such transient changes.

Methods: One female (23 years) and one male (26 years) were respectively tested for 29 and 20 consecutive days in time-locked experimental sessions including brain imaging, venipuncture/salivary sampling and self-report questionnaires. We computed the S-A axis as our measure of functional cortical organization by using diffusion map embedding to reduce the dimensionality of functional connectivity matrices at each timepoint within participants. We quantified intra-individual variability in the S-A axis as the standard deviation of parcel loadings across sessions, decoded these patterns of variability with multimodal publicly available brain maps, and tested for local differences in variability between participants with Levene's test for equality of variances. Next, independently in both participants, we used linear models to probe local- and system-level effects of daily changes in hormone levels and perceived stress on S-A axis loadings and measures of network topography, namely within- and between-network dispersion, which quantify the spread of functional networks along the S-A axis. First, we specifically assessed effects of steroid hormones that are most predominant within each sex, i.e., estradiol and progesterone in the female participant, and testosterone (and cortisol, given its availability) in the male participant. Second, we tested for sex-specific effects of common steroid hormones in both participants, i.e., estradiol and testosterone, allowing a direct comparison of effects between the female and male participants. To correct for multiple comparisons, false discovery rate correction was applied to local-level results (across 400 Schaefer parcels), and Bonferroni correction was applied to system-level results (across 7 networks for within-network dispersion and 21 pairwise network comparisons for between-network dispersion), in addition to spin permutation testing (1000 permutations) to control for spatial autocorrelation.

Results: Overall, participants showed unique cortical patterns of intra-individual variability in S-A axis loadings, with similar cortical areas (i.e., temporal limbic and ventral prefrontal regions) displaying the largest amount of variability across participants and male variability extending further across the cortex. We found statistically significant greater intra-individual variability exclusively in the male participant, as well as associations between male whole-brain patterns of intra-individual variability and a range of brain features pertaining to brain metabolism, structure, electrophysiology, genetics, and phylogeny. When testing for local- and system-level effects of steroid hormones and perceived stress on functional organization, we found only a few effects that survived our statistical corrections. However, we observed distinctly diverging patterns of hormone and perceived stress effects on network topology in the female and male participants under study.

Conclusion: Using a dense sampling approach, we showed daily variations in human functional organization in two healthy subjects. Collectively, our findings suggest subtle inter-individual differences in intra-individual daily variability along a major principle of functional cortical organization and hint at potential sex-specific neuroendocrine processes that require further testing in larger samples.

Capturing cortical hierarchy and dual stream architecture with precision functional MRI at 7T

Yezhou Wang¹, Jordan DeKraker¹, Raul Rodriguez Cruces¹, Donna Gift Cabalo¹, Bin Wan^{2,3}, Casey Paquola², Sofie L. Valk^{2,3}, Seok-Jun Hong⁴, Alan C Evans¹, Boris Bernhardt¹

¹ McConnell Brain Imaging Centre, Montreal Neurological Institute and Hospital, McGill University, Montreal, Quebec, Canada; ² Institute of Neuroscience and Medicine (INM-7), Forschungszentrum Jülich, Jülich, Germany; ³ Cognitive Neurogenetics, Max Planck Institute for Human Cognitive and Brain Sciences, Leipzig, Germany; ⁴ Department of Biomedical Engineering, Sungkyunkwan University, Suwon, Republic of Korea

INTRODUCTION:

Understanding the functional processing hierarchy of the human cerebral cortex is a longstanding challenge in neuroscience. Foundational hierarchical models of the cortex, formulated in non-human primates, presume the interaction of feedforward and feedback processes [1-3]. There is increasing support for a dual stream architecture, in which the laminar origin of projection patterns determines feedback vs feedforward signaling, especially for long-range connectivity patterns. Here, we expand this research to the human cortex, capitalizing on ultra-high-resolution 7 Tesla magnetic resonance imaging (7T MRI) [4]. Combining directional functional connectivity modelling with geodesic distance mapping across cortex, we specifically tested whether feedback signalling to primary sensory systems derives from deeper layers with increasing anatomical distance between different cortical areas.

METHODS:

We analyzed 7T MRI data of 10 unrelated healthy adults (age: 26.80 ± 4.61 years, 5 females). Each participant underwent three separate sessions, during which structural (resolution 0.5mm) and resting-state functional MRI (rs-fMRI; 1.9mm) scans were acquired. We sampled deep- and superficial-layer timeseries using rs-fMRI data. Regression dynamic causal models (rDCM) [5] were applied to these timeseries, resulting in effective connectivity matrices. To evaluate patterns of feedback streams, we defined the deep source ratio (DSR). For area V1, we assessed DSR of the feedback stream from regions in visual network (VN), dorsal attention network (dAN), and default mode network (DMN). For each region, we calculated Spearman's correlation coefficients between its DSR and its geodesic distance to the regions of interest (ROI). We performed similar analyses on somatomotor network (SMN) and auditory network (AN). We integrated all ROIs together and examined associations by controlling inter-ROI differences using a mixed linear model. To further enhance the precision of defining superficial and deep layers, we reconstructed the effective connectivity matrix by incorporating cortical layer information from a histological dataset (**Figure 2.A**) [6].

Subsequently, we reran all main analyses based on the updated effective connectivity matrix.

RESULTS:

We derived effective connectivity matrices for each participant (**Figure 1.A**). Individual matrices were averaged to obtain the group-level matrix for subsequent analyses. Our initial investigation focused on V1, revealing a significant association between DSR and geodesic distance, especially in VN+dAN+DMN ($r=0.45$, $p=0.002$; **Figure 1.B**). Similar findings were observed for S1 in SMN+dAN+DMN ($r=0.37$, $p=0.042$; **Figure 1.C**) and for A1 in AN ($r=0.60$, $p=0.034$; **Figure 1.D**). Combining all regions using a mixed model revealed significant associations ($r=0.49$, $p<0.001$; **Figure 1.E**). Finally, we cross-validated findings after adjusting definitions of deep and superficial surfaces by incorporating cortical layer information from a histological dataset [6] (**Figure 2.A**). We repeated the main analyses and obtained similar results in VN ($r=0.43$, $p=0.002$), SMN ($r=0.43$, $p=0.016$), AN ($r=0.62$, $p=0.027$), and all regions together ($r=0.46$, $p<0.001$; **Figure 2.B**).

CONCLUSION:

Our findings reveal a clear hierarchical organization within the human cortex, particularly in the feedback stream from unimodal and heteromodal association cortex to V1, S1, and A1. These results indicate the presence of well-defined, distance-dependent feedback pathways in both the superficial and deep layers, consistent with the notion of feedback connections providing a generative network [7].

KEYWORDS: laminar architecture, 7T MRI, cortical hierarchy, neuroimaging, functional connectivity

REFERENCES

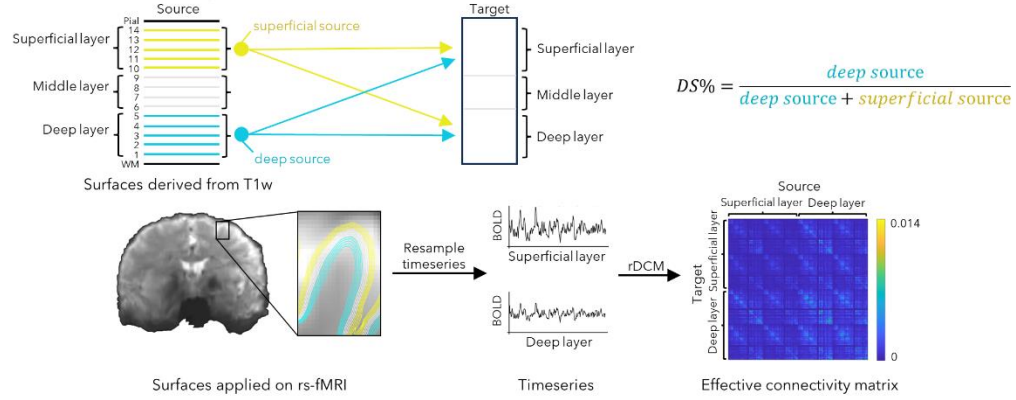
1. Felleman DJ, Van Essen DC. (1991), Distributed Hierarchical Processing in the Primate Cerebral Cortex. *Cereb Cortex*. 1(1):1-47. doi: 10.1093/cercor/1.1.1-a.
2. Mesulam MM. (1998), From sensation to cognition. *Brain*. 121(6):1013-52. doi: 10.1093/brain/121.6.1013.
3. Pascal B, Alexandre B, Kenneth K, Henry K. (2000), Laminar Distribution of Neurons in Extrastriate Areas Projecting to Visual Areas V1 and V4 Correlates with the Hierarchical Rank and Indicates the Operation of a Distance Rule. *J Neurosci*. 20(9):3263. doi: 10.1523/JNEUROSCI.20-09-03263.2000.
4. van der Kolk AG, Hendrikse J, Zwanenburg JJM, Visser F, Luijten PR. (2013), Clinical applications of 7T MRI in the brain. *Eur J Radiol*. 82(5):708-18. doi: <https://doi.org/10.1016/j.ejrad.2011.07.007>.
5. Cruces RR, Royer J, Herholz P, Larivière S, Vos de Wael R, Paquola C, et al. (2022), Micapipe: A pipeline for multimodal neuroimaging and connectome analysis. *Neuroimage*. 263:119612. doi: <https://doi.org/10.1016/j.neuroimage.2022.119612>.
6. Wagstyl K, Larocque S, Cucurull G, Lepage C, Cohen JP, Bludau S, et al. BigBrain 3D atlas of cortical layers: (2020) Cortical and laminar thickness gradients diverge in sensory and motor

cortices. PLoS Biol. 18(4):e3000678. doi: 10.1371/journal.pbio.3000678.

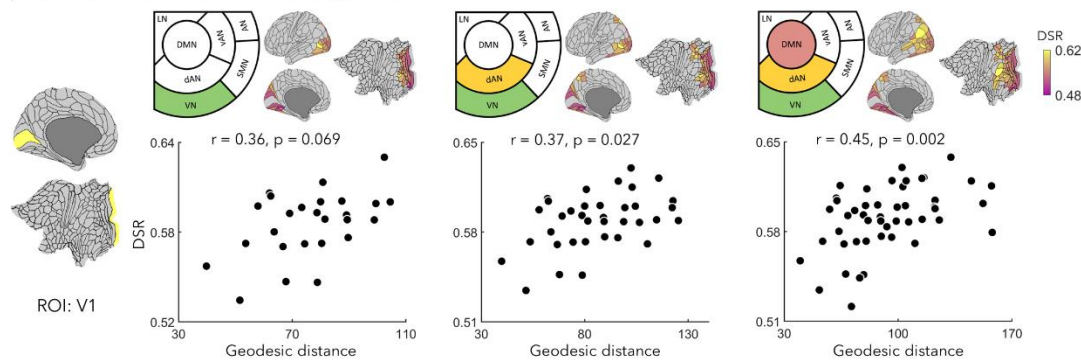
7. Vezoli J, Magrou L, Goebel R, Wang X-J, Knoblauch K, Vinck M, et al. (2021), Cortical hierarchy, dual counterstream architecture and the importance of top-down generative networks. Neuroimage. 225:117479. doi: <https://doi.org/10.1016/j.neuroimage.2020.117479>.

Figures.

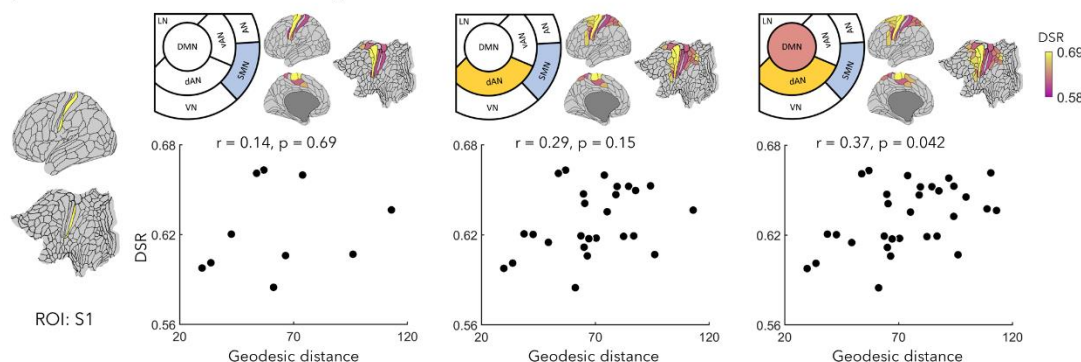
A | Generation of depth specific effective connectivity matrix



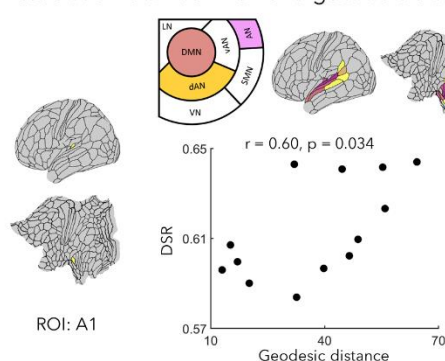
B | Association between DSR and geodesic distance in VN



C | Association between DSR and geodesic distance in SMN



D | Association between DSR and geodesic distance in AN



E | Associations in multiple cortical networks

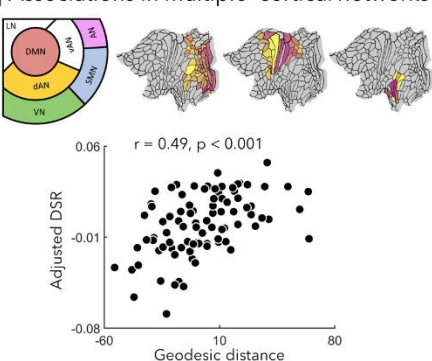
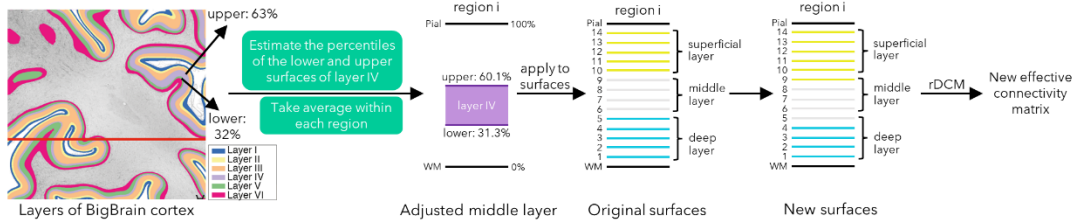


Figure 1. A) Generation of depth specific effective connectivity matrix. 14 equivolumetric intracortical surfaces were generated from high resolution structural MRI, and divided into superficial, middle and deep cortical depths. Following cross-modal registration, rs-fMRI

timeseries of deep and superficial depths were resampled and were used as input of rDCM to generate effective connectivity matrix. DSR was defined as shown in the formulation, following the theory proposed in prior study [9]. **B) Association between DSR and GD in VN.** DSR and GD of each region to the ROI V1 was computed in VN, and additional regions in dAN and DMN. Spearman's correlation coefficients between DSR and GD were estimated. **C) Association between DSR and GD in SMN.** DSR and GD of each region to the ROI S1 was computed in SMN, dAN and DMN. Spearman's correlation coefficients were also estimated. **D) Association between DSR and GD in AN.** DSR and GD of each region to the ROI A1, and Spearman's correlation coefficients between them were computed in AN. **E) Associations in multiple cortical networks.** Associations between DSR and GD in VN, SMN, AN, dAN and DMN were estimated. **Abbreviation:** GD: geodesic distance; VN: visual network; SMN: somatomotor network; AN: auditory network; dAN: dorsal attention network; vAN: ventral attention network; DMN: default mode network; LN: limbic network.

A | Adjusted effective connectivity matrix based on cortical layers defined by histological data



B | Association between DSR and geodesic distance in multiple networks

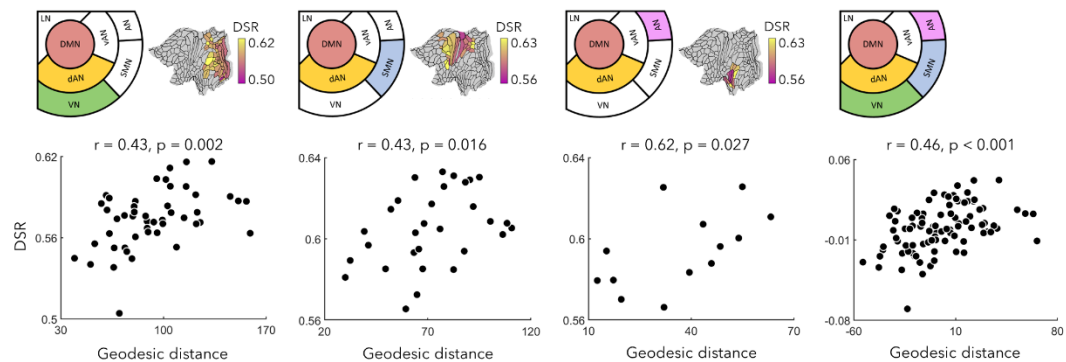


Figure 2. A) Adjusted effective connectivity matrix based on cortical layers defined by histological data. For region i, we utilized the position information of layer IV from the BigBrain dataset [8] to refine the middle layer, resulting in new surfaces. This process improved the precision of defining the superficial and deep layers of the cortex. Subsequently, we resampled timeseries using these new surfaces and reran rDCM to generate the adjusted effective connectivity matrix. **B) Associations between DSR and GD in multiple networks.** We evaluated the associations between DSR and GD in VN, SMN and AN using a new effective connectivity matrix. **Abbreviation:** GD: geodesic distance; DS: deep source.

Empathising-systemising along the unimodal-transmodal axis

Marcin A. Radecki^{1,2}, Amin Saberi^{3,4,5}, Bin Wan^{3,4}, Dorothea L. Floris^{6,7,8}, Richard A. I. Bethlehem⁹,

Meng-Chuan Lai^{2,10,11}, Michael V. Lombardo¹², Luca Cecchetti¹, Simon Baron-Cohen^{2,†}, &

Sofie L. Valk^{3,4,5,†}

1. *Social and Affective Neuroscience Group, IMT School for Advanced Studies Lucca, Lucca, Italy*
2. *Autism Research Centre, Department of Psychiatry, University of Cambridge, Cambridge, UK*
3. *Otto Hahn Group Cognitive Neurogenetics, Max Planck Institute for Human Cognitive and Brain Sciences, Leipzig, Germany*
4. *Institute of Neuroscience and Medicine (INM-7: Brain and Behaviour), Research Centre Jülich, Jülich, Germany*
5. *Institute of Systems Neuroscience, Heinrich Heine University Düsseldorf, Düsseldorf, Germany*
6. *Methods of Plasticity Research, Department of Psychology, University of Zürich, Zürich, Switzerland*
7. *Donders Institute for Brain, Cognition and Behaviour, Radboud University, Nijmegen, Netherlands*
8. *Department of Cognitive Neuroscience, Radboud University Medical Center, Nijmegen, Netherlands*
9. *Department of Psychology, University of Cambridge, Cambridge, UK*
10. *The Margaret and Wallace McCain Centre for Child, Youth & Family Mental Health and Azrieli Adult Neurodevelopmental Centre, Campbell Family Mental Health Research Institute, Centre for Addiction and Mental Health, Toronto, ON, Canada*
11. *Department of Psychiatry, Temerty Faculty of Medicine, University of Toronto, Toronto, ON, Canada*
12. *Laboratory for Autism and Neurodevelopmental Disorders, Center for Neuroscience and Cognitive Systems, Istituto Italiano di Tecnologia, Rovereto, Italy*

† denotes senior authors

Introduction

The cortical *unimodal-transmodal* gradient (G1) [1] was shown to differentiate meta-analytic activations of cognitive and affective empathy – understanding others' mental states and responding to them with an appropriate emotion, respectively [2]. We hypothesised that G1 reflects the “D-score” – the drive to systemise (understand and build systems) relative to empathise [3] – and that the two empathy maps selectively align with brain phenotypes that differentiate the unimodal and transmodal cortices [4].

Methods

One hundred typical adults ($M_{age} = 29 \pm 7$ years, 43 female [5]) had their multi-band resting-state fMRI data from two runs parcellated [6] (*Fig. 1A*), and 10 gradients were extracted via diffusion-map embedding [7] with normative HCP gradients [8] as the alignment reference (*Fig. 1B-C*). G1 loadings were averaged within: two meta-analytically thresholded empathy clusters [2]; four novel empathy clusters based on these; and seven canonical functional networks [9] (*Fig. 1D-F*). The D-score was the standardised difference between the 75-item Systemising Quotient – Revised and the 40-item Empathy Quotient; the higher the D-score, the stronger the drive to systemise relative to empathise [10]. Based on the D-score percentiles, we identified those of Type E (“empathisers”; 0-35th), Type B (“balanced”; 35-65th), and Type S (“systemisers”; 65-100th). Eight brain phenotypes were leveraged from the HCP and neuromaps [4].

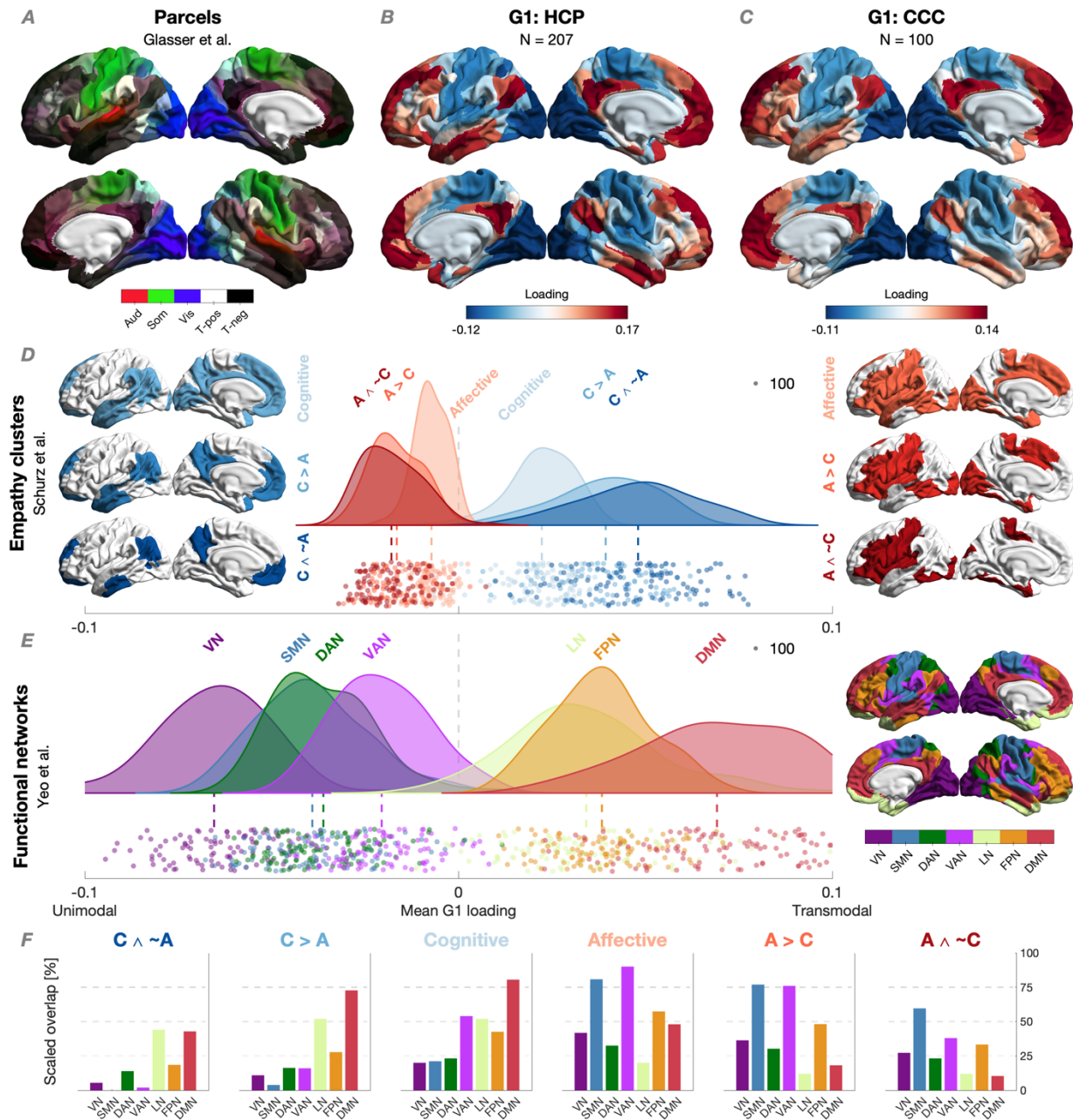


Figure 1

Results

We tested whether mean G1 loadings within four empathy clusters (*Fig. 2A*) had a relationship with the D-score and E-S type, controlling for sex, age, head motion, and multiple testing in a robust linear regression. “ $A > C$ ” and “ $A \wedge \sim C$ ” G1 loadings correlated positively with the D-score (*Fig. 2B*) and differed by E-S type, becoming progressively *transmodal* from Type E to Type S – although these two groups differed on every cluster (*Fig. 2C*). No single parcel survived FDR correction in relation to the D-score. We then spatially correlated these uncorrected standardised betas with the cognitive- and affective-empathy maps as well as their contrast (*Fig. 2D*). The spin test (2,500 permutations) showed that the D-score map correlated negatively with the cognitive map and positively with the affective map; a stronger meta-analytic loading of the parcel reflected its stronger *unimodal* or *transmodal* relationship with the D-score, respectively. These opposite relationships were further corroborated by the contrast map (*Fig. 2E*). Finally, the cognitive map aligned with maps of the first principal component (PC1) of gene expression, intracortical myelination, cortical thickness, evolutionary expansion, task-activation PC1, and G1 – but not cerebral-blood flow or the visual-somatomotor G2. Conversely, the affective map aligned with the cortical-thickness map only (*Fig. 3*).

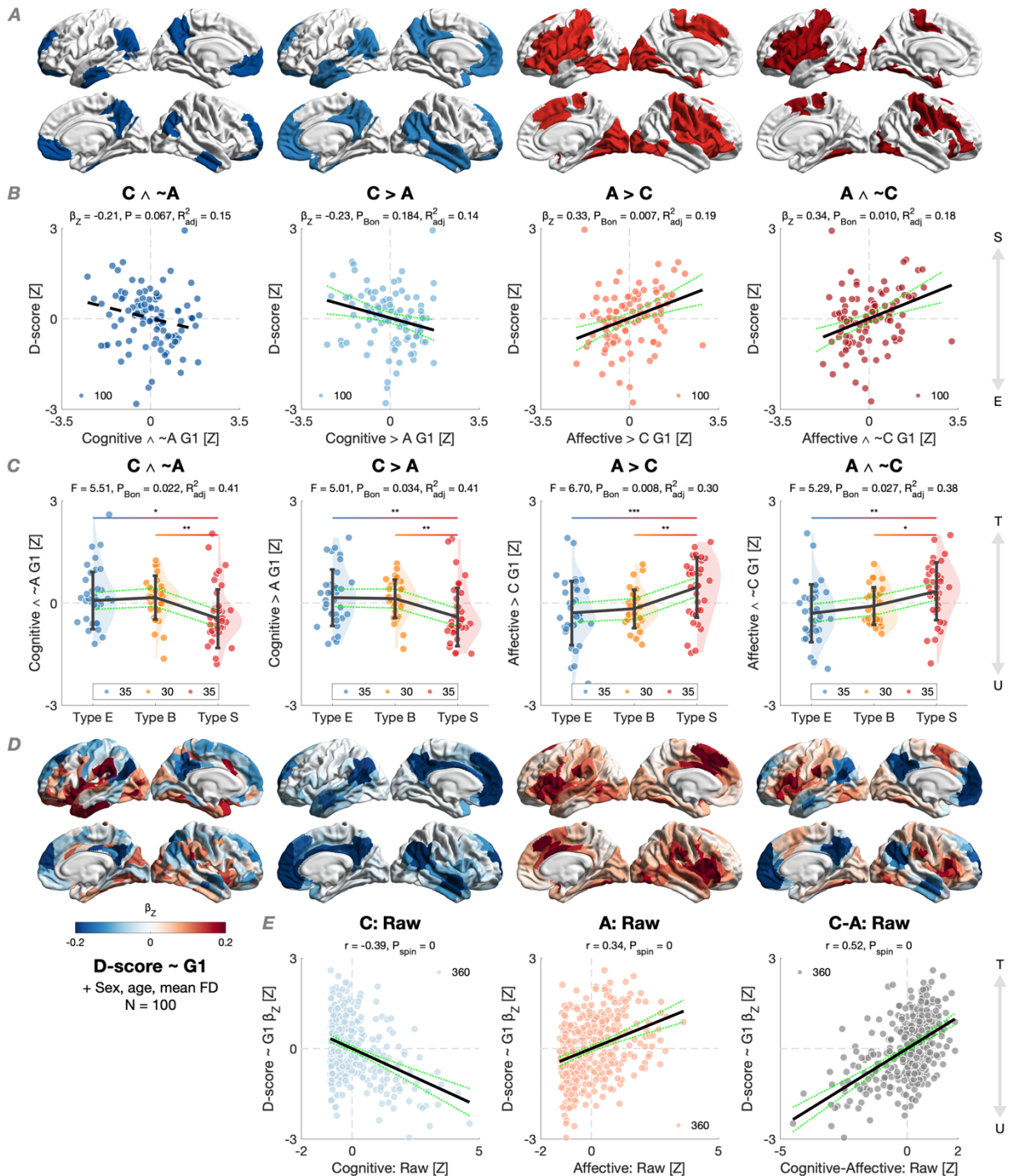


Figure 2

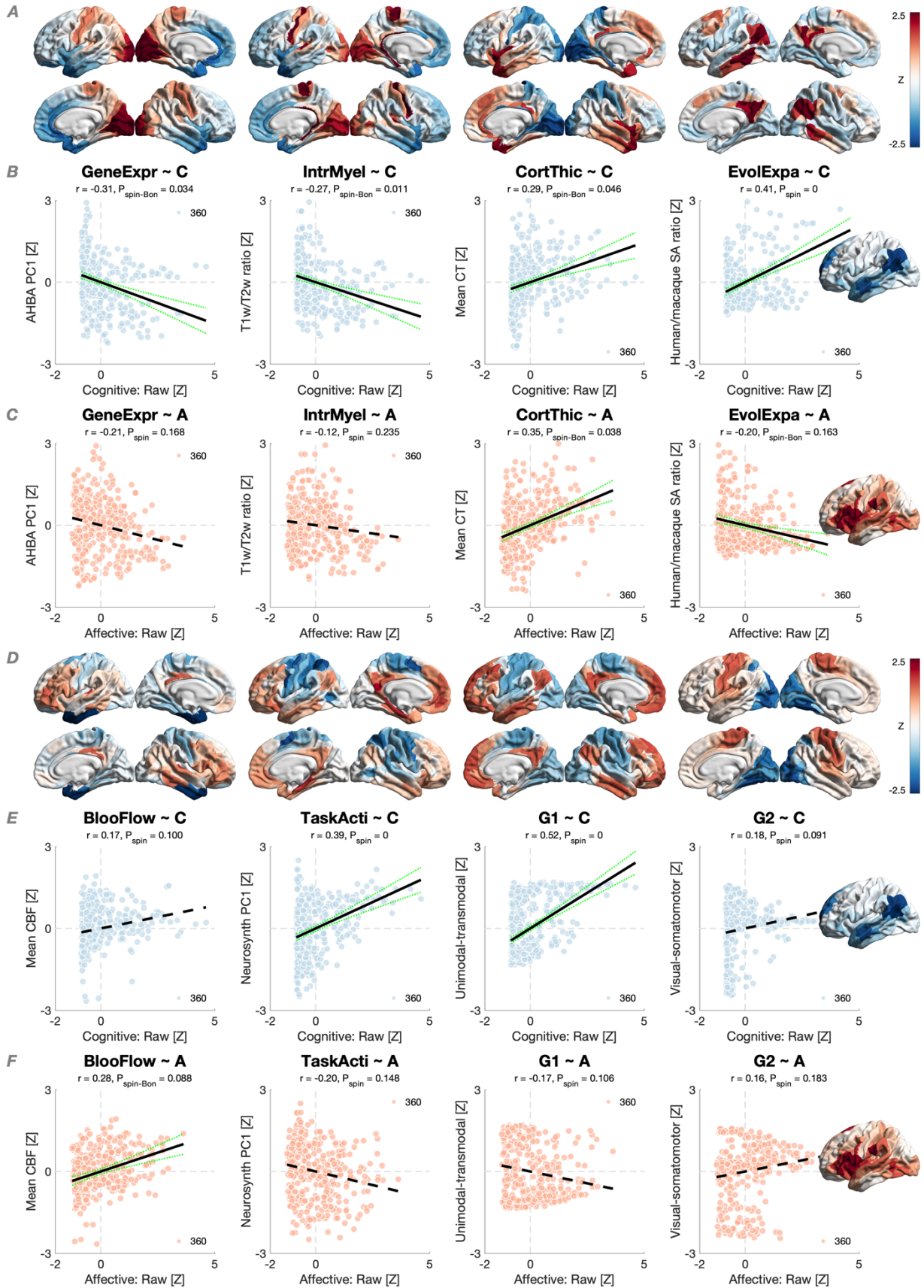


Figure 3

Conclusions

Affective-empathy G1 loadings correlated positively with the D-score and differed by E-S type; a stronger *transmodal* loading reflected a stronger drive to systemise relative to empathise. Across the cortex, the D-score showed opposite relationships with cognitive and affective empathy, which in turn showed selective brain-phenotypic relationships. These findings suggest that the D-score tracks the empathic distinction in brain function and that this distinction is informed by genetic, structural, and evolutionary factors.

References

- [1] Margulies, D. S. et al. (2016). Situating the default-mode network along a principal gradient of macroscale cortical organization. *Proceedings of the National Academy of Sciences of the United States of America*, 113(44), 12574–12579. <https://doi.org/10.1073/pnas.1608282113>
- [2] Schurz, M. et al. (2021). Toward a hierarchical model of social cognition: A neuroimaging meta-analysis and integrative review of empathy and theory of mind. *Psychological Bulletin*, 147(3), 293–327. <http://doi.org/10.1037/bul0000303>
- [3] Baron-Cohen, S. (2002). The extreme male brain theory of autism. *Trends in Cognitive Sciences*, 6(6), 248–254. [https://doi.org/10.1016/s1364-6613\(02\)01904-6](https://doi.org/10.1016/s1364-6613(02)01904-6)
- [4] Markello, R. D., Hansen, J. Y., Liu, Z.-Q., Bazinet, V., Shafiei, G., Suárez, L. E., ... Misic, B. (2022). neuromaps: Structural and functional interpretation of brain maps. *Nature Methods*, 19(11), 1472–1479 (2022). <https://doi.org/10.1038/s41592-022-01625-w>
- [5] Kliemann, D. et al. (2022). Caltech Conte Center, a multimodal data resource for exploring social cognition and decision-making. *Scientific Data*, 9(1), 138. <https://doi.org/10.1038/s41597-022-01171-2>

- [6] Glasser, M. F. et al. (2016). A multi-modal parcellation of human cerebral cortex. *Nature*, 536(7615), 171–178. <https://doi.org/10.1038/nature18933>
- [7] Vos de Wael, R. et al. (2020). BrainSpace: A toolbox for the analysis of macroscale gradients in neuroimaging and connectomics datasets. *Communications Biology*, 3(1), 103. <https://doi.org/10.1038/s42003-020-0794-7>
- [8] Larivière, S. et al. (2021). The ENIGMA Toolbox: Multiscale neural contextualization of multisite neuroimaging datasets. *Nature Methods*, 18(7), 698–700. <https://doi.org/10.1038/s41592-021-01186-4>
- [9] Yeo, B. T. T. et al. (2011). The organization of the human cerebral cortex estimated by intrinsic functional connectivity. *Journal of Neurophysiology*, 106(3), 1125–1165. <https://doi.org/10.1152/jn.00338.2011>
- [10] Greenberg, D. M. et al. (2018). Testing the Empathizing-Systemizing theory of sex differences and the Extreme Male Brain theory of autism in half a million people. *Proceedings of the National Academy of Sciences of the United States of America*, 115(48), 12152–12157. <https://doi.org/10.1073/pnas.1811032115>

Integrated Effective Connectivity Reveals Mesulam's Cortical Hierarchy in the Human Brain

Younghyun Oh^{1,2,3}, Yejin Ann^{1,4}, Takuya Ito⁵, Sean Froudist-Walsh⁶, Boris Bernhardt⁷, Casey Paquola⁸, Micahel Milham^{9,10}, Choong-Wan Woo^{1,2,3,4,*}, Seok-Jun Hong^{1,2,3,4,10*}

¹IBS Center for Neuroscience Imaging Research, Sungkyunkwan University, Suwon, South Korea, ²Department of Biomedical Engineering, Sungkyunkwan University, Suwon, South Korea, ³Life-inspired Neural networks for Prediction and Optimization (LNPO) Group, ⁴Department of Intelligence Precision Health Care, Sungkyunkwan University, Suwon, South Korea, ⁵T.J. Watson Research Center, IBM Research, Yorktown, NY, United States, ⁶Bristol Computational Neuroscience Unit, Faculty of Engineering, University of Bristol, Bristol, United Kingdom, ⁷McConnell Brain Imaging Centre, Montreal Neurological Institute and Hospital, McGill University, Montreal, QC, Canada, ⁸Institute of Neuroscience and Medicine, Forschungszentrum Jülich, Germany, ⁹Nathan S. Kline INstitute for Psychiatric Research, ¹⁰Center for the Developing Brain, Child Mind Institute, New York, NY, United States,

* Co-corresponding author

Seok-Jun Hong
hong.seok.jun@gmail.com
Choong-Wan Woo
choongwan.woo@gmail.com

Introduction. Identifying macro-scale directed functional flows between the brain regions, *i.e.* effective connectivity (EC), is key to understanding the emergence of our complex behaviors. However, reliable EC mapping remains as a daunting task, due to a lack of consensus across existing EC algorithms. This absence of methodological integration hinders a deeper investigation of neural dynamics along the brain architectures. Here, we sought to address these issues by introducing a new analytical framework, “integrated EC” (iEC), which combines the strengths of individual EC algorithms to create synergistic effects on sensitivity and reliability. Our framework revealed distinct connectome profiles across large-scale cortical hierarchy, demonstrating the utility of iEC as a robust tool for network neuroscience.

Methods. To implement the iEC framework, we first selected the major EC algorithms based on their mathematical uniqueness (**Fig 1a**). The iEC was then obtained by linear combination of the individual algorithms via Bayesian optimization (**Fig 1b**). We validated the inferred EC by assessing whether it could recover a FC pattern from rs-fMRI (**Fig 1e**). Next, we investigated the connectome profile, signal flows, and functional hierarchy using iEC to elucidate the organization of the human brain. For connectome profile, we assessed in-/out-degree and computed the ratio of their positive/negative connections. We further mapped the signal flow along the iEC by solving an equation ‘ $x(t) = e^{At}x_0$ ’, where x_0 is a binary vector initialized with ones at seed brain regions and A is a the iEC matrix. Finally. the cortical hierarchy was determined based on the established method¹, which involved conducting a general linear model in the form $g(E[EC_{ij}]) = \theta_i - \theta_j$, with θ_i representing the hierarchical level of brain region *i*.

Results. Prior to implementing the iEC framework, we first assessed face validity of EC algorithms using Hopf model² based on the ground-truth directed connectivity (**Fig 1c**). Across different network resolutions, iEC showed a superior performance over individual algorithms, showing mean correlation values of 0.82 and 0.41 with ground-truth networks of 50 and 180 nodes, respectively (**Fig 1d**). This validity was confirmed by a subsequent analysis based on experimental rs-fMRI data, in which we recovered FC from EC and tested the model fit between simulated and empirical FCs (**Fig 1e**). Again, the iEC showed better FC recovery compared to individual algorithms (**Fig 1f**; model fit $r=0.83$, **Fig 1h**), with a notable improvement by the inclusion of negative connections (**Fig 1g**). The connectome profile of iEC showed two distinct network characteristics (**Fig 2a, b**): *i*) generally higher in/out-degree in the default mode network (DMN) and *ii*) a clear positive-negative connection ratio along the sensory-fugal axis. This distinct topology informs the observed signal propagation pattern (**Fig 2c, d**): Positive signals predominantly originated from lower sensory regions, whereas negative signals propagated mostly from the higher association areas. Building on these findings, we posited that the positive/negative connections might correspond with feedforward/feedback connections, respectively, enabling us to deduce a cortical hierarchy from the discerned iEC. (**Fig 2e**). Our hierarchy map diverged from the established principal gradient⁴, particularly by positioning interoceptive regions at the top of hierarchy, instead of DMN (**Fig 2f-g**), which fully reflects the original concept of cortical diagram proposed by Mesulam⁴ (**Fig 2h**).

Conclusions. Our proposed iEC method is designed to resolve the bottleneck that the current neuroimaging has suffered in terms of connectome directionality inference. By integrating existing methods, we have enhanced both accuracy and validity of EC mapping, which we believe the two key factors in uncovering novel principles of the human brain organization.

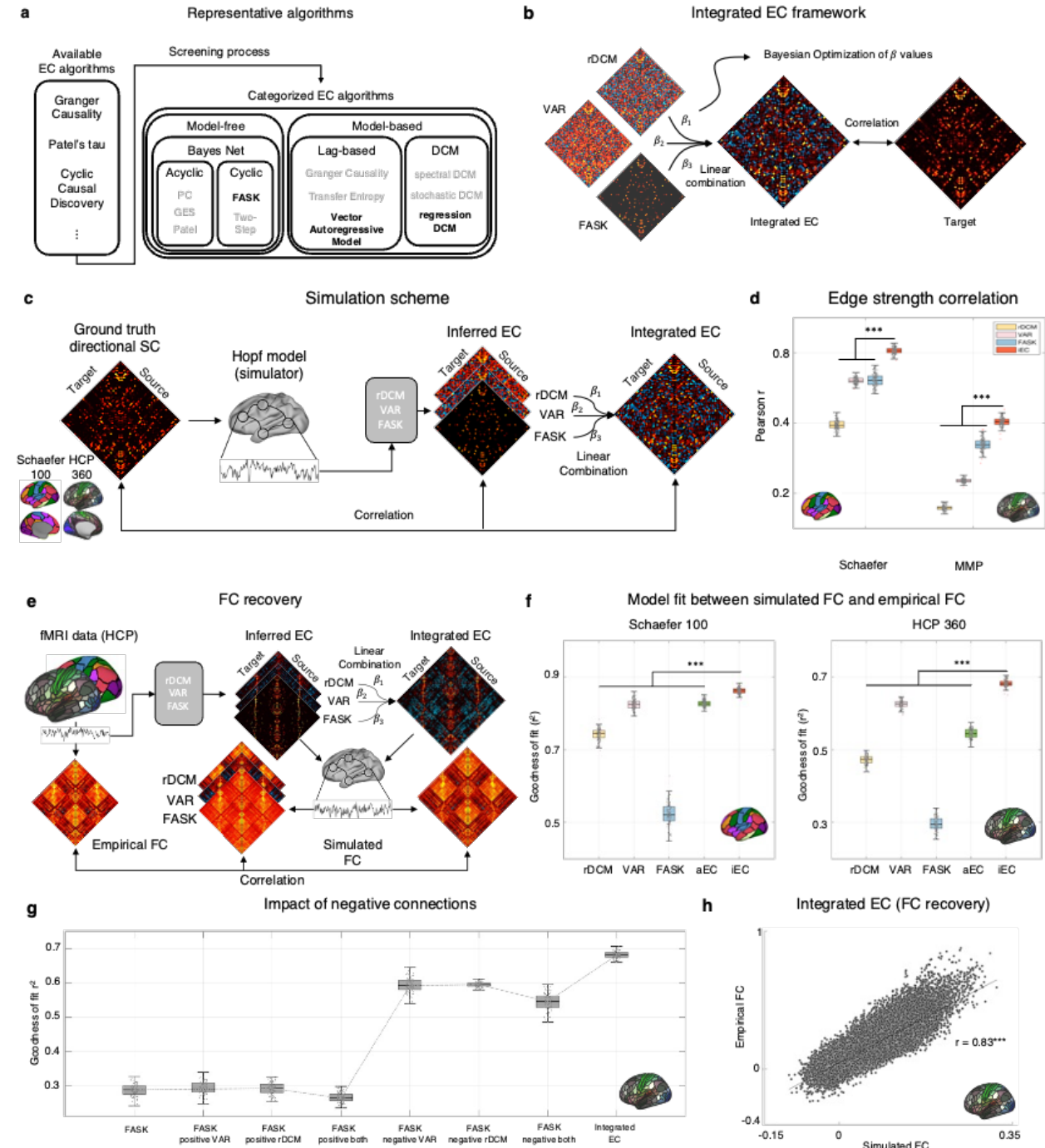
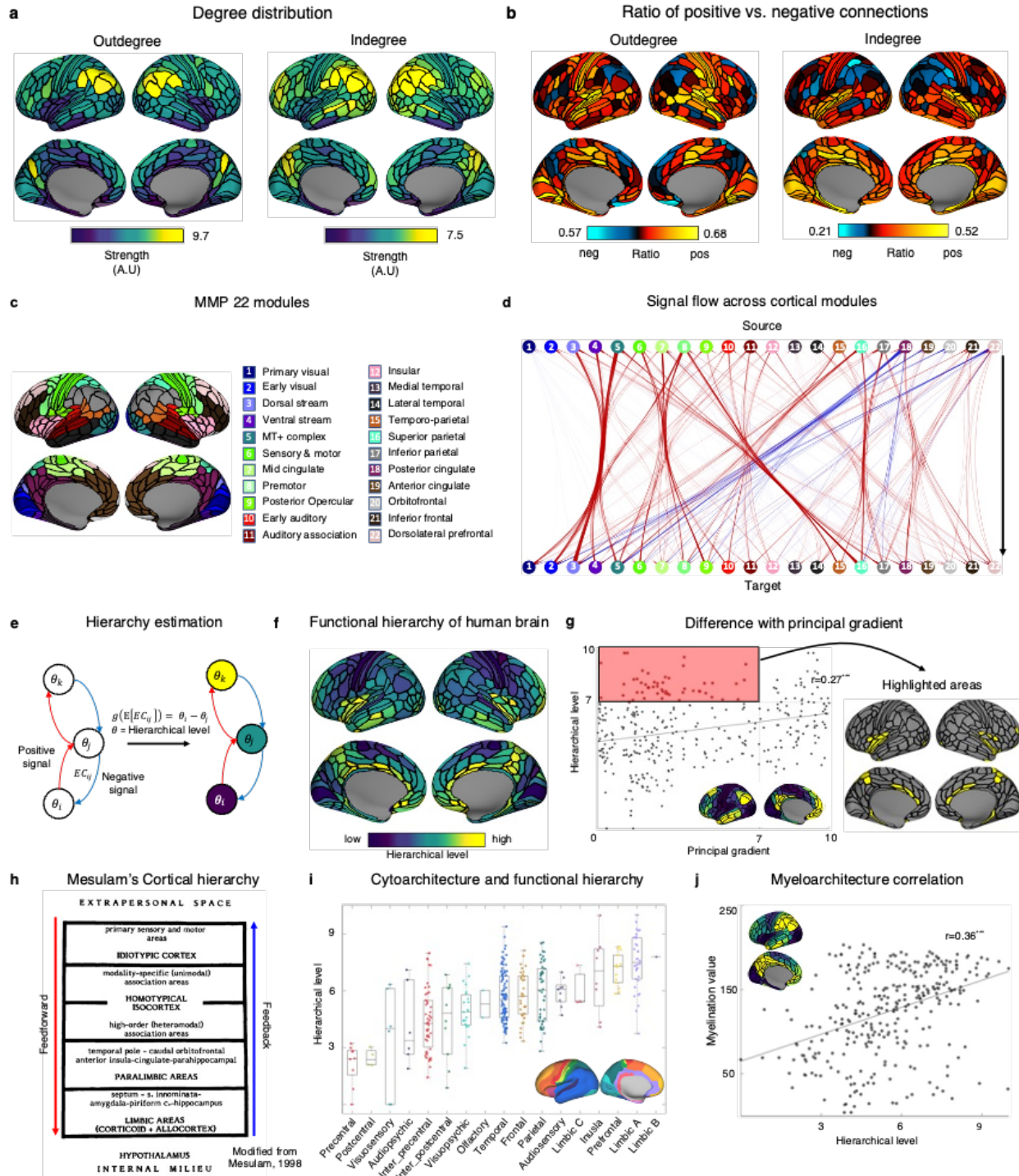
Figure 1

Figure 2

References

1. Markov, N. T. *et al.* Anatomy of hierarchy: feedforward and feedback pathways in macaque visual cortex. *J. Comp. Neurol.* **522**, 225–259 (2014).
2. Deco, G., Krriegelbach, M. L., Jirsa, V. K. & Ritter, P. The dynamics of resting fluctuations in the brain: metastability and its dynamical cortical core. *Sci. Rep.* **7**, 3095 (2017).
3. Margulies, D. S. *et al.* Situating the default-mode network along a principal gradient of macroscale cortical organization. *Proc. Natl. Acad. Sci. U. S. A.* **113**, 12574–12579 (2016).
4. Mesulam, M. M. From sensation to cognition. *Brain* **121** (Pt 6), 1013–1052 (1998).

Organizational principles of semantic control in the human brain

Kaixiang Zhuang¹, Xinyu Liang¹, Cheng Liu², Theodoros Karapanagiotidis³, Jonathan Smallwood⁴, Elizabeth Jefferies⁵, Deniz Vatansever¹

¹*Institute of Science and Technology for Brain-Inspired Intelligence, Fudan University, Shanghai, China*

²*Faculty of Psychology, Southwest University, Chongqing, China*

³*School of Psychology, University of Sussex, Sussex, UK*

⁴*Department of Psychology, Queen's University, Ontario, Canada*

⁵*Department of Psychology, University of York, York, UK*

Introduction: The human semantic system affords a multi-dimensional conceptual space through which we ascribe meaning to various words and objects around us. Notably, accessing concepts that are more remotely connected in this space is suggested to require higher levels of demand for semantic control [1]. However, the precise neural signature of semantic control, and its distributed organization within the cortical hierarchy remains unclear. By combining an fMRI-based semantic retrieval task [2], a natural language processing model [3] and multivoxel pattern analysis (MVPA) [4], here we captured a neural signature associated with varying demands for semantic control and charted its distribution within the cortical connectivity gradients [5]. We demonstrate that semantic control requires the engagement of multiple brain networks, dispersed along two principal gradients relevant to different aspects of semantic processing. This offers new insights into how the brain's functional networks are architecturally specialized to support semantic cognition.

Methods: A group of 46 healthy young adults (mean = 21.31 years old, 21/25 Word List A to B ratio) completed a 3-alternative forced choice semantic retrieval fMRI task, in which they were probed with a cue word and asked to select the most conceptually associated target word amongst two other distractors across 80 trials. Crucially in each trial, semantic distance between word pairs, defined by the cosine distance within 300-dimensional GloVe vectors, were used to systematically manipulate the demand for semantic control (Fig. 1a-b). Next, we employed thresholded partial least squares T-PLS [6] and GLMsingle derived single-trial beta maps [7] to identify a whole-brain multivariate signature of semantic control (Fig. 1c), which served as a predictive model for semantic distance during semantic retrieval. After a series of rigorous assessments, the feature weights of semantic control signature were projected onto a continuous 2D space of functional connectivity gradients in order to characterize its organizational principles within the large-scale cortical hierarchy.

Results: The identified neural signature of semantic control spanned areas sensitive to both high and low-demand semantic decisions (e.g. left IFG, pMTG, mPFC, PCC), as well as bilateral anterior insula and primary visual cortices (Fig. 1c). In addition to demonstrating high accuracy and generalizability (Fig. 1d-e), the semantic control signature distinguished subtle differences between word pairs (Fig. 1f), and accurately captured the response speed of participants during semantic retrieval (Fig. 1g). Furthermore, the identified semantic control signature exhibited spatial correlations with two out of 10 principal

gradients (Fig. 2a). Specifically, we observed clear boundaries in the 2D space constituted by Gradients 6 and 10, which demarcated positive and negative feature weights of the neural signature (Fig. 2b). Based on the NeuroSynth meta-analytic decoding, we further revealed that both gradients were closely related to semantic cognition (Fig. 2c). While Gradient 6 arranged brain regions in a cognitive continuum from “low to high demand semantic cognition”, Gradient 10 arranged brain regions from “verbal to visual semantic cognition”.

Conclusions: Based on a semantic retrieval task and machine learning approach, we revealed a robust and generalizable neural signature sensitive to varying levels of semantic control demands. Notably, the identified signature was constrained by two functional connectivity gradients, both of which related to different aspects of semantic cognition. Together, our findings demonstrate how disparate regions within the cortical organization unite within a lower dimensional space to facilitate the control of semantic cognition.

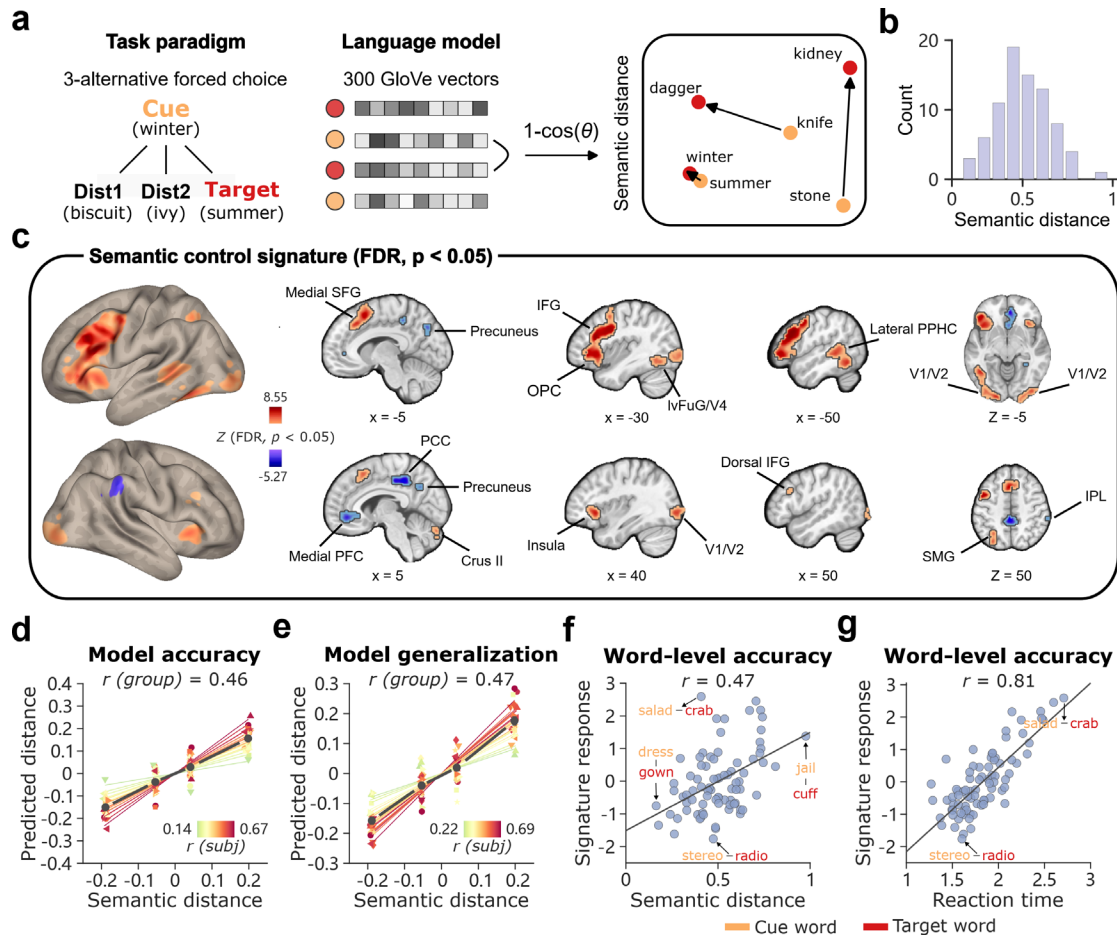


Figure 1. Experimental procedure and model evaluation. (a) Experimental procedure. A group of healthy young adult participants took part in an fMRI session designed to probe semantic memory retrieval utilizing a 3-alternative forced choice (3-AFC) paradigm. T-PLS was employed to identify a whole-brain neural signature of semantic control. (b) Distribution of semantic distance. 300 dimensional GloVe word vectors were employed to quantify semantic distance between the cue and target word pairs. (c) Semantic control signature. The map was thresholded using a 5,000-sample bootstrap procedure at FDR $p < 0.05$. (d) Evaluation of model accuracy. Subject-level prediction-outcome correlation: $r = 0.46 \pm 0.12 \text{ SE}$; group-level prediction-outcome correlation: $r = 0.46$. (e) Evaluation of model generalizability. Subject-level prediction-outcome correlation: $r = 0.48 \pm 0.09 \text{ SE}$ in the generalization of A-to-B; group-level prediction-outcome correlation: $r = 0.47$ in A-to-B. (f) Word level prediction for semantic distance. The identified neural signature was used to predict semantic distance between word pairs. The beta maps corresponding to each word pair were averaged across all trials. Correlation between signature response and semantic distance: $r = 0.47$. (g) Word level prediction of reaction time (RT). The identified neural signature was used to distinguish the differences in RT between word pairs. The beta maps and RTs corresponding to each word pair were averaged across all trials. Correlation between signature response and RTs: $r = 0.81$.

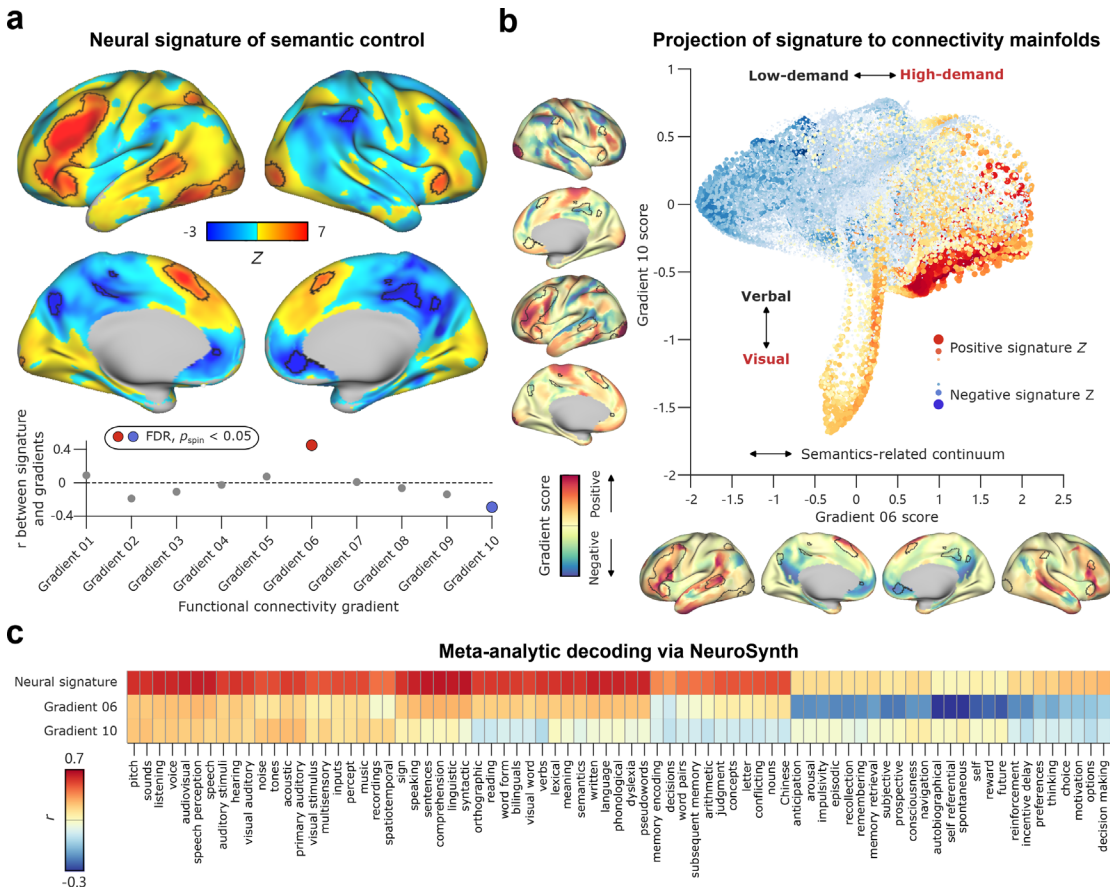


Figure 2. Neural signature for semantic control projected to low-dimensional cortical connectivity gradients. (a) Relationship between semantic control signature and functional connectivity gradients. The ‘spin’-based method was used to correct the p values for potential confounding effects of spatial autocorrelation. $r = 0.45$ for gradient 0.6, $r = -0.29$ for gradient 1.0, FDR, $p_{\text{spin}} < 0.001$. (b) Projection of semantic control signature onto the specific 2D gradient space. Gradient scores were adjusted according to the correlation direction of each gradient with the semantic control signature. (c) Distribution of correlation coefficients for the three brain patterns of interest in the NeuroSynth feature matrix. Top 30 cognitive terms (features) from the NeuroSynth database are displayed for both the positive and negative extrema of each brain pattern.

References:

- [1] Ralph, M. A. L., Jefferies, E., Patterson, K., & Rogers, T. T. (2017). The neural and computational bases of semantic cognition. *Nature reviews neuroscience*, 18(1), 42-55.
- [2] Vatansever, D., Smallwood, J., & Jefferies, E. (2021). Varying demands for cognitive control reveals shared neural processes supporting semantic and episodic memory retrieval. *Nature communications*, 12(1), 2134.
- [3] Pennington, J., Socher, R., & Manning, C. D. (2014). Glove: Global vectors for word representation. In Proceedings of the 2014 conference on empirical methods in natural language processing (EMNLP)
- [4] Spisak, T., Bingel, U., & Wager, T. D. (2023). Multivariate BWAS can be replicable with moderate sample sizes. *Nature*, 615(7951), E4-E7.
- [5] Citation: Lee, S., Bradlow, E. T., & Kable, J. W. (2022). Fast construction of interpretable whole-brain decoders. *Cell Reports Methods*, 100227.
- [6] Mars, R. B., Passingham, R. E., & Jbabdi, S. (2018). Connectivity fingerprints: from areal descriptions to abstract spaces. *Trends in cognitive sciences*, 22(11), 1026-1037.
- [7] Prince, J. S., Charest, I., Kurzawski, J. W., Pyles, J. A., Tarr, M. J., & Kay, K. N. (2022). Improving the accuracy of single-trial fMRI response estimates using GLMsingle. *Elife*, 11, e77599.

Title: Reproducible Gradients of Microstructural Development along White Matter Tracts in Youth

Authors: Audrey C. Luo, Valerie J. Sydnor, Joëlle Bagautdinova, Deanna M. Barch, Aaron Alexander-Bloch, Fengling Hu, Bart Larsen, Alex R. Franco, Marc Jaskir, Arielle S. Keller, Steven L. Meisler, Michael P. Milham, David R. Roalf, Ariel Rokem, Golia Shafiei, Russell T. Shinohara, Jason Yeatman, Fang-Cheng Yeh, Matthew Cieslak, Theodore D. Satterthwaite

Introduction: White matter (WM) undergoes protracted microstructural changes in youth that refine communication between spatially distributed cortical regions critical for complex behavior. Post-mortem human and animal studies have shown posterior-to-anterior, inferior-to-superior, and central-to-peripheral maturational patterns of myelination. Work in animals has also revealed variation in myelin sheath thickness along an axon, which can profoundly impact neural transmission. However, the few human neuroimaging studies that have examined developmental variation along WM tracts are limited by small sample sizes and lack of a clear biological framework to interpret such variation. We propose that within-tract variation in developmental change is linked to the distinct roles of different parts of a tract, which come together to facilitate neural transmission. Here, we used two large-scale neuroimaging datasets (total N=1,786) to test the hypothesis that maturation of WM progresses systematically along tracts, with gradients of development reflecting adaptations that optimize neural communication between cortical regions.

Methods: We used diffusion MRI data from the Human Connectome Project: Development (HCP-D; N=569; ages 8-22) and Healthy Brain Network (HBN; N=1217; ages 5-22). All images were processed using *QSIPrep* 0.19.1. The *QSIPrep* reconstruction workflow included multi-tissue constrained spherical deconvolution and tractography using *MRtrix3*, followed by segmenting 22 major WM tracts using PyAFQ. Mean diffusivity (MD), which may be more sensitive to age-related changes than fractional anisotropy in this age window, was measured at 100 equidistant nodes along each tract. To model linear and non-linear associations between age and MD at each node, we fit generalized additive models, with age as a smooth term and sex and in-scanner motion as covariates. The age effect at each node was quantified by the change in adjusted R² between a full model and reduced model with no age term. The relationship between age effect and position along a tract was evaluated using Pearson correlations.

Results: WM microstructure markedly varied along each tract, with portions of tracts deeper in WM having significantly lower MD than portions of each tract closer to tract endpoints. Though tract-averaged MD displayed overall decreases with age, we observed graded developmental changes within tracts. The magnitude of age effects showed a strong correlation with the relative position of a given node within its tract, indicating greater age-related decreases in MD closer to tract endpoints. This deep-to-superficial gradient of development was consistent across datasets

in 18 total cortico-cortical tracts including bilateral arcuate fasciculus (HCPD: $r=0.90$, $p_{FDR}<0.0001$; HBN: $r=0.84$, $p_{FDR}<0.0001$), bilateral inferior longitudinal fasciculus (HCPD: $r=0.59$, $p_{FDR}<0.0001$; HBN: $r=0.81$, $p_{FDR}<0.0001$), bilateral superior longitudinal fasciculus (HCPD: $r=0.84$, $p_{FDR}<0.0001$; HBN: $r=0.96$, $p_{FDR}<0.0001$), and forceps minor (HCPD: $r=0.80$, $p_{FDR}<0.0001$; HBN: $r=0.91$, $p_{FDR}<0.0001$), with a mean correlation of 0.63 in HCP-D and 0.78 in HBN. Lastly, age effects increased from inferior to superior regions of bilateral corticospinal tract (HCPD: $r=0.72$, $p_{FDR}<0.0001$; HBN: $r=0.35$, $p_{FDR}<0.0001$).

Discussion:

To our knowledge, this is the largest study of maturation along WM tracts from childhood to young adulthood. We delineate reproducible deep-to-superficial and inferior-to-superior gradients of WM development in two independent datasets. Deeper tract regions may myelinate earlier to reduce interference from crossing tracts carrying distinct neuronal signals, while regions near cortex may dynamically interact with cortical development. Further analyses are necessary to investigate these hypotheses and to characterize the link between WM development and psychopathology. This work establishes the importance of studying spatial variation along WM tracts in understanding brain development and function.

Changes in structural connectome manifolds in patients with episodic migraine

Eunchan Noh¹, Jong Young Namgung², Yeongjun Park³, Yurim Jang⁴, Mi Ji Lee^{5*}, and Bo-yong Park^{2,4,6*}

¹ College of Medicine, Inha University, Incheon, Republic of Korea

² Department of Data Science, Inha University, Incheon, Republic of Korea

³ Department of Electrical and Computer Engineering, Sungkyunkwan University, Suwon, Republic of Korea

⁴ Department of Statistics and Data Science, Inha University, Incheon, Republic of Korea

⁵ Department of Neurology, Seoul National University Hospital, Seoul National University College of Medicine, Seoul, Republic of Korea

⁶ Center for Neuroscience Imaging Research, Institute for Basic Science, Suwon, Republic of Korea

<Objectives>

Migraine is a neurological disease characterized by recurrent headaches [1], and neuroimaging studies have found significant alterations in connectivity in patients with migraine. Gradient analysis has recently been introduced to investigate whole-brain connectome organization with multiple low-dimensional representations [2, 3]. In this study, we aimed to assess whole-brain structural connectome changes in patients with episodic migraine using gradient analysis.

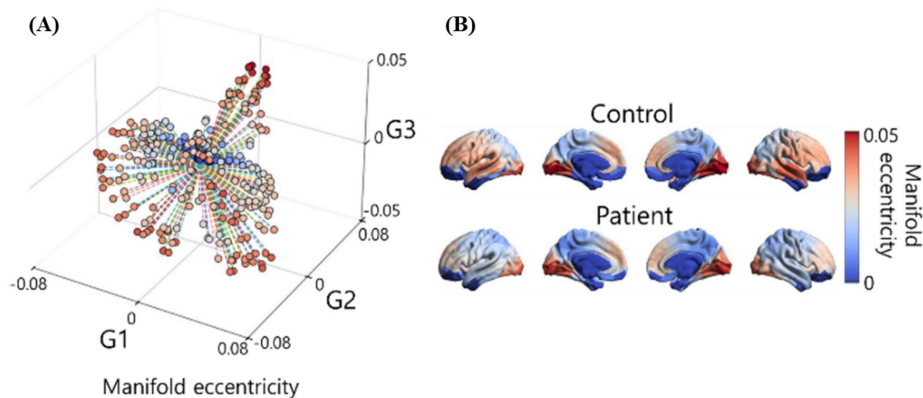


Fig. 1. Schema of manifold eccentricity. (A) The manifold eccentricity is defined by calculating the Euclidean distance between each data point and the center of the data in a three-dimensional manifold space consisting of three gradients (G1, G2, and G3). (B) Group-averaged manifold eccentricity of control and patient groups.

<Methods>

We obtained T1-weighted and diffusion MRI of 47 patients with migraine (age = 34.3 ± 8.3 , 74.5% female) and 41 healthy controls (age = 35.2 ± 7.7 , 75.6% female). T1-weighted data were preprocessed with the fusion of neuroimaging preprocessing (FuNP) surface-based pipeline [4], and diffusion MRI data were preprocessed with MRtrix3 [5]. Neuronal streamlines were estimated using probabilistic tractography, and the structural connectivity matrix was generated based on the sub-parcellation of the Desikan-Killiany atlas with 300 cortical regions [6]. We applied a nonlinear dimensionality reduction technique to the connectivity matrix to estimate gradients. The individual gradients were aligned to a template gradient calculated from the group representative connectivity matrix constructed using distance-dependent thresholding [7]. We calculated manifold eccentricity, the Euclidean distance between each data point and the center of the data in the low-dimensional manifold space [8] (Fig. 1). Comparisons of manifold eccentricity between patients with migraine and healthy controls were conducted using 10,000 permutation tests, controlling for age and sex. Multiple comparisons across brain regions were corrected using a false discovery rate (FDR). Additionally, we assessed shifts in subcortical connectivity in patients with migraine using the degree values of subcortico-cortical connectivity.

<Results>

The orbitofrontal cortex, temporal pole, and somatomotor regions showed significant shifts in manifold eccentricity in patients with migraine (**Fig. 2A**). With summarization of statistics according to seven functional networks and four cortical hierarchical levels, the largest effect was observed in the limbic areas. The caudate, amygdala, and accumbens showed significant between-group differences in the subcortico-cortical connectivity (**Fig. 2B**).

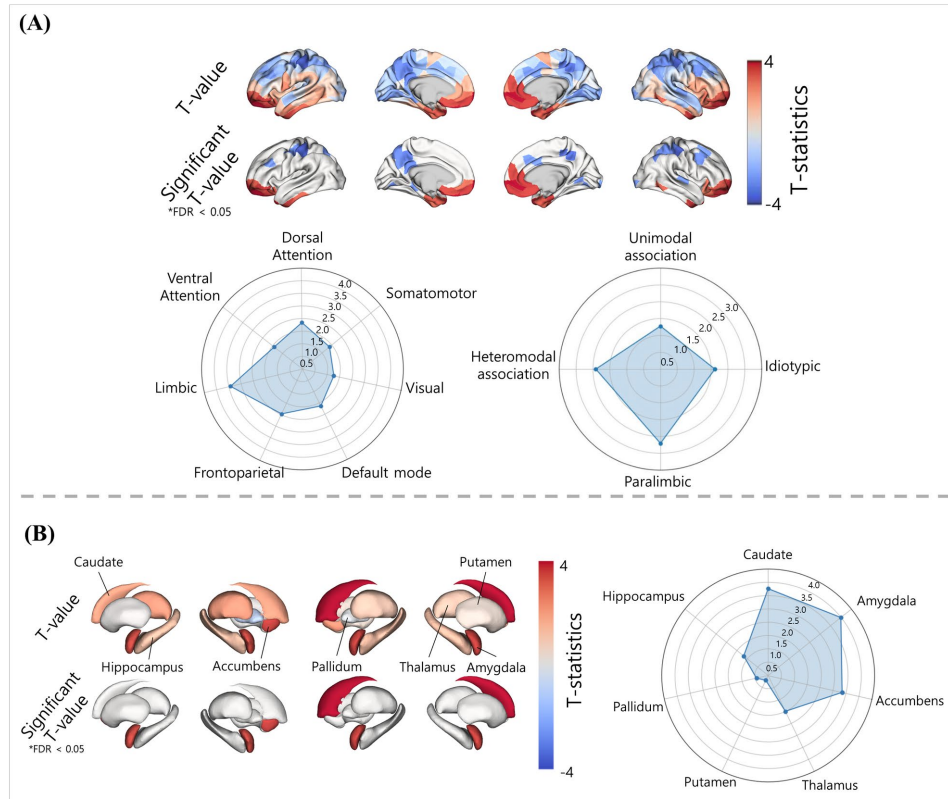


Fig. 2. Between-group differences in manifold eccentricity and subcortico-cortical connectivities. (A) T-statistics of the whole brain and the regions that showed significant effects are shown on the brain surfaces. The t-statistics were summarized according to functional networks and cortical hierarchical levels. (B) Between-group differences in subcortico-cortical degree values. FDR, false discovery rate.

<Conclusion>

Our results may contribute to a deeper understanding of structural connectome changes in patients with migraine, potentially aiding in developing migraine diagnostic or prognostic models.

<Acknowledgements>

This research was supported by the National Research Foundation of Korea (NRF-2020R1A2B5B01001826; NRF-2022R1A5A7033499), Institute for Information and Communications Technology Planning and Evaluation (IITP) funded by the Korea Government (MSIT) (No. 2022-0-00448, Deep Total Recall: Continuous Learning for Human-Like Recall of Artificial Neural Networks; No. RS-2022-00155915, Artificial Intelligence Convergence Innovation Human Resources Development (Inha University); No. 2021-0-02068, Artificial Intelligence

Innovation Hub), Institute for Basic Science (IBS-R015-D1), and the Korea Medical Device Development Fund grant funded by the Korean government (the Ministry of Science and ICT, the Ministry of Trade, Industry and Energy, the Ministry of Health & Welfare, the Ministry of Food and Drug Safety) (Project number: RS-2023-00229484).

<References>

1. Walter K (2022) What Is Migraine? *JAMA* 327:93. <https://doi.org/10.1001/jama.2021.21857>
2. Margulies DS, Ghosh SS, Goulas A, et al (2016) Situating the default-mode network along a principal gradient of macroscale cortical organization. *Proceedings of the National Academy of Sciences* 113:12574–12579
3. Vos de Wael R, Benkarim O, Paquola C, et al (2020) BrainSpace: a toolbox for the analysis of macroscale gradients in neuroimaging and connectomics datasets. *Commun Biol* 3:103. <https://doi.org/10.1038/s42003-020-0794-7>
4. Park B, Byeon K, Park H (2019) FuNP (Fusion of Neuroimaging Preprocessing) Pipelines: A Fully Automated Preprocessing Software for Functional Magnetic Resonance Imaging. *Front Neuroinform* 13:
5. Tournier J-D, Smith R, Raffelt D, et al (2019) MRtrix3: A fast, flexible and open software framework for medical image processing and visualisation. *Neuroimage* 202:116137. <https://doi.org/https://doi.org/10.1016/j.neuroimage.2019.116137>
6. Desikan RS, Ségonne F, Fischl B, et al (2006) An automated labeling system for subdividing the human cerebral cortex on MRI scans into gyral based regions of interest. *Neuroimage* 31:968–980. <https://doi.org/https://doi.org/10.1016/j.neuroimage.2006.01.021>
7. Betzel RF, Griffa A, Hagmann P, Mišić B (2019) Distance-dependent consensus thresholds for generating group-representative structural brain networks. *Network Neuroscience* 3:475–496. https://doi.org/10.1162/netn_a_00075
8. Park B, Bethlehem RAI, Paquola C, et al (2021) An expanding manifold in transmodal regions characterizes adolescent reconfiguration of structural connectome organization. *Elife* 10:e64694. <https://doi.org/10.7554/eLife.64694>

Title: Characterizing the developmental trajectory of functional hierarchy in autism

Authors: Jong-eun Lee, Hyunjin Park

Abstract:

Autism is a neurodevelopmental disorder marked by a wide range of symptoms among patients. The coexistence of high-level social impairments and low-level sensory symptoms in autism complicates the understanding of its neural mechanisms. The functional connectome gradient, which places unimodal sensory networks at one end and the transmodal default mode network (DMN) at the other, has been suggested to explain system-level abnormalities in autism, emphasizing disruptions in functional hierarchy. Since hierarchical brain systems undergo maturation during youth, it is essential to examine age-dependent developmental effects on the functional gradient. However, the manifestation of developmental changes in the functional gradient and the abnormal trajectories in autism remain largely unknown. In this study, we used a normative modeling approach to estimate the developmental trajectories of the functional gradient. We discovered that the macroscale segregation between sensory networks and the DMN becomes more pronounced with age in typically developing individuals, while this diverging pattern is weakened in autism, particularly in the DMN. Furthermore, we observed more significant differences in the functional gradient when considering developmental effects compared to group comparisons that did not account for these effects. Our findings offer new insights into the development of autism, highlighting its atypical functional hierarchical system.

Title : Comparison of different group-level templates in gradient-based multimodal connectivity analysis

Authors: Sunghun Kim, Hyunjin Park

Abstract:

The study of large-scale brain connectivity is increasingly adopting unsupervised approaches that derive low-dimensional spatial representations from high-dimensional connectomes, referred to as gradient analysis. When translating this approach to study interindividual variations in connectivity, one technical issue pertains to the selection of an appropriate group-level template to which individual gradients are aligned. Here, we compared different group-level template construction strategies using functional and structural connectome data from neurotypical controls and individuals with autism spectrum disorder (ASD) to identify between-group differences. We studied multimodal magnetic resonance imaging data obtained from the Autism Brain Imaging Data Exchange (ABIDE) Initiative II and the Human Connectome Project (HCP). We designed six template construction strategies that varied in whether: (1) they included typical controls in addition to ASD; or (2) they mapped from one dataset onto another. We found that aligning a combined subject template of the ASD and control subjects from the ABIDE Initiative onto the HCP template exhibited the most pronounced effect size. This strategy showed robust identification of ASD-related brain regions for both functional and structural gradients across different study settings. Replicating the findings on focal epilepsy demonstrated the generalizability of our approach. Our findings will contribute to improving gradient-based connectivity research.

Changes in connectome gradient according to body mass index in manifold space

Yurim Jang¹, Eunchan Noh², Bo-yong Park ^{1,3,4}

Department of Statistics and Data Science, Inha University, Incheon, Korea¹

College of Medicine, Inha University, Incheon, Republic of Korea²

Department of Data Science, Inha University, Incheon, Korea³

Center for Neuroscience Imaging Research, Institute for Basic Science, Suwon, Korea⁴

Introduction:

Obesity is a prevalent condition worldwide[1] and is easily measured using the body mass index (BMI). Neuroimaging studies based on Magnetic Resonance Imaging (MRI) have revealed differences in brain morphology and inter-regional brain connections associated with BMI[2]. Here, we analyzed how the structural connectome organization changes according to BMI using a manifold learning approach and examined its relationship with eating behaviors.

Methods:

We obtained T1-weighted and diffusion MRI data of 283 participants (mean \pm standard deviation [SD] age = 38.32 ± 13.80 years; male: female = 102: 181) from the enhanced Nathan Kline Institute-Rockland Sample database[3]. T1-weighted data were processed using the fusion of neuroimaging preprocessing (FuNP), and diffusion MRI data were preprocessed using MRtrix3. Spherical-deconvolution informed filtering of tractograms (SIFT2) was applied to optimize the cross-section multipliers. The streamlines were reconstructed by mapping onto the Schaefer atlas with 200 parcels. We utilized the diffusion map embedding to estimate low-dimensional representations of the cortex-wide structural connectivity. We generated three eigenvectors and calculated gradient eccentricity, which is defined as the Euclidean distance between the manifold origin and all data points within the manifold space (Fig 1A-B)[4]. Additionally, we calculated gradient differentiation, which is defined as the Euclidean distance between different nodes within the manifold space (Fig 1C). We then associated BMI with gradient eccentricity and differentiation, respectively. Multiple comparisons across brain regions were corrected using the false discovery rate (FDR). To assess the communication mechanisms of the BMI-manifold association, we calculated search information and path transitivity. Search information quantifies the accessibility of paths connecting source nodes to target nodes within a network, measuring the amount of information needed to access the path[5]. Path transitivity measures the density of local detours along the given shortest path (Fig 2A)[6]. The search information and path transitivity between different networks were correlated with BMI. Finally, we associated the estimated three gradients with well-established self-assessment tools measuring eating behaviors, the Three-Factor Eating Questionnaire (TFEQ) and the Eating Disorder Examination Questionnaire (EDEQ), to assess whether the gradient features are linked to dietary habits. Specifically, we examined the associations between eating behavior scores and the gradient values of the brain regions, which showed significant associations between gradient eccentricity and BMI.

Results:

We found that individuals with high BMI show expansions of the gradient eccentricity in the dorsolateral prefrontal cortex (DLPFC) and dorsomedial prefrontal cortex (DMPFC) (Fig 1B). When we assessed the association between gradient differentiation and BMI, individuals with higher BMI exhibited greater differentiation within transmodal regions and between transmodal-sensory regions (Fig 1C). In other words, high BMI may be related to network segregation in the transmodal areas. For communication measures, we observed positive associations between search information and BMI between overall networks, except for the somatomotor and dorsal/ventral attention networks (Fig. 2B). The path transitivity showed negative associations, except for the ventral attention-limbic network (Fig. 2C). The findings indicate that higher BMI is generally linked to inefficient communication (Fig 2B). Finally, we found that the gradient values in the DLPFC/DMPFC were significantly associated with eating behaviors, particularly with the EDEQ subscales (EDEQ-E [eating concern]: $t=1.828$, $p=0.034$; EDEQ-S [shape concern]: $t=2.476$, $p=0.007$; and EDEQ-W [weight concern]: $t=2.922$, $p=0.002$ (Fig 3B).

Conclusions:

We investigated structural connectome organization associated with BMI using the gradient eccentricity and differentiation measures. We found that individuals with high BMI exhibit increased segregation of the DLPFC/DMPFC from other networks, which might be linked to inefficient communication mechanisms, and errant eating behaviors.

Funding:

National Research Foundation of Korea (NRF-2022R1A5A7033499), Institute for Information and Communications Technology Planning and Evaluation (IITP) funded by the Korea Government (MSIT) (No. 2022-0-00448, Deep Total Recall: Continual Learning for Human-Like Recall of Artificial Neural Networks; No. RS-2022-00155915, Artificial Intelligence Convergence Innovation Human Resources Development (Inha University); No. 2021-0-02068, Artificial Intelligence Innovation Hub), Institute for Basic Science (IBS-R015-D1).

Reference:

- [1] V. S. Malik, W. C. Willett, and F. B. Hu, “Global obesity: trends, risk factors and policy implications,” *Nat Rev Endocrinol*, vol. 9, no. 1, pp. 13–27, Jan. 2013, doi: 10.1038/nrendo.2012.199.
- [2] K. A. Carbone, K. M. Duraccio, A. Hedges-Muncy, K. A. Barnett, C. B. Kirwan, and C. D. Jensen, “White matter integrity disparities between normal-weight and overweight/obese adolescents: an automated fiber quantification tractography study,” *Brain Imaging Behav*, vol. 14, no. 1, pp. 308–319, Feb. 2020, doi: 10.1007/s11682-019-00036-4.
- [3] K. B. Noonan *et al.*, “The NCI-Rockland Sample: A Model for Accelerating the Pace of Discovery Science in Psychiatry,” *Front Neurosci*, vol. 6, 2012, doi: 10.3389/fnins.2012.00152.
- [4] B. Park *et al.*, “An expanding manifold in transmodal regions characterizes adolescent reconfiguration of structural connectome organization,” *eLife*, vol. 10, Mar. 2021, doi: 10.7554/eLife.64694.

- [5] K. Sneppen, A. Trusina, and M. Rosvall, “Hide-and-seek on complex networks,” *Europhysics Letters (EPL)*, vol. 69, no. 5, pp. 853–859, Mar. 2005, doi: 10.1209/epl/i2004-10422-0.
- [6] M. D. E. Conder and C. E. Praeger, “Remarks on Path-transitivity in Finite Graphs,” *European Journal of Combinatorics*, vol. 17, no. 4, pp. 371–378, May 1996, doi: 10.1006/eujc.1996.0030.

Figure:

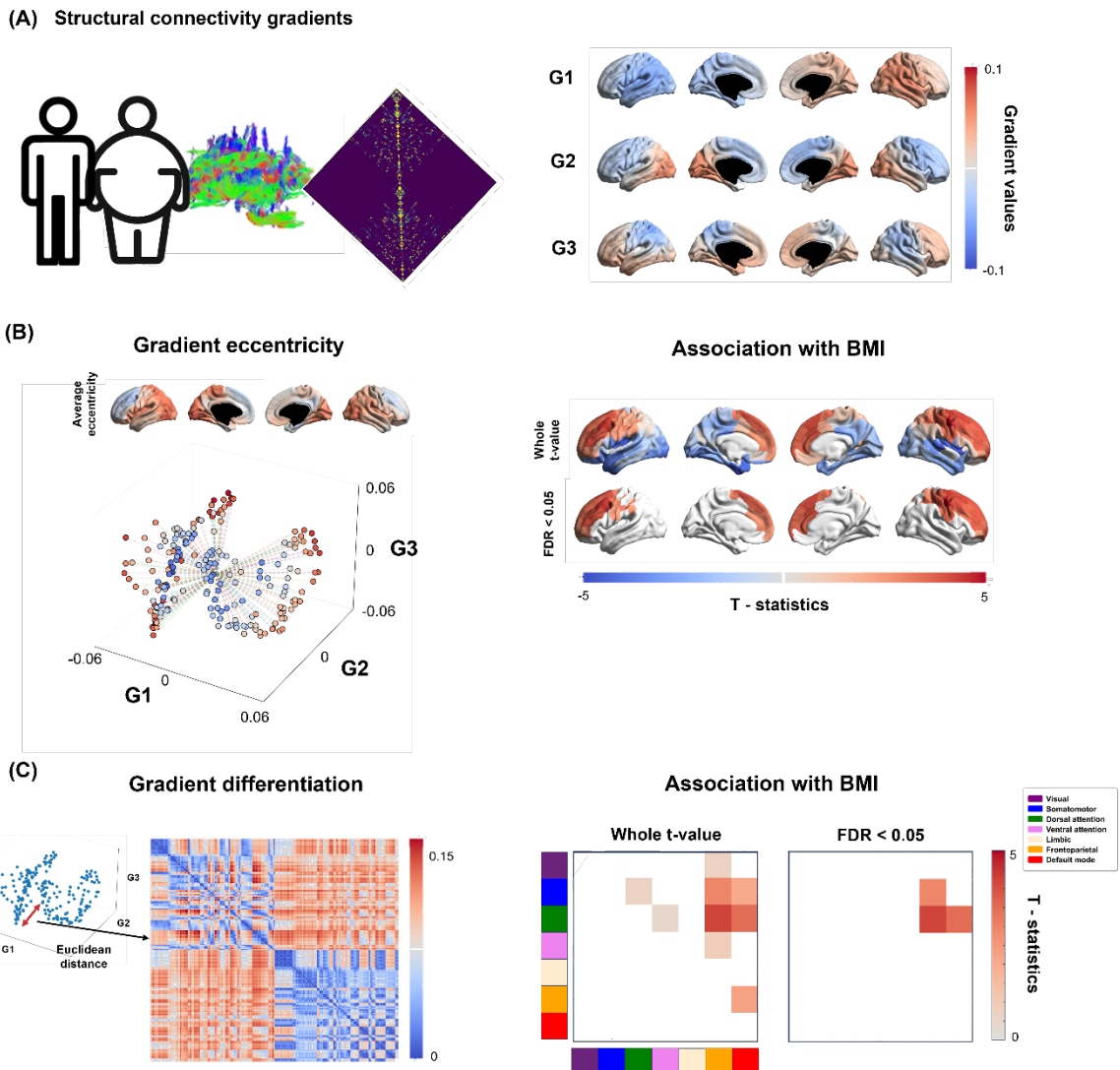


Figure 1 Manifold learning based on gradient eccentricity and differentiation. (A) A schema of obesity and structural connectivity is shown (left). Structural gradients are generated and visualized on brain surfaces (right). (B) We calculated gradient eccentricity (left) and associated with body mass index (BMI) (right). (C) We analyzed the association between gradient differentiation (left) and BMI (right).

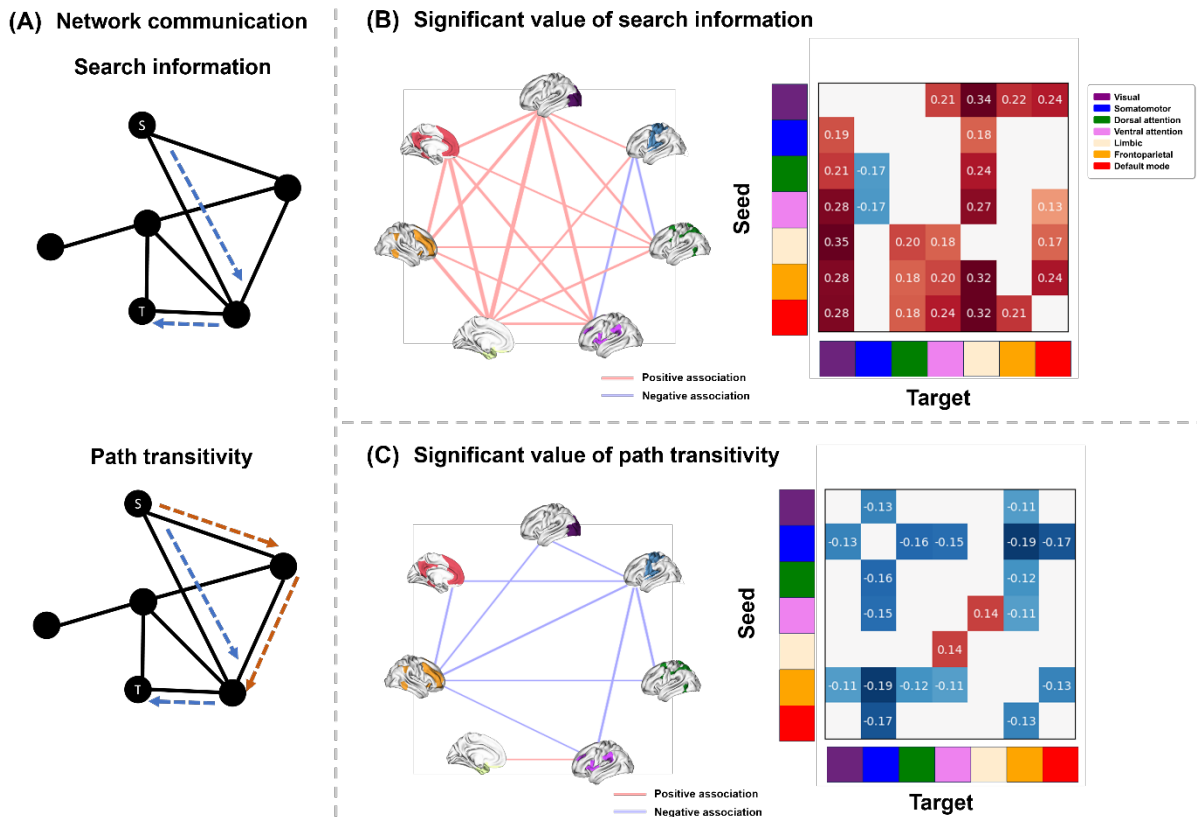


Figure 2 Association between network communication measures and body mass index.
 (A) A schema of brain network communication. (B) Significant correlations between BMI and search information or (C) path transitivity are shown in the spider plot and matrix.

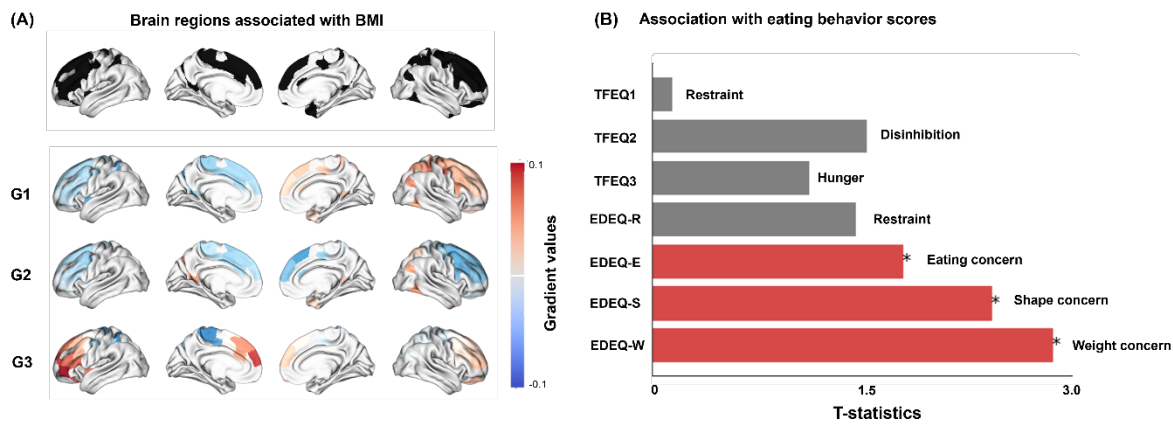


Figure 3 Eating behavior subtypes associated with gradients. (A) Three gradients of brain regions that showed significant association with body mass index. (B) The bar plot shows the association between the gradients and eating behaviors.

fMRI-based Encoding for Self-supervised Deep Predictive Coding in the Human Brain

Jungmin Lee^{1,2,3}, Sungwoo Lee^{1,2,3}, Sunghyoung Hong^{1,2},
Choongwan Woo^{1,2,3}, Seok Jun Hong^{1,2,3,4}

¹Center for Neuroscience Imaging Research, Institute for Basic Science, Suwon, South Korea,

²Department of Biomedical Engineering, Sungkyunkwan University, Suwon, South Korea, ³Life-inspired Neural networks for Prediction and Optimization (LNPO) Group, ⁴Center for the Developing Brain, Child Mind Institute, New York, NY, United States

Introduction. The ability to anticipate future outcomes is of utmost importance in human cognition. Predictive coding theory provides a parsimonious model for this phenomenon, conceptualizing the brain as a self-supervised hierarchical generative model minimizing prediction errors by reconciling top-down information with bottom-up sensory input. Despite its significance, the neuroscientific evidence supporting this theory remains scarce, especially at the whole-brain level. Here, we employed ‘PredNet’, a predictive coding-inspired deep learning model, and correlated its temporal activation with movie-watching fMRI in order to explore the representation of prediction and prediction error across the human brain.

Methods. The model was trained on a 3-hour movie, ‘Titanic’, and subsequently tested on a 2-hour movie, ‘ForrestGump’. The fMRI data of this test movie was obtained from StudyForrest, an open source repository providing audio-visual movie watching fMRI data from 15 subjects. For the next-frame video prediction task, we employed PredNet, a convLSTM model with four hierarchical layers, each containing four computational units: \mathbf{R} (representation), \mathbf{Ahat} (prediction), \mathbf{A} (input), \mathbf{E} (error). Features from both prediction and prediction error units were extracted for voxel-wise encoding. Principal component analysis (PCA) was applied to this feature matrix to preserve 90% of its variance, followed by hemodynamic response convolution of 4 seconds and down-sampling to the actual fMRI rate. The feature matrix was used to train an encoding model via ridge regression, ensuring a robust evaluation through 9-fold cross-validation. During training, we estimated regression coefficients (β), which were then used to predict BOLD signals. Finally, we correlated this signal with experimental fMRI data to assess the encoding performance.

Results. We identified the distinct patterns of PredNet-Brain correspondence for both prediction and prediction error across the whole brain. Specifically, the prediction exhibited a more pronounced correlation in the early visual areas (i.e. V1-4), with average encoding performance values of 0.05, 0.13, and 0.19 in accordance with the hierarchy of PredNet. In comparison, the prediction error exhibited a stronger performance across widespread brain areas, persisting even at the lowest PredNet layer, and showed a layerwise increase, with averaged encoding accuracy values of 0.26, 0.33, and 0.40. This implies that the computation of prediction error occurs on the whole-brain level, as sensory information is initiated for the processing and intensifies from the lower visual to higher dorsal attention networks. Subsequently, we focused on 8 regions of interest including V1-4, MT, and FFC, known for

their relevance to visual processing, to assess how each prediction and prediction error could be mapped along the PredNet layer orders. For further analysis, we also mapped β as a means to identify the most explanatory features of prediction and prediction error within the layer, and examined their dominance ratio. Notably, at layer 1, the prediction error initially showed a predominant pattern which, by layer 2, gradually shifted towards the prediction taking over the dominance. At the highest layer, both the prediction and prediction error displayed a comparatively balanced dominance ratio.

Conclusions. The study showed unique signal pathways for each prediction and prediction error across the macroscale network, revealing a dynamic processing shift. By demonstrating a proof-of-concept for the biological plausibility of predictive coding, our study provides an important avenue to comprehending the intricate dynamics of macroscale information processing in the human brain.

Transdiagnostic mapping of corticostriatal circuit for behavior and cognition in autism and ADHD

Han Byul Cho¹, Hyunhoe An^{1,2} Shinwon Park³, Seok-Jun Hong^{1,2,4,5}

1. Center for Neuroscience Imaging Research, Institute for Basic Science, Suwon, Republic of Korea
2. Department of Biomedical Engineering, Sungkyunkwan University, Suwon, Republic of Korea
3. Autism Center, Child Mind Institute, New York, United States
4. Life-inspired Neural network for Prediction and Optimization Research Group, Suwon, South Korea
5. Center for the Developing Brain, Child Mind Institute, New York, United States

Abstract

Autism spectrum disorder (ASD) and attention-deficit/hyperactivity disorder (ADHD) are the two highly comorbid developmental conditions that are characterized by heterogeneous behavioral phenotypes^{1,2}. Previous studies targeting both ASD and ADHD suggested that some of their behavioral symptoms are commonly linked to the altered function of the corticostriatal circuit—a core structure for executive function³⁻⁶. However, those studies mainly compared between case-control groups informed by clinically diagnosed labels, which leaves space for further exploration into the essence of 'transdiagnostic research'. Here, we address this issue by performing a fully dimensional approach, where we pool the data of all individuals with ASD or/and ADHD and comprehensively phenotype the relationship between their behavioral spectrum and corticostriatal functional connectivity (FC), regardless of their labels.

We analyzed the male-only data of 23 ASD, 111 ADHD, 61 comorbid ASD+ADHD and 35 neurotypical (NT) individuals derived from Healthy Brain Network⁷ (6-21 years). The two dimensionality reduction techniques were employed: 1) Factor analysis to identify the bases underlying common variance of behavioral symptoms across all subjects, 2) the Partial least squares (PLS) analysis to investigate the correlation between resting-state FC of corticostriatal circuits and behavior symptoms. We employed a permutation test (1,000 iterations) for the significance of the PLS analysis. Moreover, the composite scores from PLS were sorted out into three different bins (bottom 20%, middle 60%, top 20%) to quantitatively assess the gradual changes on this brain-behavior axis. After these analyses, we further performed ANOVA to identify the differences of factor scores and cognitive performance⁸ between the diagnostic labeled groups as well as between the three binned groups based on the PLS scores above.

Factor analysis identified four behavioral bases (i.e., 'social problems', 'impulsive behavior', 'emotional problems', and 'repetitive behavior'), each providing a component score across all individuals. The following PLS analysis revealed a significant association between these behavioral component scores and corticostriatal FC (permutation $p = 0.05$) across individuals, regardless of the diagnostic groups. We also checked the effect of diagnosis by extracting the PLS component scores

for both corticostriatal FC and behavior symptoms and comparing them between the clinically labeled groups including NT. In this analysis, the comorbid group showed the most negative PLS score, suggesting their severe symptoms and corticostriatal connectivity abnormalities. In the one-way ANOVA with clinical diagnosis as an independent variable, each behavior score in ASD and ADHD exhibited significant impairment compared to other groups. In particular, the ASD group showed a significantly lower score for cognitive flexibility, corroborating previous findings⁹. The same analysis based on the three binned groups revealed significant differences for the behavior scores. In the assessment of cognitive performance, however, the score showed only a trend of positive correlation, except for the working memory.

In this study, we found compelling evidence of a common biological axis that transgresses the boundaries of clinically diagnosed ASD, ADHD, and their comorbid groups. This axis revealed the spectrum of transdiagnostic pathogenicity on brain-behavior relationships as well as on cognitive performance, potentially indicating their shared developmental etiology and manifestation. Our findings can provide a novel insight to a neuroimaging-based disease modeling in the future RDoC research¹⁰.

References

1. Sinzig J et al., (2009) 'Attention deficit/hyperactivity disorder in children and adolescents with autism spectrum disorder' *Journal of Attention Disorders* 13(2):117-2
2. Simonoff E. et al., (2008) 'Psychiatric disorders in children with autism spectrum disorders: prevalence, comorbidity, and associated factors in a population-derived sample' *Journal of the American Academy of Child and Adolescent Psychiatry* 47, 921–929.
3. Di Martino A et al., (2011) 'Aberrant striatal functional connectivity in children with autism' *Biological Psychiatry* 69(9): 847–56.
4. Tomasi D et al., (2012) 'Abnormal functional connectivity in children with Attention-Deficit/Hyperactivity Disorder' *Biological Psychiatry* 71 (5): 443–50.
5. Uddin LQ, (2021) 'Cognitive and behavioural flexibility: neural mechanisms and clinical considerations' *Nature Reviews Neuroscience* 22(3): 167–79.
6. Westbrook A et al., (2021) 'A mosaic of cost-benefit control over cortico-striatal circuitry' *Trends in Cognitive Sciences* 25(8): 710–21.
7. Alexander LM et al., (2017) 'An open resource for transdiagnostic research in pediatric mental health and learning disorders' *Scientific data* 4, 170181
8. www.nihtoolbox.org
9. Cho HB et al., Transdiagnostic mapping of striatal connectivity and behavior-circuit modeling in autism and ADHD. Canada. 2023.07.22-26. OHBM 2023.
10. RDoC Matrix. <https://www.nimh.nih.gov/research/research-funded-by-nimh/rdoc/constructs/rdoc-matrix>

Hierarchical organization of intersubject correlations parallels functional gradients during naturalistic viewing

Meaghan Smith¹, Ahmad Samara¹, Jeffrey Eilbott³, Hallee Shearer², Tamara Vanderwal^{2,3*}, Boris Bernhardt^{1*}

¹ McGill University, Montreal, Quebec, ²University of British Columbia, Vancouver, British Columbia, ³BC Children's Hospital Research Institute, Vancouver, British Columbia

*joint senior authors

Despite approaching BOLD-signal time-courses from different perspectives and with different analyses, both functional connectivity (FC) gradients and intersubject correlations (ISCs) appear to capture core features of functional architecture (1, 2). By examining the relationship between these two measures, we might better understand what each analytical technique reveals about functional brain organization. Here, we leverage movie-fMRI to generate modality-specific movie gradients that have previously been shown to enhance brain-behavior associations (3). **We perform parcel-wise correlation of these movie gradients with ISC scores. Our goal is to identify which of the main axes of functional organization in the brain are most aligned with patterns of reliable stimulus-response across subjects.**

These analyses use minimally preprocessed movie-watching data from the Human Connectome Project (HCP) 7T data release (4, 5). From the complete dataset, 95 participants (58 females, mean age 29.5 ± 3.3) from 64 families were selected based on head motion and data availability. One hour of movie data was collected over the course of four 15-minute runs across two sessions. All analyses were first conducted in a discovery dataset of 45 subjects and replicated in the remaining 50 subjects. Gradient analyses were performed parcel-wise using the Schaefer-1000 parcellation (6). The mean time series for each parcel was correlated with the mean time course of all other parcels in the brain to create subject-level FC matrices. Diffusion embedding was performed at the subject level using the BrainSpace toolbox (7), and individual gradients were aligned to a group-mean template before being averaged to yield group-level gradients. BOLD-signal timeseries data at the Schaefer-1000 level were used to compute intersubject correlations using a group mean approach. Each subjects' time course at each parcel was correlated with the group average time course at that parcel to provide a single ISC score per region. Spatial autocorrelation-preserving null-models (8) were used to assess the significance of correlations between ISCs and scores along the top three gradients. Spin permutation tests were used to generate 10,000 null-models for each comparison.

ISCs and movie gradients followed trends in the literature (2, 3). ISCs were high in superior temporal and occipital regions. The top three gradient poles were situated in the somatosensory, visual, and auditory cortices respectively and radiated towards heteromodal association systems such as the default and frontoparietal networks. There was a significant spatial correlation between ISC scores and Gradient 2 scores ($r = 0.74$, $p < 0.05$), such that regions with the highest and lowest ISC scores were situated at the poles of the second gradient (i.e., visual and default networks). This relationship was reproduced in the replication dataset ($r = 0.75$, $p < 0.05$).

These results provide further support for a macroscale processing hierarchy within the brain that is exemplified under naturalistic conditions. These findings also suggest that when the brain is active and processing complex and ecologically valid stimulus, there is a strong correspondence between functional connectivity patterns at a whole-brain level, and BOLD signal response reliability across subjects at a parcel-level.

- (1) Margulies, D. S. (2016). Situating the default-mode network along a principal gradient of macroscale cortical organization. *Proceedings of the National Academy of Sciences*, 113(44), 12574–12579. <https://doi.org/10.1073/pnas.1608282113>
- (2) Hasson, U. (2004). Intersubject synchronization of cortical activity during natural vision. *Science*, 303(5664), 1634–1640. <https://doi.org/10.1126/science.1089506>
- (3) Samara, A. (2023). Cortical gradients during naturalistic processing are hierarchical and modality-specific. *NeuroImage*, 271, 120023. <https://doi.org/10.1016/j.neuroimage.2023.120023>
- (4) Glasser, M. F. (2013). The minimal preprocessing pipelines for the Human Connectome Project. *NeuroImage*, 80, 105–124. <https://doi.org/10.1016/j.neuroimage.2013.04.127>
- (5) Van Essen, D. C. (2013). The Wu-minn human connectome project: An overview. *NeuroImage*, 80, 62–79. <https://doi.org/10.1016/j.neuroimage.2013.05.041>
- (6) Schaefer, A. (2017). Local-global parcellation of the human cerebral cortex from intrinsic functional connectivity MRI. *Cerebral Cortex*, 28(9), 3095–3114. <https://doi.org/10.1093/cercor/bhx179>
- (7) Vos de Wael, R. (2020). BrainSpace: A toolbox for the analysis of macroscale gradients in neuroimaging and Connectomics datasets. *Communications Biology*, 3(1). <https://doi.org/10.1038/s42003-020-0794-7>
- (8) Alexander-Bloch, A. F. (2018). On testing for spatial correspondence between maps of human brain structure and function. *NeuroImage*, 178, 540–551. <https://doi.org/10.1016/j.neuroimage.2018.05.070>

Microstructural asymmetry in the human cortex

Bin Wan ^{1,2,3,4}, Amin Saberi ^{1,4,5}, Casey Paquola ⁴, H. Lina Schaare ^{1,4}, Meike D. Hettwer ^{1,4,5,6},
Jessica Royer ⁷, Alexandra John ^{1,4}, Lena Dorfschmidt ^{8,9}, Şeyma Bayrak ^{1,3,4}, Richard A.I.
Bethlehem ^{9,10}, Simon B. Eickhoff ^{4,5}, Boris C. Bernhardt ⁷, Sofie L. Valk ^{1,4,5}

1. *Otto Hahn Research Group Cognitive Neurogenetics, Max Planck Institute for Human Cognitive and Brain Sciences, Leipzig, Germany.*
2. *International Max Planck Research School on Neuroscience of Communication: Function, Structure, and Plasticity (IMPRS NeuroCom), Leipzig, Germany.*
3. *Department of Cognitive Neurology, University Hospital Leipzig and Faculty of Medicine, University of Leipzig, Leipzig, Germany.*
4. *Institute of Neuroscience and Medicine (INM-7: Brain and Behavior), Research Center Jülich, Jülich, Germany.*
5. *Institute of Systems Neuroscience, Heinrich Heine University Düsseldorf, Düsseldorf, Germany.*
6. *Max Planck School of Cognition, Leipzig, Germany*
7. *McConnell Brain Imaging Centre, Montréal Neurological Institute and Hospital, McGill University, Montréal, QC, Canada.*
8. *Department of Biostatistics, Epidemiology and Informatics, University of Pennsylvania, Philadelphia, PA, USA.*
9. *Department of Psychiatry, University of Cambridge, Cambridge, UK.*
10. *Department of Psychology, University of Cambridge, Cambridge, UK.*

Abstract

While macroscale brain asymmetry and its relevance for human cognitive function have been consistently shown, the underlying neurobiological signatures remain an open question. Here, we probe layer-specific microstructural asymmetry of the human cortex using intensity profiles from *post-mortem* cytoarchitecture. An anterior-posterior cortical pattern of left-right asymmetry was found, varying across cortical layers. A similar anterior-posterior pattern was observed using *in vivo* microstructural imaging, with *in vivo* asymmetry showing the strongest similarity with layer III. Microstructural asymmetry varied as a function of age and sex and was found to be heritable. Moreover, asymmetry in microstructure corresponded to asymmetry of intrinsic function, in particular in sensory areas. Last, probing the behavioral relevance, we found differential association of language and markers of mental health with asymmetry, illustrating a functional divergence between inferior-superior and anterior-posterior microstructural axes anchored in microstructural development. Our study highlights the layer-based patterning of microstructural asymmetry of the human cortex and its functional relevance.

Keywords: Asymmetry, Cortical microstructure, BigBrain, Structure-function, Mental health, Language

Correspondence to Bin Wan (binwan@cbs.mpg.de) and Sofie L. Valk (valk@cbs.mpg.de), Max Planck Institute for Human Cognitive and Brain Sciences, Leipzig, Germany and Institute of Neuroscience and Medicine (INM-7: Brain and Behaviour), Research Centre Jülich, Jülich, Germany.

Assessing Reliability and Geometric Influence in Organization of Structural Brain Connectivity

Sunghyoung Hong^{1,2*}, Seulk Yoo^{3*}, Boyong Park^{1,4,5†}, Seok Jun Hong^{1,2,6†}

¹IBS Center for Neuroscience Imaging Research, Sungkyunkwan University, Suwon, Republic of Korea,

²Department of Biomedical Engineering, Sungkyunkwan University, Suwon, Republic of Korea, ³Convergence Research Institute, Sungkyunkwan University, Suwon, Republic of Korea, ⁴Department of Data Science, Inha University, Incheon, Republic of Korea, ⁵Department of Statistics and Data Science, Inha University, Incheon, Republic of Korea, ⁶Center for the Developing Brain, Child Mind Institute, New York, NY, United States

Introduction. Understanding the functional mechanism of human cognitive systems prerequisites a precise mapping of underlying physical brain networks. Structural connectivity (SC) based on diffusion tractography has been instrumental in this purpose, as it allows to grasp the configuration of whole-brain physical connections in a single matrix form. However, the prohibitively high dimensionality of SC matrices, together with inconsistent results depending on the tractography-related parameters (e.g. tractography method, parcellation, filtering strategy) have hindered the effort to use this technique in capturing the principles of structural brain organization¹. Here, we sought to address these issues by applying a low-dimensional connectome mapping approach on SC², which provides a smooth transition of connectivity profiles across the whole brain (also known as “*connectome gradient*”). Moreover, inspired by a recent study demonstrating a significant role of gross cortical geometry on human brain function¹, we further tested the association between this SC gradient and cortical geometry to investigate a fundamental constraint in the manifestation of the structural brain organization.

Methods. We analyzed structure and diffusion MRI of 86 young-adult subjects from Human Connectome Project (HCP)⁴ (51 females; age range: 22-36). To generate SC matrices, we used three different tractography algorithms (FACT and SD STREAM: both for deterministic; iFOD2 for probabilistic)⁵, three parcellations (Schaefer 400⁶, Glasser 360⁷, and vosdewael 400⁸), and two filtering methods (SIFT2⁹ and COMMIT2⁹). Gradients were then generated from these SCs using Brainspace, specifically based on the diffusion map algorithm for non-linear dimensionality reduction with zero sparsity². To compare this gradient with cortical geometry, we also calculated eigenmodes from a group-averaged mid-thickness cortical surface using the Laplace-Beltrami operator⁹. Next, gradients and SC were reconstructed by cumulatively adding geometric eigenmodes weighted by their corresponding coefficients.

Results. We profiled the gradients of structural connectivities from 18 different combinations of tractography algorithms (3 tractography methods×3 parcellations×2 filtering algorithms). Among these, we found that the gradient showed high reproducibility, particularly in the 1st-4th components, between different algorithmic combinations (**Fig1A**). When we examined the variance explained by each principal component, however, it turned out that the first 3 components account for the majority of connectom data (=43% on average; determined by an elbow point in the scree plot of **Fig1B**). These 3 principal components showed 1) the left to right, 2) the anterior to posterior, and 3) the sensory to transmodal axes (**Fig1C**). This suggests that even if the original SC matrices were seemingly complex, their underlying structures could be recapitulated by a parsimonious set of low-dimensional bases. Notably, as hypothesized, when we visualized the tractography results at each gradient, all of them

seemed greatly affected by cortical geometric effects (**Fig 1D**). Our post-hoc analysis confirmed this visual inspection that there are strikingly similar patterns between the eigenmodes of cortical surface and SC gradients (**Fig 2A, 1C**). Indeed, when we reconstructed the SC gradient based on cortical eigenmodes, >95% of accuracy was achieved with a minimal number of eigenmodes (only 4, 2, and 4 eigenmodes for the gradient 1-3, respectively, **Fig 2B, 2D**). This strong geometric effect was also observed in the SC matrix (**Fig 2C, 2D**).

Conclusion. Here, our study systematically investigated the principles of SC organization using a non-linear dimensionality reduction approach. Our main finding, *i.e.* a strong geometric effect on SC gradients, suggests that the topology of structural brain networks may be predominantly determined by the connectivity from the adjacent cortical areas (*e.g.*, a short-range U fibers), a potential signature of evolutionarily shaped brain organization that prioritizes energy efficiency.

References

1. Motwani, R., Naor, J. S., & Naor, M. (1994). The probabilistic method yields deterministic parallel algorithms. *Journal of Computer and System Sciences*, 49(3), 478-516.
2. Vos de Wael R, Benkarim O, Paquola C, Lariviere S, Royer J, Tavakol S, Xu T, Hong S, Langs G, Valk S, Misic B, Milham M, Margulies D, Smallwood J, Bernhardt B (2020). BrainSpace: a toolbox for the analysis of macroscale gradients in neuroimaging and connectomics datasets. *Commun Biol* 3, 103.
3. Pang, J. C., Aquino, K. M., Oldehinkel, M., Robinson, P. A., Fulcher, B. D., Breakspear, M., & Fornito, A. (2023). Geometric constraints on human brain function. *Nature*, 1-9.
4. WU-Minn, H. C. P. (2017). 1200 subjects data release reference manual. URL <https://www.humanconnectome.org>, 565.
5. J.-D. Tournier, R. E. Smith, D. Raffelt, R. Tabbara, T. Dhollander, M. Pietsch, D. Christiaens, B. Jeurissen, C.-H. Yeh, and A. Connelly. *MRtrix3*: A fast, flexible and open software framework for medical image processing and visualisation. *NeuroImage*, 202 (2019), pp. 116–37.
6. Schaefer, A., Kong, R., Gordon, E. M., Laumann, T. O., Zuo, X. N., Holmes, A. J., ... & Yeo, B. T. (2018). Local-global parcellation of the human cerebral cortex from intrinsic functional connectivity MRI. *Cerebral cortex*, 28(9), 3095-3114.
7. Glasser, M. F., Coalson, T. S., Robinson, E. C., Hacker, C. D., Harwell, J., Yacoub, E., ... & Van Essen, D. C. (2016). A multi-modal parcellation of human cerebral cortex. *Nature*, 536(7615), 171-178.
8. Desikan RS, Ségonne F, Fischl B, et al. An automated labeling system for subdividing the human cerebral cortex on MRI scans into gyral based regions of interest. *Neuroimage* 2006;31:968-980.
9. Schiavi, S., Ocampo-Pineda, M., Barakovic, M., Petit, L., Descoteaux, M., Thiran, J. P., & Daducci, A. (2020). A new method for accurate *in vivo* mapping of human brain connections using microstructural and anatomical information. *Science advances*, 6(31), eaba8245.

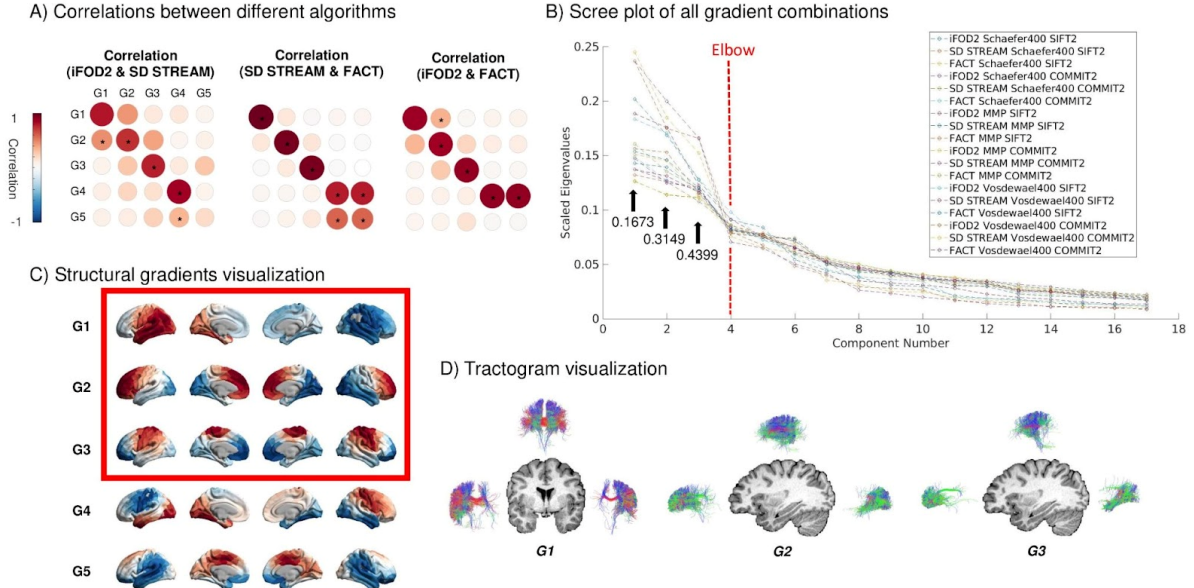


Fig 1. Consistency of structural gradients, their principal components and tractography visualization. A) Gradients 1st-4th between different tractography algorithms have a high correlation. B) Scree plot of all gradient combinations shows that the first three gradients have, on average, a fairly high explanatory power of more than 0.43. C) Among five principal gradients, the first gradient appears to be the left to right, the second gradient looks like the anterior to posterior, and the third gradient seems to be the sensory to transmodal axes. This gradient was made of iFOD2, Vosdewael 400, SIFT2, diffusion map, and sparsity 0. Based on A) and B), we decided to focus on the first three gradients of the analysis after it. D) It shows seed-based tractography along the progress of each gradient. Seed points are parcels with the largest, the medium, and the smallest value.

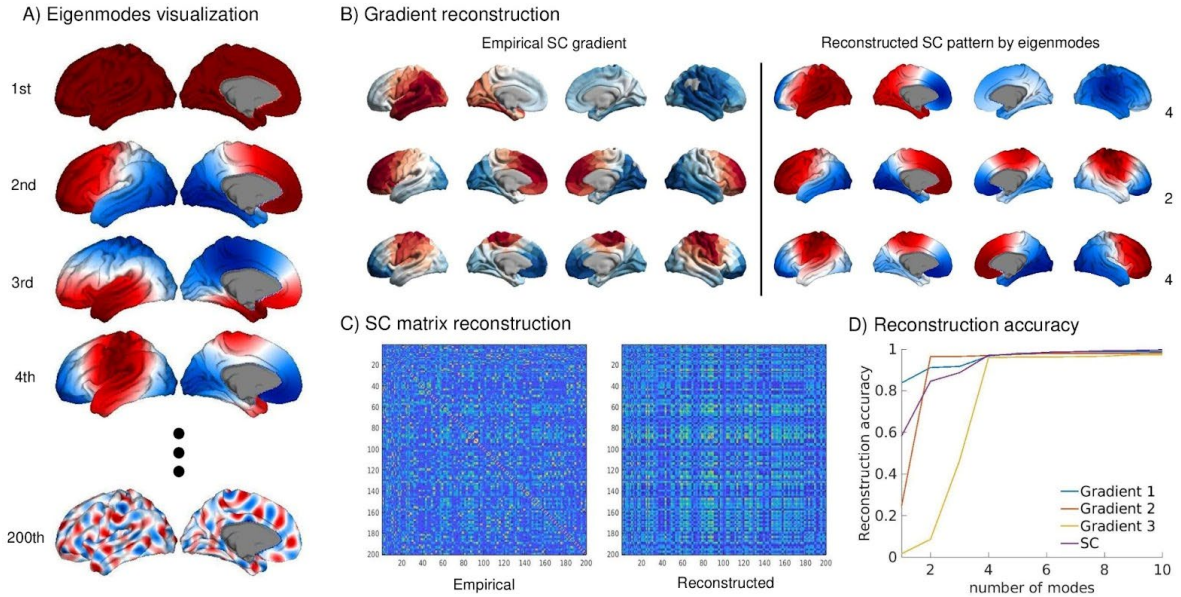


Fig 2. Eigenmodes and reconstruction of structural gradient and connectivity with them. A) Total 200 geometric eigenmodes were generated of group-averaged mid-thickness cortical surface. 1st, 2nd, and 4th eigenmodes are very similar with 1st, 2nd, and 3rd gradients, respectively. B) Each gradient was reconstructed by cumulatively adding eigenmodes multiplied by each coefficient. The numbers in the lower right of each gradient are the minimum number of eigenmodes to achieve reconstruction accuracy of more than 95%. C) Group-averaged left hemisphere structural connectivity was reconstructed in the same way. Only 4 eigenmodes were needed to reconstruct more than 95% accuracy. D) It is shown that the graph of the reconstruction accuracy is saturated using more than four eigenmodes in both gradient and structural connectivity.

Title

Structurally Informed Resting-State Effective Connectivity Recapitulates Cortical Hierarchy

Authors and Affiliations

Matthew D. Greaves ^{a, b, *}, Leonardo Novelli ^{a, b}, Adeel Razi ^{a, b, c, d}.

- a. Turner Institute for Brain and Mental Health, School of Psychological Sciences, Monash University, Melbourne, Australia
- b. Monash Biomedical Imaging, Monash University, Melbourne, Australia
- c. Wellcome Centre for Human Neuroimaging, University College London, London, UK
- d. CIFAR Azrieli Global Scholars Program, CIFAR, Toronto, Canada

* Corresponding author: matthew.greaves@monash.edu

Introduction

Interregional brain communication is mediated by the brain's physical wiring (i.e., structural connectivity). Yet, it remains unclear whether models describing directed, functional interactions between latent neuronal populations—effective connectivity—benefit from incorporating macroscale structural connectivity. Here, we assess a hierarchical empirical Bayes method: structural connectivity-based priors constrain the inversion of group-level resting-state effective connectivity, using subject-level posteriors as input; subsequently, group-level posteriors serve as empirical priors for re-evaluating subject-level effective connectivity. This approach permits knowledge of the brain's structure to inform inference of (multilevel) effective connectivity.

Methods

Functional and structural data in this study were sourced from the Human Connectome Project. Test (face-validation) and retest datasets include data from 100 healthy adults (54 female, age 22–35) acquired on two different days (session 1 and session 2, respectively); and two out-of-sample validation datasets which include data from 50 healthy adults (24 female, age 22–35) acquired on two different days. We perform deterministic tractography utilizing the fiber assignment by continuous tractography algorithm. To account for distance- and volume-related biases, for both the test-retest and validation samples, we generated distance-based consensus structural connectivity matrices. At the first level, spectral dynamic causal modelling (DCM) was used to infer subject-level effective connectivity. We then used the hierarchical empirical Bayes procedure to infer structurally informed (multilevel) effective connectivity (see Fig. 1).

Results

In 17 resting-state brain networks, we find that a positive, monotonic relationship between structural connectivity and the prior probability of group-level effective connectivity generalizes across sessions and samples. To examine inter-network differences in the degree to which structural connectivity influenced—i.e., was linearly coupled with—effective connectivity, we compared the weight (or slope) parameters of the Bayesian model-average variance transformations (see Fig. 2). The coupling between structural connectivity and third-level priors was highest in the default mode network that comprised hub regions: posterior cingulate cortex and medial prefrontal cortex. We show that the value of these weight parameters is situated along an axis that describes an approximate unimodal (sensory) to transmodal (integrative) processing spectrum.

Conclusions

Our study further elucidates the role that structural connectivity exerts in shaping effective connectivity. By leveraging a novel two-step hierarchical empirical Bayes method, we reveal that a positive, monotonic relationship between structural connectivity and the prior probability of group-level effective connectivity generalizes out of session and out of sample, increasing model evidence at both group and subject levels. The recapitulation of a unimodal-transmodal cortical hierarchy through inter-network variation in the coupling between structural and effective connectivity highlights the role that structurally constrained lower-order dynamics play in shaping patterns in higher-order statistical dependencies between brain regions. Our findings recommend a shift towards more integrative approaches in DCM-based research, in which the fusion of structural and effective connectivity models could offer novel insights into functional integration in health and disease.

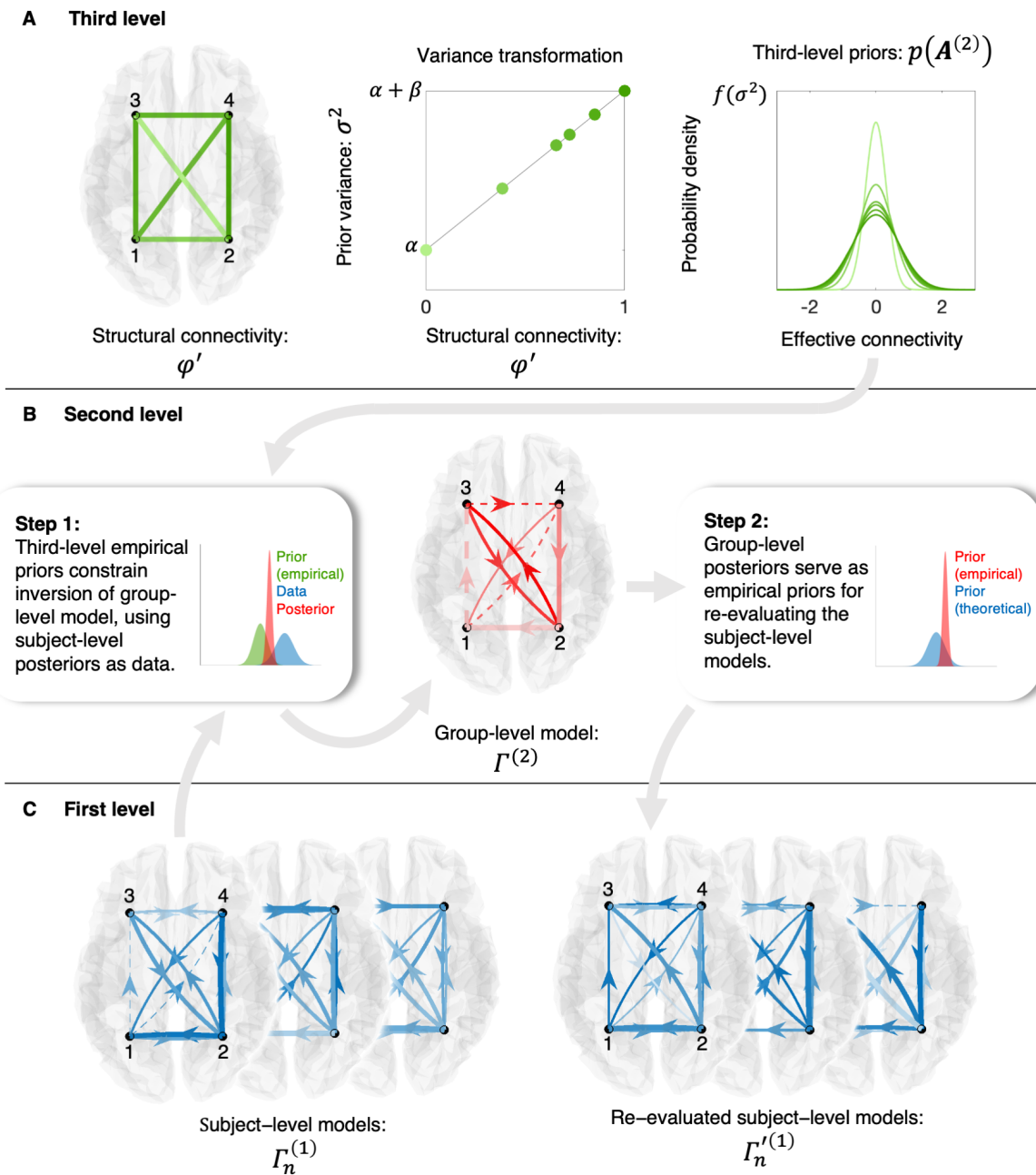


Fig 1. Two-step, hierarchical empirical Bayes model. The three rows represent the levels of the hierarchical model. Inset text boxes and arrows describe the processes via which empirical data are integrated at multiple levels of the hierarchy. The left inset box displays a plot containing three probability density functions: a structure-based prior (in green), data (in blue), and the resulting posterior (in red), illustrating the Bayesian updating of priors. The right inset box shows a similar plot, in which the red probability density function represents the updated (empirical) prior used for re-evaluating subject-level models. This prior is contrasted with the initial (theoretical) prior (in blue), with the difference in precision reflecting a search for more precise or reduced models. **(A)** At the third level, structure-based priors are furnished by linearly mapping (normalized) structural connectivity weights to variances of zero-mean Gaussian priors. In this row, the undirected structural connectivity graph is formatted such that the weights are represented by the saturation of the color, with more saturated lines indicating stronger connectivity. **(B)** At the second level, a group-level model is furnished. Here, we represent a (directed) effective connectivity graph that is formatted such that solid (dashed) lines represent positive (negative) connections, with line weight representing the connection strength—the higher the weight the stronger the connection—and saturation of the color representing the precision of the estimate (with more saturated lines indicating more precise estimates). **(C)** At the first level, subject-level models—i.e., dynamic causal models—both serve as data (step 1), and are re-evaluated (step 2). The subject-level effective connectivity graphs are formatted per the conventions employed for the group-level effective connectivity graph.

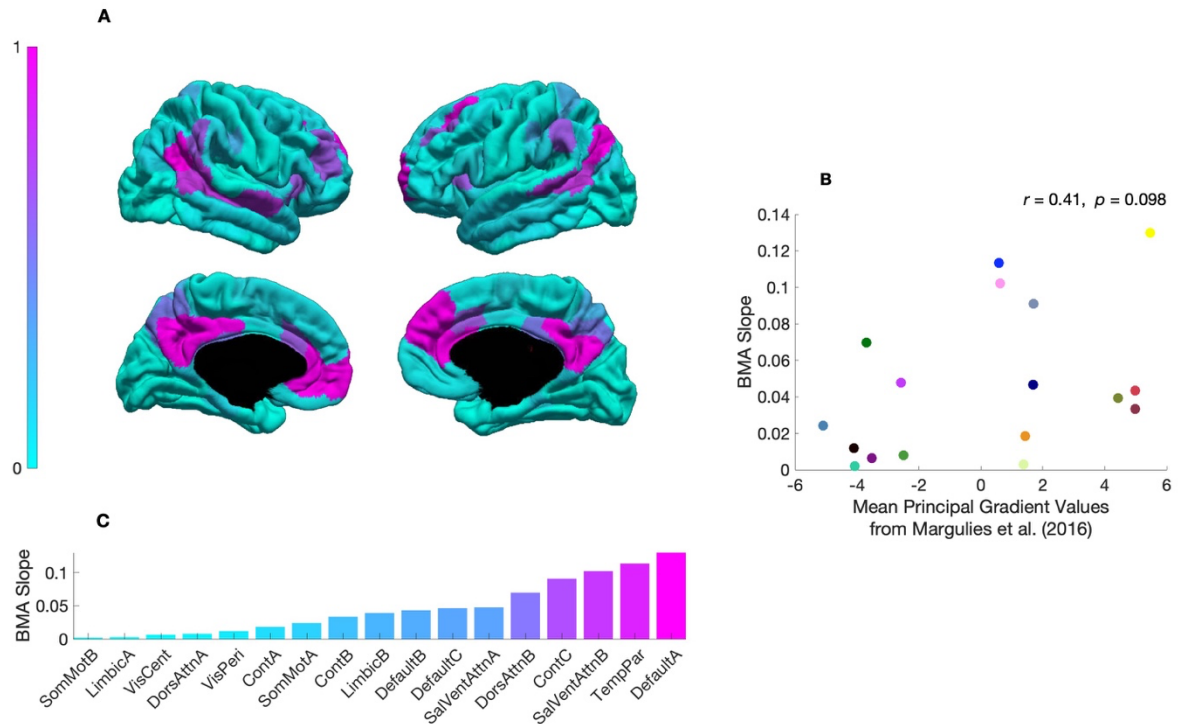


Fig 2. Coupling between structural and effective connectivity across the cortex. (A) Relative weight (or slope) parameters for the network-specific Bayesian model-average (BMA) variance transformations on sagittal views of a cortical pial surface. The colormap indicates that regions in magenta (cyan) have relatively higher (lower) coupling between structural connectivity and effective connectivity. (B) Scatter plot showing the relationship between network-specific BMA slope parameter estimates—we refer the reader to Figs. 1-3 for the corresponding color legend—and the mean principal gradient values per network from Margulies et al. (2016). (C) Bar plot showing that the rank-ordered network-specific BMA beta slope parameter estimates capture key aspects of a well-known cortical (processing) hierarchy. Namely, transmodal (unimodal) networks tend to have been given a relative greater (lesser) weight, with coupling highest in a default mode (DefaultA) network, and lowest in a somatomotor (SomMotB) network.

Multiscale structural architecture of human neural dynamics

Jessica Royer¹, Casey Paquola³, Raul Rodriguez-Cruces¹, Hans Auer¹, Alexander Ngo¹, Ella Sahlas¹, Daniel Mansilla De Latorre^{1,4}, Raluca Pana¹, Jeffrey Hall¹, Birgit Frauscher², Boris C. Bernhardt¹

1) Montréal Neurological Institute and Hospital, McGill University, Montreal, Québec, Canada

2) Duke University School of Medicine, Durham, North Carolina, United States

3) Institute for Neuroscience and Medicine (INM-7), Forschungszentrum Jülich, Jülich, Germany

4) Neurophysiology Unit, Department of Neurosurgery, Institute of Neurosurgery, Asenjo, Santiago, Chile.

Neural dynamics are complex and heterogeneous across the cortex. Local spectral signatures are constrained by structural properties ^{1,2}, but the relationship between neural dynamics and cortical structure remains incompletely understood. The present work explores this question by investigating the balance of extrinsic and intrinsic structural constraints on regional neural dynamics. We provide an integrated account of this interplay by combining the high temporal and spatial precision of intracranial electroencephalography (iEEG) with multiscale measures of cortical wiring, specifically inter-regional distance, structural connectivity estimated from diffusion-weighted MRI tractography, and microstructural profile similarity.

The *MNI open iEEG atlas*³ provides iEEG recordings acquired during conditions of resting wakefulness in 106 patients with intractable epilepsy (*atlas dataset*; **Fig1A**). By excluding channels involved in ictal and inter-ictal activity, this dataset provides a putative reference space for normal human neurophysiology. Data pre-processing included band-pass filtering (0.5-80Hz), downsampling (200Hz), and demeaning. We computed each channel's power spectral density (PSD; Welch's method; 2-second blocks, 1-second overlap, Hamming window weighting). Channel PSDs were log-transformed, mapped to a single hemisphere, and parcellated⁴. Parcel-wise PSDs were cross-correlated while controlling for the average PSD across all channels and underwent Fisher R-to-Z transformation. We then applied diffusion map embedding to derive principal axes of variation in neural dynamics (**Fig1B**)⁵. In a second dataset of 20 patients (*multimodal dataset*; 13F; mean±S.D. age=33.90±9.02years), iEEG was recorded during resting wakefulness, and pre-operative, high-resolution structural (T1-weighted, quantitative T1, 0.8mm isovoxels) and multi-shell diffusion-weighted MRI (DWI; 1.6mm isovoxels) were acquired, enabling dataset-specific correlations between brain wiring and macroscale neural dynamics. We used micapipe⁶ to derive subject-specific measures of geodesic distance, microstructural profile similarity, and structural connectivity across all node pairs. Electrophysiological data underwent identical processing as in the atlas dataset. Channel-level PSDs were averaged across patients within each parcel (**Fig2A**), and multimodal dataset embeddings were aligned to the atlas embedding space using Procrustes rotation. We assessed structure-function coupling with a multiple linear regression model using three structural features as predictors of inter-node distances in the multimodal dataset embedding space.

The first gradient (G1) of neural dynamics differentiated primary motor and surrounding frontal cortices from occipito-temporal regions, segregating channels with dominant beta and gamma-range activity (>13hz) from those with high-delta, theta, and alpha-range peaks (<13Hz) (**Fig1C**). The second gradient (G2) differentiated unimodal sensory cortices, encompassing channels with peaks in the alpha frequency range (8-13Hz), from limbic and paralimbic regions with strong low frequency activity (<4Hz). This compact representation reflected distinct spectral signatures of unimodal sensory, motor, and association areas (**Fig1D**), and could be replicated in the multimodal dataset (median $r=0.34$; **Fig2B**). Structural features explained up to 60% of variance in distances within the embedding space: highest R^2 values were observed in frontopolar and lateral temporal areas (**Fig2C**). This model outperformed models implementing different functional response variables (**Fig 2D**). These results show diverse contributions of cortical wiring to regional neural dynamics, with variable coupling strengths observed across the neocortical.

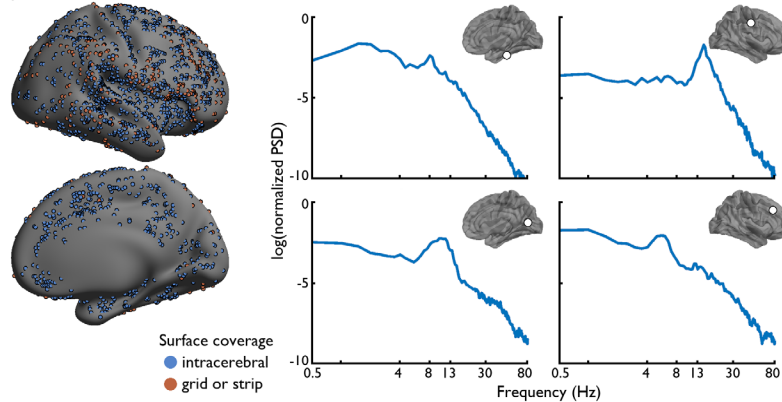
By mapping gradients of neural dynamics, our approach resolves macroscale trends in spectral similarity of local cortical regions and opens the way for assessments of structure-function coupling from direct measurements of neural activity.

References

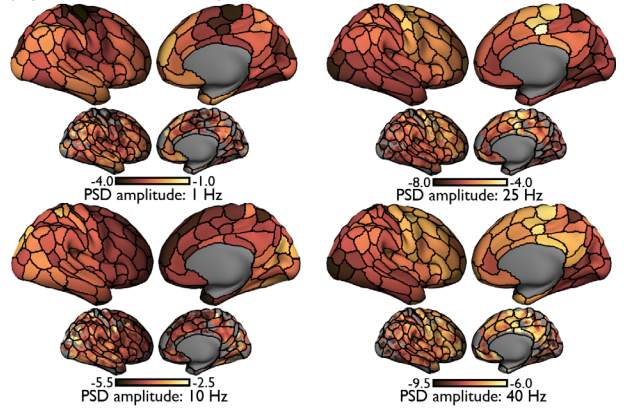
1. Shafiei G, Markello RD, De Wael RV, Bernhardt BC, Fulcher BD, Misic B. Topographic gradients of intrinsic dynamics across neocortex. *Elife*. 2020;9:e62116.
2. Wang X-J. Macroscopic gradients of synaptic excitation and inhibition in the neocortex. *Nature Reviews Neuroscience*. 2020/03/01 2020;21(3):169-178. doi:10.1038/s41583-020-0262-x
3. Frauscher B, von Ellenrieder N, Zelmann R, et al. Atlas of the normal intracranial electroencephalogram: neurophysiological awake activity in different cortical areas. *Brain*. 2018;141(4):1130-1144. doi:10.1093/brain/awy035
4. Schaefer A, Kong R, Gordon EM, et al. Local-global parcellation of the human cerebral cortex from intrinsic functional connectivity MRI. *Cerebral cortex*. 2018;28(9):3095-3114.
5. Vos de Wael R, Benkarim O, Paquola C, et al. BrainSpace: a toolbox for the analysis of macroscale gradients in neuroimaging and connectomics datasets. *Communications biology*. 2020;3(1):1-10.
6. Cruces RR, Royer J, Herholz P, et al. Micapipe: A pipeline for multimodal neuroimaging and connectome analysis. *NeuroImage*. 2022;263:119612.

A | Mapping neural dynamics with intracranial EEG

i | Atlas of the normal intracranial EEG

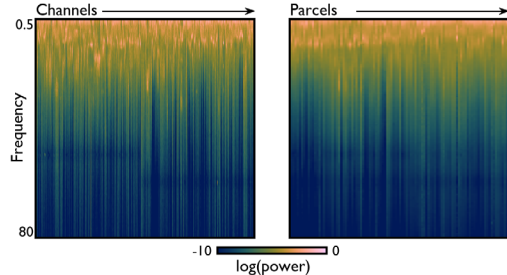


ii | Spatial shifts in PSD amplitudes

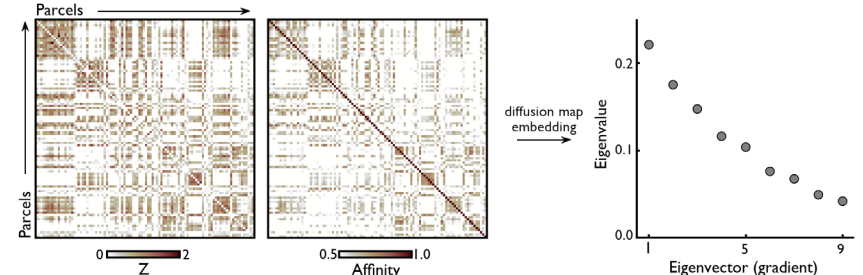


B | Cortex-wide PSD similarity

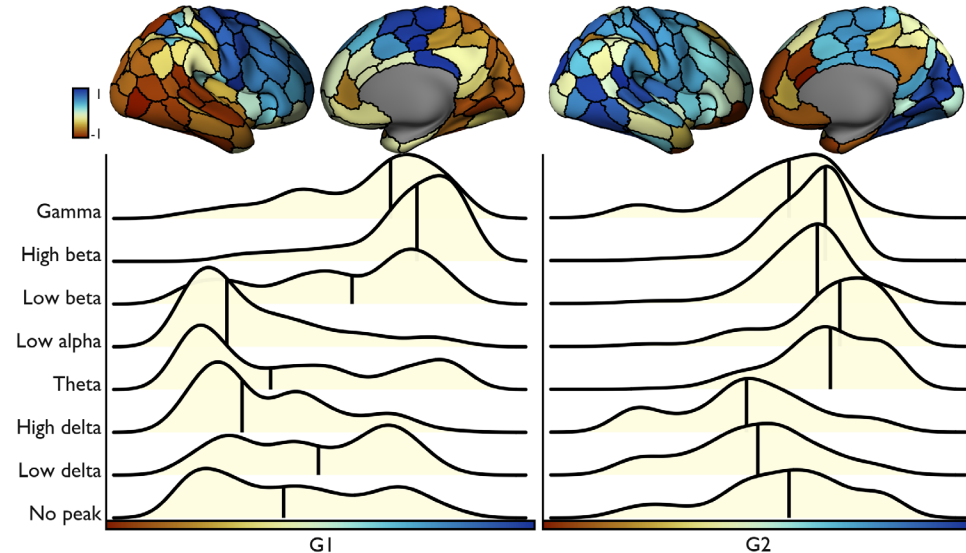
iii | Parcellate channel PSDs



iv | Apply dimensionality reduction to PSD similarity matrix



C | Principal gradients of neural dynamic similarity



D | 2D gradient space

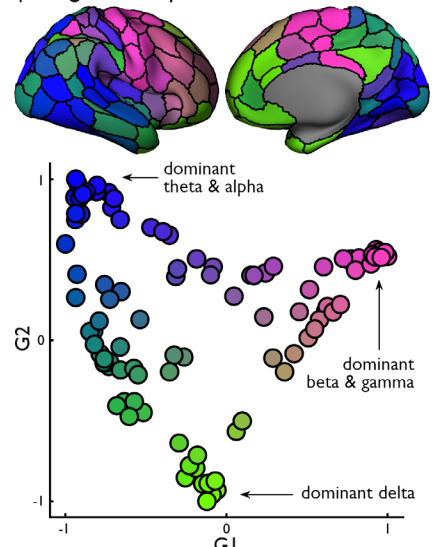


Figure 1. Cortical gradients of neural dynamics. (A) Channel coordinates from the MNI open iEEG atlas were mapped to the right hemisphere and registered to the fs-LR 32k-vertex surface template. The PSD of each channel was computed and normalized as in previous work (i). Channel PSDs were mapped to single vertices, expanded to 5mm regions surrounding each assigned vertex (channel region), and averaged within regions defined by the Schaefer-200 parcellation. PSD amplitude at selected frequencies (1-10-25-40Hz) mapped to channel regions (bottom) and the Schaefer-200 parcellation (top) highlight the spatial heterogeneity of neural dynamics across the cortex (ii). (B) After averaging channel-wise PSDs within parcels (iii), features were cross-correlated to generate large-scale gradients of neural rhythm similarity using diffusion map embedding (iv). We retained the first two gradients explaining the most variance in the data for further analyses. (C) Projected to the cortical surface, these gradients emphasized strong differentiation of neural dynamics between anterior-posterior (G1) and sensory-limbic (G2), cortices. Ridge plots show that each gradient captured unique channel-level variations in PSD features, segregating channels according to their respective spectral peaks. (D) The scatter plot depicts node positions in the 2D gradient space, coloured according to proximity to axis limits, alongside an equivalent representation on the cortical surface.

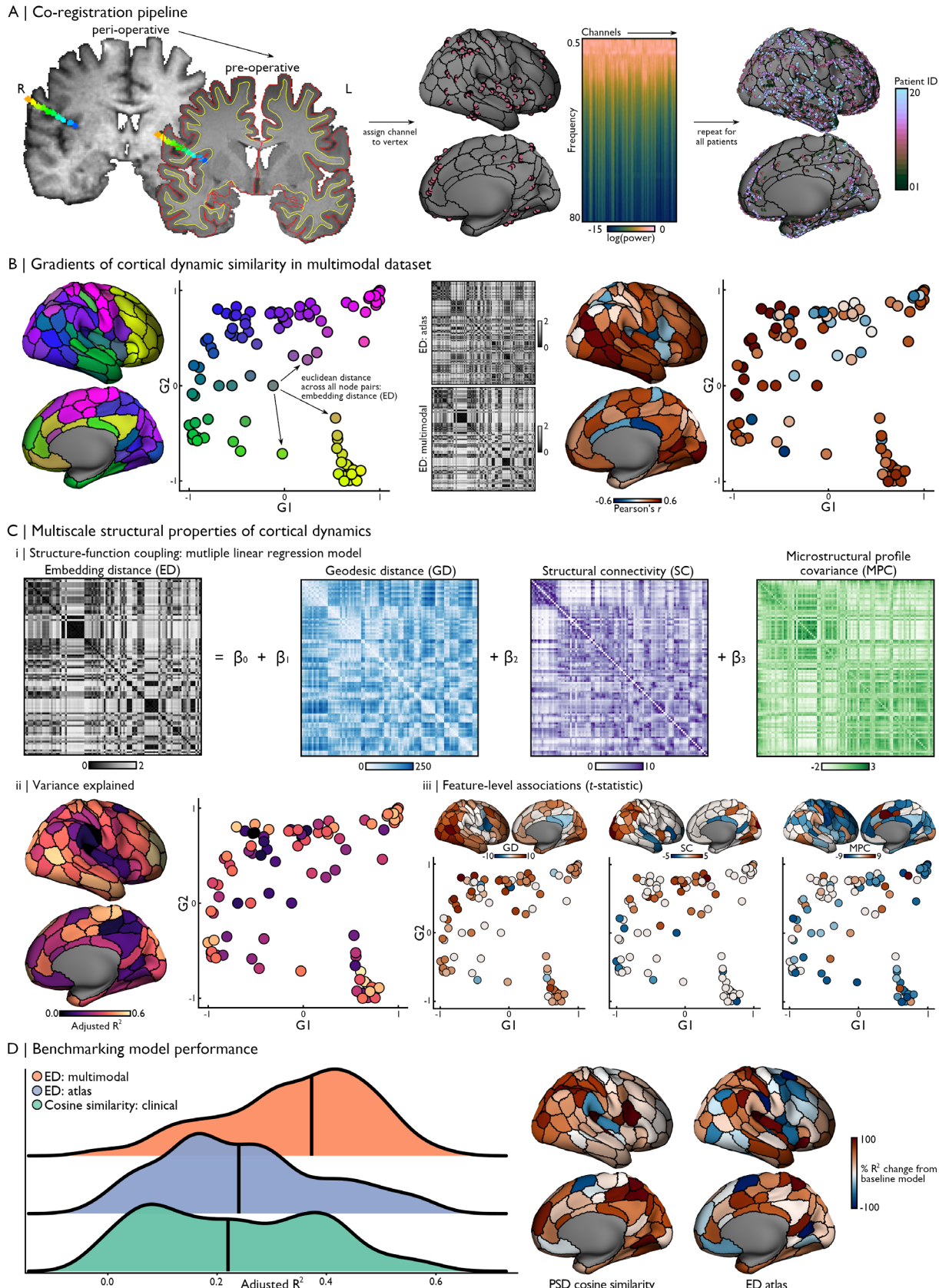


Figure 2. Multiscale structural architecture of human neural dynamics. (A) Peri- and pre-implantation anatomical scans were linearly co-registered in each patient. Each bipolar channel was assigned to vertices along patient-specific neocortical surface segmentations resampled from native FreeSurfer space to a single hemisphere of the fs-LR surface template (~32k vertices). Repeating this procedure across all 20 patients yielded widespread sampling of the neocortical gray matter. (B) Generating gradients of PSD similarity in the clinical sample partially recovered the layout of the normative space, with segregation of sensory, motor, and paralimbic structures. However, we found stronger differentiation of frontal lobe structures in the clinical sample relative to the normative space. Comparing embedding distance matrices, generated by computing the Euclidean distance between all node pairs in each space, showed generally consistent positioning of nodes across both embedding spaces (median $r=0.34$). (C) (i) A multiple linear regression model was used to predict each node's embedding distance profile from its multiscale structural properties including geodesic distance along the neocortical surface, structural connectivity strength, and microstructural profile similarity. (ii) The model showed the best prediction of neocortical function from structure along the edges of the embedding space (median adjusted $R^2=0.37$). (iii) Each structural feature differentially contributed to the accuracy of predictions across regions as quantified using node-wise t-statistic (thresholded at $t>2$ and $t<-2$ for visualization). (D) This model outperformed predictions of cosine similarity of clinical sample PSDs (median adjusted $R^2=0.22$) and embedding distance computed from the normative atlas (median adjusted $R^2=0.24$).

Title: Disentangling the functional relationship between neural networks of social cognition

Lara Z. Maliske¹, Matthias Schurz^{2,3,4}, Philipp Kanske^{1,5}

¹Clinical Psychology and Behavioral Neuroscience, Faculty of Psychology, Technische Universität Dresden, Dresden, Germany

²Institute of Psychology and Digital Science Center, University of Innsbruck, Innsbruck, Austria

³Donders Institute for brain, Cognition, & Behavior, Radboud University, Nijmegen, Netherlands

⁴Wellcome Centre for Integrative Neuroimaging, Department of Experimental Psychology, University of Oxford, Oxford, United Kingdom

⁵Max Planck Institute for Human Cognitive and Brain Sciences, Leipzig, Germany

Recent advances in the study of empathy and Theory of Mind (ToM) demonstrate the need to investigate the two in interaction: naturalistic settings often blur the distinction between affect and cognition and demand the simultaneous processing of such different stimulus dimensions. Here, we followed up on the results of a recent coordinate-based meta-analysis and hierarchical clustering analysis, as well as a follow-up meta-analytic connectivity modeling analysis that described a hierarchical model of social affect and cognition, and how neural representations of empathy and ToM were enabled through network co-activation and connectivity. Specifically, we investigated the relationship between social affective, cognitive, and complex social neural activation maps by projecting them along a principal gradient of macroscale cortical organization (Margulies et al., 2016), and comparing them to other neural activation patterns related to social cognition.

We re-analyzed data from a meta-analytic hierarchical clustering (Schurz et al., 2021) including 188 empathy and ToM studies across 11 more narrow tasks groups, clustering into three overarching patterns of neural activation related to social affect and cognition (cognitive, intermediate, affective cluster). Furthermore, we re-analyzed data from a follow-up meta-analytic connectivity modeling study (Maliske et al., 2023) including 140 studies associated with the right anterior cingulate cortex, right posterior cingulate cortex, left temporoparietal junction, and left anterior insula.

We determined overlap between neural activation maps using a variant of the dice score (indicating the percentage of voxels in i1 that overlap with i2). Specifically, we calculated the overlap between meta-analytic (co-activation) maps and a) continuous changes in the functional spectrum described by the principal gradient (in increments of 5%), as well as b) more narrow task groups related to social affect and cognition (see Schurz et al., 2021).

Meta-analytic (co-activation) maps related to social affect and cognition were positioned at separable locations along the principle gradient, while meta-analytic (co-activation) maps related to complex social cognition (intermediate cluster) tended to overlap with the locations of both the affective (located towards the sensory/ unimodal part of the gradient, 30-55th percentile) and the cognitive cluster (located towards the transmodal end of the gradient, 80-95th percentile).

The cognitive cluster showed most pronounced overlap with the false belief task (e.g., Saxe & Kanwisher, 2002; overlap ranging from 81-95%). Neural (co-)activation patterns related to social affect and complex social cognition showed overlap with diverse task profiles, although some trends emerged (e.g., a larger overlap of affective cluster and observing pain, as well as reading the mind in the eyes meta-analytic maps).

Re-analysis of coordinate-based meta-analyses and meta-analytic connectivity modeling allowed us to further probe the relationship between neural activation patterns related to social affect, cognition, as well as complex social tasks. More precisely, in contrasts to the notion of independence of empathy and ToM-related neural networks, the results presented here indicate that complex social tasks (intermediate cluster) rely on cross-network interaction (network integration), and their neural

activation are similar to a neural activation patterns related to a range of different tasks measuring empathy and ToM.

References:

Schurz, M. (2021). ‘Towards a Hierarchical Model of Social Cognition: A Neuroimaging Meta-Analysis and Integrative Review of Empathy and Theory of Mind’, *Psychological Bulletin*, vol. 147, no. 3, pp. 293-327.

Maliske, L. (2023). ‘Interactions within the social brain: Co-activation and connectivity among networks enabling empathy and Theory of Mind’, *Neuroscience & Biobehavioral Reviews*, vol. 147, article 105080, pp. 1-13.

Margulies, D. (2016). ‘Situating the default-mode network along a principal gradient of macroscale cortical organization’, *Proceedings of the National Academy of Sciences*, vol. 113, no. 44, pp. 12574-12579.

Saxe, A. (2003). ‘People thinking about thinking people. The role of the temporo-parietal junction in “theory of mind”’, *NeuroImage*, vol. 19, pp. 1835-1842.

key words: Social cognition; fMRI; Meta-analysis; Co-activation; functional gradient; overlap analysis

Geodesic Distances on the Cortical Surface Predict Reading Performance

R. Austin Benn¹, Francesco Alberti¹, Wei Wei¹, Victoria Shevchenko¹, Ulysse Klatzmann¹, Robert Scholz^{1,2,3}, Carla Pallavicini¹, Pierre-Louis Bazin⁴, Daniel Margulies¹

Institutions

1. Université Paris Cité, INCC UMR 8002, CNRS, Paris, France
2. Max Planck School of Cognition, Leipzig, Germany,
3. Wilhelm Wundt Institute for Psychology, Leipzig University, Leipzig, Germany,
4. Full brain picture Analytics, Leiden, The Netherlands

This study explores the relationship between the intrinsic geometry of the cortical surface and its influence on reading performance and language processing, as measured by the Oral Reading Recognition Test (ORRT). The ORRT engages multimodal and widely distributed cortical areas to perform a task dependent on visual perception, semantic memory, and motor planning. Using data from the Human Connectome Project (HCP), we adapted connectome-based predictive modeling (CPM) to predict reading performance in the ORRT using geodesic distance measured on the cortical surface.

With a cohort of 887 subjects from the HCP, we measured geodesic distance on the reconstructed midthickness surface from high-resolution T1-weighted images and constructed a distance matrix between all parcels of the Schaefer 400 parcellation. Using a 10x10K-fold cross-validation scheme, we identified distances consistently associated with ORRT performance across all training folds. These associated distances were split based on their sign and used to define two summary measures corresponding to increased distance (positive feature) or decreased distance (negative feature) associated with ORRT performance. These summary measures were then used as predictors in a linear model to establish

the predictive capacity of spatial relationships on the cortex for ORRT performance.

The distances associated with ORRT performance were widely localized to regions pertaining to the language network and the visual word form area. Based on the summary measures, we built three predictive models using the positive and negative summaries as individual predictors, and a third joint model using both summary measures. The joint model achieved the highest predictive accuracy, highlighting that both expansion and contraction between cortical areas support better performance in reading ability. Our results underscore the role of cortical geometry in specialized functions and show that the spatial configuration of areas relative to each other facilitates efficient language processing.

In conclusion, this study finds that the intrinsic geometry of the cortical surface is a significant predictor of reading performance, advancing our understanding of how the spatial organization of the cortex relates to cognitive function.

PRECISION NEUROIMAGING AND GRADIENTS IN THE INDIVIDUAL HUMAN BRAIN AT ULTRA-HIGH FIELDS

Donna Gift Cabalo^{1,2}, Yezhou Wang^{1,2}, Ilana Leppert², Risa Thevakumaran², Jordan DeKraker^{1,2}, Youngeun Hwang^{1,2}, Yigu Zhou^{1,2}, Jessica Royer^{1,2}, Valeria Kebets^{1,2}, Shahin Tavakol^{1,2}, Oualid Benkarim^{1,2}, Nicole Eichert³, Casey Paquola⁴, Christine Lucas Tardif², David Rudko², Jonathan Smallwood⁵, Raul Rodriguez-Cruces^{1,2*}, Boris C. Bernhardt^{1,2*}

¹Multimodal Imaging and Connectome Analysis Lab, McGill University, Montreal, QC, Canada,

²McConnell Brain Imaging Centre, Montreal Neurological Institute and Hospital, Montreal, QC,

Canada; ³University of Oxford, Oxford, UK; ⁴Forschungszentrum Jülich, Jülich, Germany;

⁵Queens University, Kingston, ON, Canada.

Multimodal neuroimaging allows for non-invasive examination of human brain structure and function across multiple scales. Precision neuroimaging builds upon this foundation, enabling the mapping of brain structure, function, and connectivity patterns with high fidelity in single individuals. Ultra-high field (UHF) neuroimaging, operating at magnetic field strengths of 7 Tesla, offers even greater spatial and temporal resolution. The increased specificity provided by multimodal, UHF-precision imaging therefore, allows for more precise delineation of cortical network organization, encompassing microstructure, connectivity, and function.^{1,2} Neurosciences has increasingly benefitted from and embraced open science practices, particularly through data sharing initiatives and the dissemination of derivative data alongside the publication of processing pipelines. Large collaborative projects have produced open source datasets acquired at UHF 7T³, however, these datasets focused either on functional scans or structural sequences. Here, we provide a multimodal Precision Neuroimaging and Connectomics (PNI) dataset, utilizing UHF 7T MRI. Ten healthy individuals underwent a comprehensive MRI protocol, including T1 relaxometry, magnetization transfer imaging, T2*-weighted imaging, diffusion MRI, and multi-state functional MRI paradigms, aggregated across three imaging sessions. Alongside anonymized raw imaging data, we release cortex-wide connectomes derived from different modalities across multiple parcellation scales and supply “gradients” that compactly characterize spatial patterning

of cortical organization. These gradients span various aspects of brain organization including, structural⁴ and functional connectivity,⁵ task-based investigations,⁶ cortical morphology and microstructure^{7,8} indicating converging spatial trends.^{7,8} For example, analyses of intrinsic functional connectivity gradients have identified a principal gradient distinguishing sensorimotor systems from transmodal networks,⁵ consistent with established cortical hierarchy models.⁹ Gradient techniques, therefore, offer unification of different principles of brain organization across multiple neurobiological features and scales. From the PNI dataset, individual and group-level connectivity gradients were derived from each data modality using Brainspace¹⁰. Group-level gradients were generated using averaged subject-level matrices in Conte69 surface space. Geodesic distance (GD), microstructural profile variance (MPC) and functional connectivity (FC) matrices were thresholded to retain only the top 10% row-wise connections. Structural connectivity (SC) matrices were log-transformed before averaging to reduce variance in connectivity strength. We constructed affinity matrices using the normalized angle to measure the similarity of inter-regional patterns between regions. Affinity matrices from each modality were fed into diffusion map embedding,¹⁰ a non-linear dimensionality reduction technique to identify low-dimensional eigenvectors. To evaluate reproducibility, individual and modality-specific gradients were generated and aligned to their respective group-level templates using Procrustes rotations. Finally, we computed the averaged correlations between individual and group level gradients. As expected, the principal GD gradient (GD-G1) recapitulated the longest cortical distance axis in anterior to posterior direction¹¹. SC-G1 distinguished visual and sensorimotor surfaces, whereas rsFC-G1 describe a unimodal to transmodal pattern.⁵ MPC-G1 derived from T1, MTSAT and T2* maps were anchored in primary sensory areas and limbic regions.¹² G1-GD (mean r and SD=0.99±0.001), MPC-T1 (0.85±0.022), and FC (0.86±0.423) were highly replicable in all participants and moderately replicable for G1 SC (0.73±0.068) and MPC-MTSAT(0.56±0.140) and MPC-T2*(0.40±0.423). Our precision imaging dataset will advance our understanding of structure-function relationships in the individual human brain and is available via the [Open Science Framework](#).

1. Boyacioğlu R, Schulz J, Koopmans PJ, Barth M, Norris DG. Improved sensitivity and specificity for resting state and task fMRI with multiband multi-echo EPI compared to multi-echo EPI at 7 T. *Neuroimage*. 2015;119:352-361.
2. Betts MJ, Acosta-Cabronero J, Cardenas-Blanco A, Nestor PJ, Düzel E. High-resolution characterisation of the aging brain using simultaneous quantitative susceptibility mapping (QSM) and R2* measurements at 7 T. *Neuroimage*. 2016;138:43-63.
3. Van Essen DC, Ugurbil K, Auerbach E, et al. The Human Connectome Project: a data acquisition perspective. *Neuroimage*. 2012;62(4):2222-2231.
4. Park B-y, de Wael RV, Paquola C, et al. Signal diffusion along connectome gradients and inter-hub routing differentially contribute to dynamic human brain function. *Neuroimage*. 2021;224:117429.
5. Margulies DS, Ghosh SS, Goulas A, et al. Situating the default-mode network along a principal gradient of macroscale cortical organization. *Proceedings of the National Academy of Sciences*. 2016;113(44):12574-12579.
6. Cabalo DG, Dekraker J, Royer J, et al. Differential reorganization of episodic and semantic memory systems in epilepsy-related mesiotemporal pathology. *bioRxiv*. 2023:2023.09.28.560002.
7. Royer J, Paquola C, Valk SL, et al. Gradients of brain organization: Smooth sailing from methods development to user community. *Neuroinformatics*. 2024;1-12.
8. Bernhardt BC, Smallwood J, Keilholz S, Margulies DS. Gradients in brain organization. Elsevier; 2022. p. 118987.
9. Mesulam M-M. From sensation to cognition. *Brain: a journal of neurology*. 1998;121(6):1013-1052.
10. Vos de Wael R, Benkarim O, Paquola C, et al. BrainSpace: a toolbox for the analysis of macroscale gradients in neuroimaging and connectomics datasets. *Commun Biol*. Mar 5 2020;3(1):103. doi:10.1038/s42003-020-0794-7
11. Royer J, Rodríguez-Cruces R, Tavakol S, et al. An open MRI dataset for multiscale neuroscience. *Scientific Data*. 2022;9(1):569.
12. Paquola C, Vos De Wael R, Wagstyl K, et al. Microstructural and functional gradients are increasingly dissociated in transmodal cortices. *PLoS biology*. 2019;17(5):e3000284.

Multiparametric Mapping of Superficial White Matter Architecture Using 7T Quantitative MRI

Youngeun Hwang^{1,2}, Jordan DeKraker^{1,2}, Donna Gift Cabalo^{1,2}, Yezhou Wang^{1,2}, Ilana Leppert², Risavarshni Thevakumaran², Christine L. Tardif², David A. Rudko², Raul Rodriguez-Cruces^{1,2*}, Alan C Evans^{2,*}, Boris C. Bernhardt^{1,2*}

¹Multimodal Imaging and Connectome Analysis Lab, McGill University, Montreal, QC, Canada, ²McConnell Brain Imaging Centre, Montreal Neurological Institute and Hospital, Montreal, QC, Canada

The superficial white matter (SWM) is a layer of white matter (WM) located immediately underneath the cortex. This SWM contains subcortical U-fibers interconnecting adjacent brain gyri, which remain incompletely myelinated until later in life¹. Due to the key role of U-fibers in brain plasticity and aging, alterations in their density are observed in various disorders^{2,3,4}. Despite its importance, the SWM has been understudied, primarily due to technical difficulties and limitations⁵. Recent advances in ultra-high field 7 Tesla magnetic resonance imaging (MRI) technology have enabled precise imaging and mapping of brain microstructure, leading to reliable research on the SWM. This study focuses on standardizing qMRIs on the SWM, validating the reliability of SWM mapping, and contributing to a more comprehensive understanding of its microstructural features.

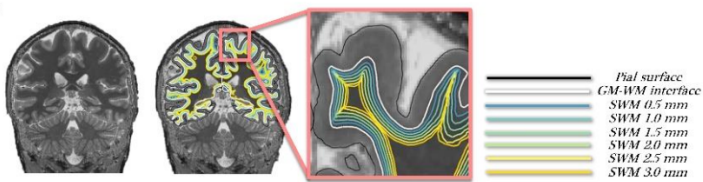
This study utilized data acquired at the Montreal Neurological Institute on a 7T Siemens Terra system. The dataset included ten healthy participants with a mean \pm SD age of 26.8 \pm 4.61 years (5females). For each MRIs were as follows: (i) T1 relaxation time maps, (ii) apparent diffusion coefficient (ADC) and fractional anisotropy (FA) derived from diffusion-weighted MRI (iii) Myelin-sensitive magnetization transfer (MT) ratio maps computed from gradient echo data with and without MT. (iv) iron-sensitive T2* relaxation time maps derived from multi-echo gradient echo. We preprocessed all MRI data using micapipe⁶. To examine the SWM, we solved the Laplace equation over the WM domain. This was achieved by initially computing a Laplace field across the WM and subsequently shifting an existing WM surface along that gradient. Stopping conditions were set by the geodesic distance traveled.

SWM surfaces were sampled at six depths, each separated by 0.5 mm, beneath the gray and WM interface (**Fig. 1A**). The microstructure intensity profiles, depicting the intensity values of qMRI features, are presented in **Fig. 1B**. The matrix illustrates the subject mean value of the profile on each SWM surface, and this mean value was subsequently mapped onto the brain mask. **Fig. 2A** presents a matrix illustrating the average microstructure intensity profile across all SWM surfaces for each qMRI. The Spearman correlation coefficient between MTsat and FA intensity profiles was found to be the highest, and there were high negative correlation coefficients between T1 map and MTsat, as well as T1 map and FA. **Fig. 2B** demonstrates vertex- wise similarities among highly correlated qMRI pairs, showing high correlations for each feature pair across all SWM depths.

In this study, we investigate the microstructural intensity profile of the SWM using 7T qMRI. By establishing quantitative relationships between qMRI features and standardizing

microstructural profiles, our work will contribute to a deeper understanding of the SWM, potentially enhancing abnormal connectivity estimation.

A | Sampling SWM microstructure



B | Microstructural intensity profiles derived from each SWM surface

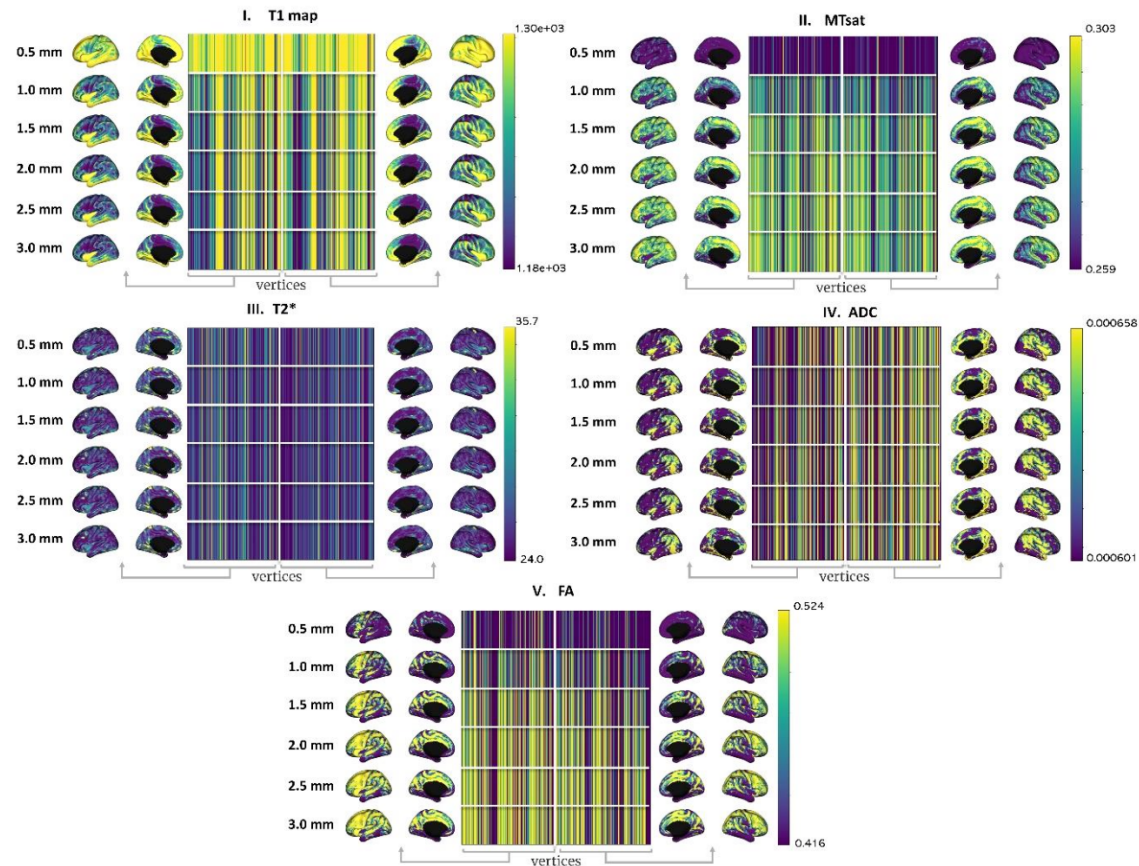
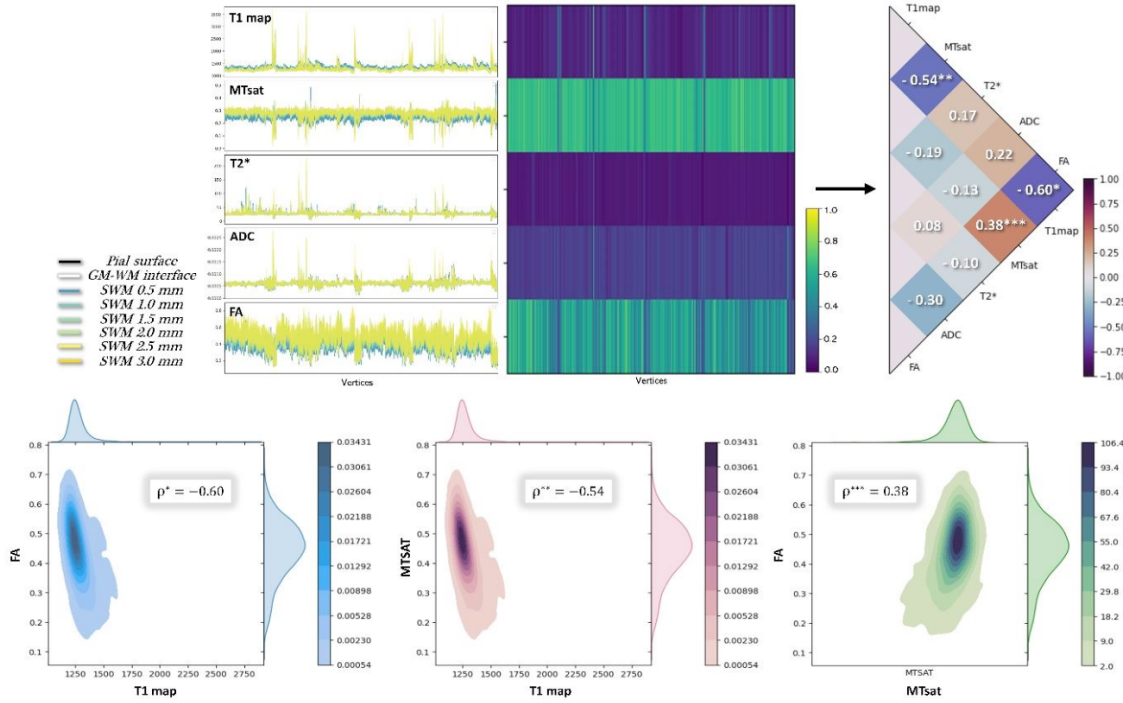


Figure 1. Depth-wise microstructural intensity variation in SWM construction. (A) SWM surface sampling. **(B)** Alterations in qMRI feature intensity according to the SWM depth.

A | Correlation matrix between group mean intensity profiles



B | Vertex-wise similarity across qMRI pairs for all SWM depths

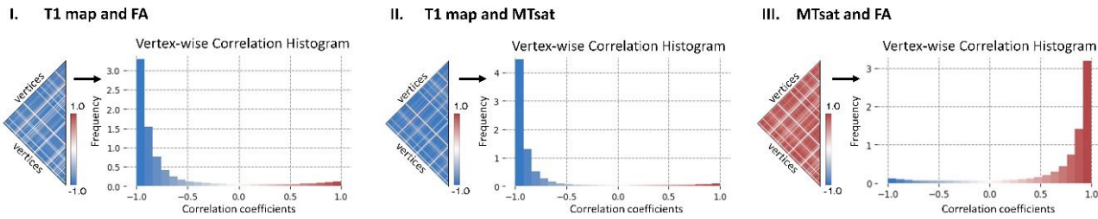


Figure 2. Comprehensive microstructural intensity profile analysis in the SWM. (A) (Top, Left) The variation in microstructure intensity profiles across different SWM surfaces. (Top, Middle) Averaged and normalized microstructural intensity profiles across SWM depths. (Top, Right) Cross-correlation matrix for mean microstructure profiles of each qMRI. (Bottom) Bivariate distribution representing all data points of qMRI pairs with the highest correlation coefficient. (B) (Left, each panel) Vertex-wise cross-correlation of qMRI features for all SWM surfaces. (Right, each panel) Histogram illustrating voxel-wise correlation.

TRANSCRIPTOMIC GRADIENTS OF THE HUMAN HIPPOCAMPUS: A VERTEX-WISE ATLAS OF *POST-MORTEM* GENE EXPRESSION

Alexander Ngo¹, Jordan DeKraker^{1,2}, Sara Larivière³, Lang Liu⁴, Jessica Royer¹, Raúl Rodríguez-Cruces¹, Jacob W. Vogel⁵, Ziv Gan-Or⁴, Alan C. Evans², Boris C. Bernhardt¹

- [1] Multimodal Imaging and Connectome Analysis Laboratory, Montreal Neurological Institute and Hospital, McGill University, Montreal, Quebec, Canada
- [2] McGill Centre of Integrative Neuroscience, Montreal Neurological Institute and Hospital, McGill University, Montreal, Quebec, Canada
- [3] Center for Brain Circuit Therapeutics, Brigham and Women's Hospital, Harvard University, Boston, Massachusetts, United States
- [4] Department of Genetics, McGill University, Montreal, Quebec, Canada
- [5] Department of Clinical Sciences, SciLifeLab, Lund University, Lund, Sweden

Introduction. The hippocampus is involved in multiple aspects of brain function and dysfunction. Unravelling its complex organization requires the integration of multiscale data, linking molecular features to macroscale hierarchies. Gene expression is a fundamental molecular phenotype, and its profiling can provide a reference description of how microstructural features are distributed across the brain. *Post-mortem* gene expression samples, however, are often spatially discontinuous and biased towards coarse brain parcellations, thus potentially overlooking fine-grained information. Here, we charted gene expression patterns within the hippocampus with unprecedented resolution, provided a unified atlas of the hippocampal transcriptome, and related our findings to its functional and structural hierarchies.

Methods. *Allen Human Brain Atlas.* We used the structural T1w magnetic resonance imaging (MRI) and microarray expression data of six deceased human donors (five males, mean \pm SD age = 42.5 ± 13.4 years) from the Allen Human Brain Atlas—a brain-wide atlas comprised of bulk transcriptomic measures from over 20,000 genes sampled across 3,702 spatially distinct tissue samples.¹

Vertex-wise mapping of hippocampal gene expression. Donor-specific hippocampal surfaces were generated from individual structural scans using *HippUnfold*—an automated pipeline for hippocampal unfolding and novel surface-based hippocampal registration.^{2,3} In parallel, we preprocessed the microarray expression data through intensity-based filtering of microarray probes, selection of a representative probe for each gene across both hemispheres, normalization, and aggregation across donors⁴. Tissue sampled within the hippocampus ($n = 178$) were mapped to subject-specific hippocampal surfaces. We interpolated expression values across the hippocampus, weighted by the geodesic distance of a given vertex to its nearest sampled neighbour. Continuous donor-specific transcriptomic maps were averaged to generate a single expression map for each gene (**Fig 1A**).

Code and data availability. All code to preprocess imaging, microarray data, and hippocampal transcriptomic maps will be made available as part of the *HippoMaps*—a toolbox for multiscale

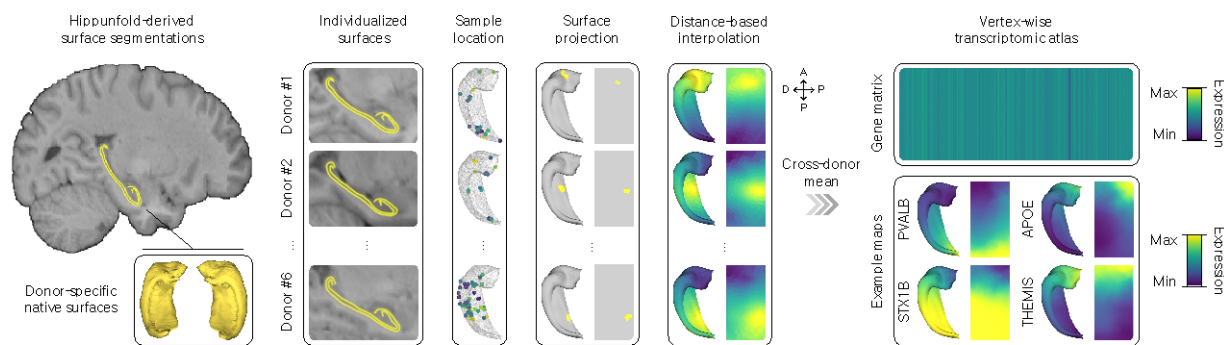
and multimodal contextualization of the hippocampus (<https://github.com/MICA-MNI/hippomaps>)⁵.

Results. We generated an atlas of vertex-wise maps of hippocampal expression for 15,630 genes. Dimensionality reduction using diffusion map embedding on gene co-expression patterns identified two main axes: (i) anterior-posterior (56.9% variance explained) and (ii) proximal-distal (27.7% variance explained) gradients (Fig 1B). Histological and MRI-derived features of the hippocampus generated (Fig 2A) and spatially correlated to genetic gradients identified herein using autocorrelation preserving null models.⁶ Cross-modality correlation analyses revealed the strongest correspondence between: (i) main functional axis and anterior-posterior gradient and (ii) microstructural organization (bielochowsky, calbindin, calretinin, mean diffusivity, qT1 intensity) and proximal-distal gradient ($p_{\text{spin}} < 0.05$; Fig 2B).

Conclusion. Capitalizing on recent imaging-transcriptomic initiatives, we generated vertex-wise maps of hippocampal gene expression from six *post-mortem* human brains, that showed distinct organizational patterns. The presence of fundamental transcriptomic distinctions within the hippocampus may be associated with varying cognitive and functional roles along its anterior-posterior axis, and with microstructural hierarchy along its proximal-distal axis.

Figures

A | Spatially dense hippocampal mapping of gene expression



B | Principle transcriptomic axes of the hippocampus

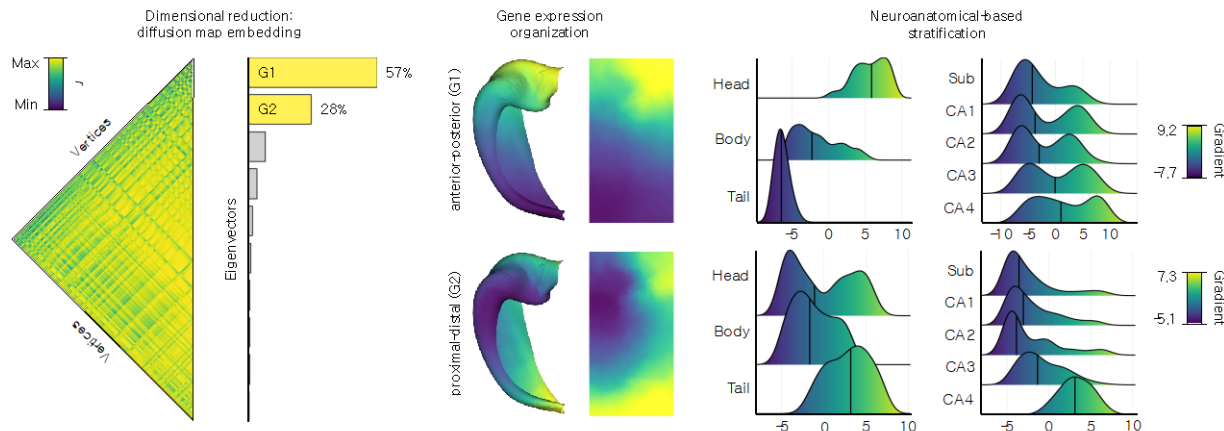
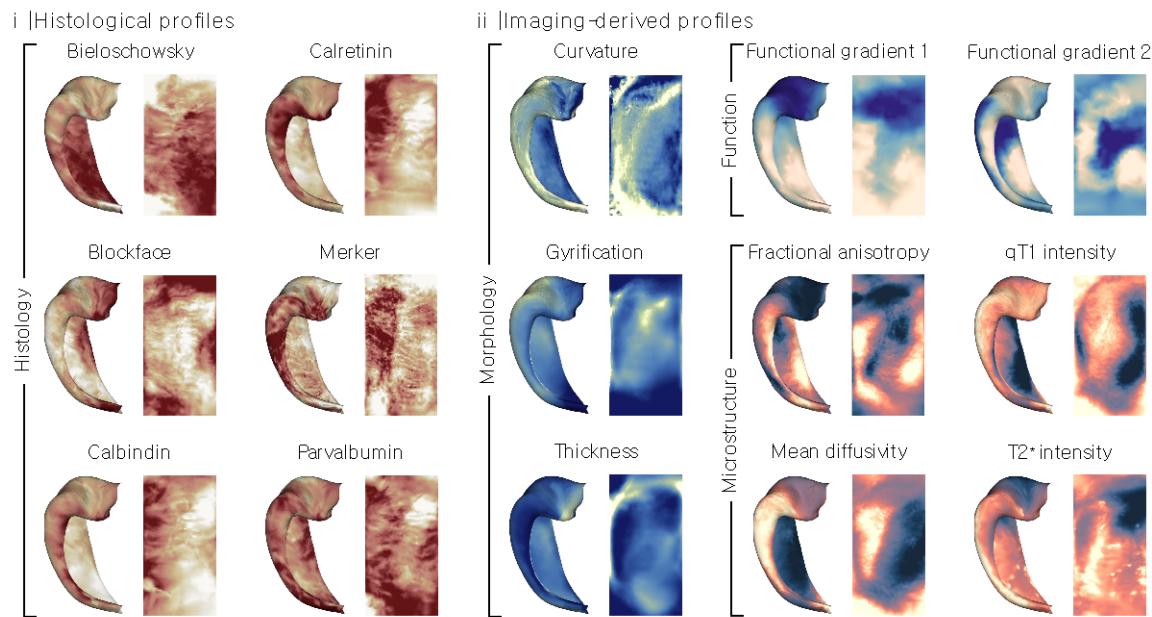


Figure 1 | Gene expression within the hippocampus. (A) Spatially discontinuous *post-mortem* microarray samples from Allen Human Brain Atlas (AHBA) were projected and interpolated along MRI-derived hippocampal surfaces to generate continuous maps of gene expression. (B) Non-linear dimensionality reduction of gene co-expression revealed predominant anterior-to-posterior and proximal-distal gradient.

A | Multimodal decoding of the hippocampus



B | Relation to organization in gene expression

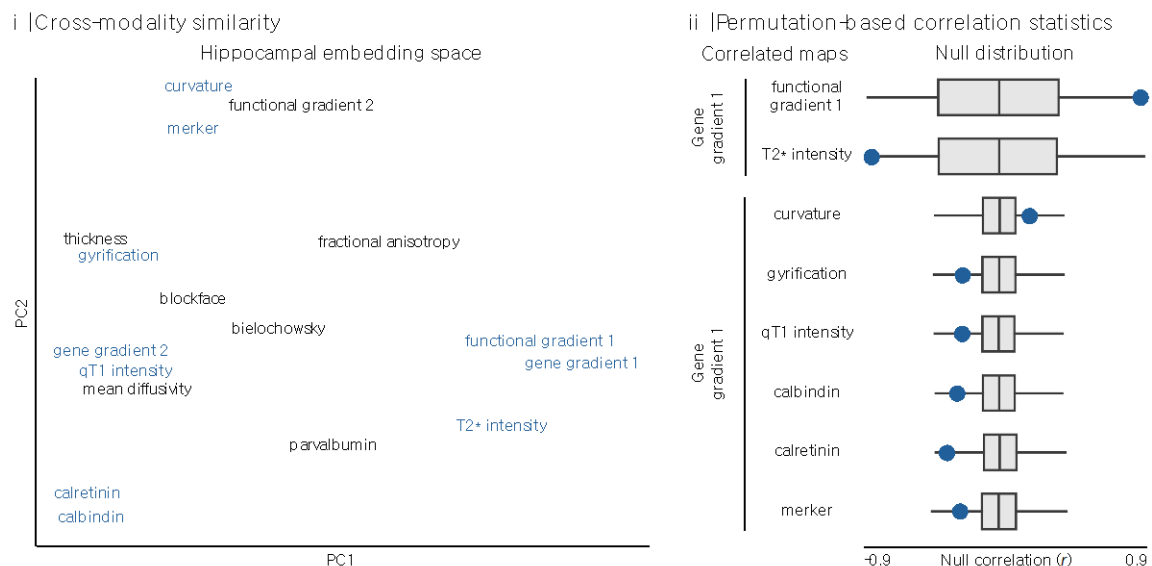


Figure 2 | Multiscale decoding of transcriptomic organization (A) Histological and MRI-derived features from BigBrain Project^a (merker), AHEAD^b (bieloschowsky, blockface, calbindin, calretinin, Parvalbumin) and MICA-MICs^c (curvature, fractional anisotropy, functional gradient,

gyrification, mean diffusivity, qT1 intensity, thickness). **(B)** Cross-modality correlation analyses revealed strong correspondence between (*i*) functional organization and anterior-posterior gene gradient and (*ii*) microstructural organization and proximal-distal gradient. ^aAmunts K et al., 2012, *Science*, 340:1472-1475, ^bAlkemade A et al. 2020, *Neuroimage*, 221:117200, ^cRoyer J et al., 2022, *Sci Data*, 9(1):569.

References

- [1] Hawrylycz MJ et al., 2012, *Nature*, 489(7416):391-399
- [2] DeKraker J et al., 2022, *eLife*, 11:e77945
- [3] DeKraker J et al., 2023, *eLife*, 12:RP88404
- [4] Arnatkeviciute A et al., 2019, *Neuroimage*, 189:353-367
- [5] DeKraker J et al., 2024, bioRxiv, doi: 10.1101/2024.02.23.581734
- [6] Alexander-Bloch AF et al., 2018, *Neuroimage*, 178:540-551

Deciphering the Dynamic Spatiotemporal Maturation from Childhood to Adolescence

Kyoungseob Byeon¹, Hyunjin Park², Seok-jun Hong², Shinwon Park¹, Jon Clucas¹, Kahini Mehta³, Matthew Cieslak³, Jonathan Smallwood³, Theodore D. Satterthwaite⁴, Michael P. Milham¹, Ting Xu¹

¹Child Mind Institute, New York, New York, USA, ²Sungkyunkwan University, Suwon, Republic of Korea, ³Queen's University, Kingston, Ontario, Canada, ⁴University of Pennsylvania, Philadelphia, Pennsylvania, USA

Introduction

Cortical maturation from childhood to adolescence is crucial for neurodevelopment, shaping cognition, emotions, and behaviors. Convergent evidence suggests that neurodevelopment follows in a hierarchical progression with heterogeneous structural and functional maturation patterns. However, the relationship between established static functional patterns and the brain's intrinsic spatiotemporal dynamics remains underexplored. To address this gap, we employ Complex Principal Component Analysis (CPCA), a technique that reduces the complexity of high-dimensional spatiotemporal data across multiple development datasets. This study aims to understand the development of spatiotemporal patterns with age, both locally and globally, focusing on three distinct propagation pathways from childhood to adolescence.

Method

We utilized resting-state fMRI data across a developmental continuum, including Human Connectome Project Development (HCP-D, ages 8.1-21.9, n=408) and Aging (HCP-A, ages 36.0-64.9, n=399) datasets. The preprocessed data were parcellated and analyzed using CPCA to extract spatiotemporal components, reordering them based on their spatial similarity with static functional gradients. Using a vector alignment approach, we reconstructed individual spatiotemporal dynamic patterns and assessed their reproducibility across cohorts and test-retest reliability across sessions. Age effects on dynamic patterns were estimated by comparing individual patterns with the adult reference from HCP-A dataset. To validate the results, we replicated the age effects with the Nathan Kline Institute Rockland Sample (NKI-RS, ages 6-18, n=259), and Chinese Color Nest Project dataset (CCNP, ages 6.5-17.9, n=152).

Result

We identified phase-dependent spatiotemporal components and focused on the first three dynamic states which were reproducible across cohorts and each explained over 10% of the variation in each datasets. High test-retest reliability was observed for the first three patterns ($r > 0.9$), revealing that individual-specific patterns can be differentiated from other participants. Compared to the adult reference, a linear increase in similarity with age ($r=.36-.56$) was observed, indicating maturation towards adult-like dynamic states. The state occurrence ratio,

representing the time spent in each dynamic state, exhibited a positive age effect for pattern 1 ($r=0.25$) but a negative age effect for pattern 2 ($r=-0.14$). A strong correlation ($r=.93$) was observed between the occurrence ratio and the explained variance of static gradient, suggesting the significant contribution of time spent in each state to their altered gradients. We also calculated the proportion of bottom-up (sensory-to-association) and top-down (association-to-sensory) contributions to the first dynamic pattern. Interestingly, with increasing age, individuals spent less time in bottom-up phases and more time in phases characterized by top-down propagation. Additionally, the amplitude of regional fluctuations for each dynamic state varied across individuals. From childhood to adolescence, the amplitude increased in dorsal attention and sensory-related networks for pattern1.

Abstract

Pharmacoresistant temporal lobe epilepsy gradually perturbs the cortex-wide excitation-inhibition balance

Ke Xie¹, Jessica Royer¹, Raul Rodriguez-Cruces¹, Linda Horwood¹, Alexander Ngo¹, Thaera Arafat¹, Hans Auer¹, Ella Sahlas¹, Judy Chen¹, Yigu Zhou¹, Sofie L. Valk², Seok-Jun Hong³, Birgit Frauscher⁴, Raluca Pana¹, Andrea Bernasconi¹, Neda Bernasconi¹, Luis Concha⁵, and Boris C. Bernhardt¹

¹Montreal Neurological Institute-Hospital, McGill University, Montreal, QC, Canada; ²Max Planck Institute for Human Cognitive and Brain Sciences, Leipzig, Germany; ³Center for Neuroscience Imaging Research, Institute for Basic Science, Sungkyunkwan University, Suwon, South Korea; ⁴Department of Neurology, Duke University, Durham, NC, USA; ⁵Institute of Neurobiology, Universidad Nacional Autónoma de Mexico, Queretaro, Mexico

Excitation-inhibition (E/I) imbalance is posited as a fundamental pathophysiological mechanism in temporal lobe epilepsy (TLE).¹ However, previous evidence supporting this hypothesis has been primarily derived from experimental studies in non-human animals. This study aims to non-invasively elucidate the cortical pattern of E/I imbalance in TLE patients and explore its associations with disease severity and cognitive impairment.

We studied 40 pharmacoresistant TLE patients (17 males; age = 35.80±11.04 years; 27/13 left/right focus) and 40 age- and sex-matched healthy controls (19 males; 34.25±3.98 years). All participants underwent multimodal MRI at 3T, as well as global cognitive testing including the Montreal Cognitive Assessment (MoCA) and EpiTrack. A subset of participants underwent follow-up MRI scans and cognitive assessment. Node-wise Hurst exponent score, reflecting scale-free properties (*i.e.*, 1/f slope) of fMRI signal and serving as a proxy for the overall E/I ratio within a given region,² was estimated via the univariate maximum likelihood method and discrete wavelet transform, modeling the resting-state fMRI timeseries as multivariate fractionally integrated processes. Quantitative and surface-wide between-group differences in Hurst exponent were assessed, with *P*-values adjusted for false discovery rate (FDR). Subsequently, we explored the relationship between TLE-related regional changes in Hurst exponent and microcircuit parameters estimated by connectome-informed biophysically computational simulations via a parametric mean-field model.³ Finally, we examined associations with clinical and cognitive measures at baseline, as well as prospective cognitive decline after a 2-year follow-up.

In both cohorts, Hurst exponent scores exhibited a sensory-fugal distribution, being highest in the visual cortex, intermediate in the frontoparietal and default mode networks, and lowest in the paralimbic network, aligning with the sensory–fugal gradient of cytoarchitectural differentiation ($\rho = -0.41$, $P_{\text{spin}} = 0.044$). TLE patients had a significantly lower Hurst exponent score across the whole brain than healthy controls (Cohen's $d = -0.75$, $P < 0.001$), indicating an overall elevated E/I ratio. Surface-based analysis further revealed marked reductions in local Hurst exponent scores in bilateral temporal lobes, dorsolateral and dorsomedial prefrontal cortices, precuneus, and occipital cortex in TLE compared to healthy controls ($P_{\text{FDR}} < 0.05$). When stratifying the topography into functional communities, pronounced effects were observed in the transmodal association system, such as the default mode, frontoparietal, and attention networks, as well as the visual system. Computational models indicated that the degree of Hurst exponent

Abstract

changes was closely related to atypical increases in recurrent connection strength in TLE ($\rho_{\text{ho}} = -0.22$, $P_{\text{spin}} = 0.015$). Finally, lower Hurst exponent scores in TLE patients were associated with longer disease duration (whole-brain, $t = -1.61$, $P = 0.028$; significant clusters, $t = -1.76$, $P = 0.021$) and poorer performance on both the MoCA ($t = 2.33$, $P = 0.006$; $t = 2.93$, $P = 0.001$) and the EpiTrack tests ($t = 2.72$, $P = 0.002$; $t = 3.06$, $P < 0.001$). Moreover, in TLE patients, Hurst exponent scores declined significantly at the 2-year follow-up time point (Cohen's $d = -0.92$, $P < 0.001$; Cohen's $d = -0.77$, $P < 0.001$), mirroring the prospective decline in MoCA scores ($t = 2.02$, $P = 0.016$; $t = 2.05$, $P = 0.015$).

In TLE, our finding of reduced Hurst exponent scores likely indicates widespread cortical excitation-inhibition changes, tilting the balance towards increased cortical excitability. These changes were found to increase with ongoing disease progression and more marked cognitive impairment, highlighting the potential of the Hurst exponent as a neuroimaging biomarker for TLE-related dysfunction.

1. Fritschy, J. M. (2008), 'Epilepsy, E/I balance and GABA(A) receptor plasticity', *Front Mol Neurosci*, vol. 1, p. 5
2. Trakoshis, S. et al. (2020), 'Intrinsic excitation-inhibition imbalance affects medial prefrontal cortex differently in autistic men versus women', *eLife*, vol. 9, p. e55684
3. Kong, X. et al. (2021), 'Sensory-motor cortices shape functional connectivity dynamics in the human brain', *Nat Commun*, vol. 12, no. 1, p. 6373

Title: Dimensions of intrinsic connectivity modulate language processing with modality-specific mechanisms.

Authors: Lidón Marin Marin^{a,b}, Susanne Eisenhauer^{a,b}, Elizabeth Jefferies^{a,b}

^aDepartment of Psychology, University of York, YO10 5DD, United Kingdom

^bYork Neuroimaging Centre, Innovation Way, York, YO10 5DD, United Kingdom

Abstract:

Introduction: Comprehension of spoken and written language entails a series of steps that are believed to be hierarchically ordered and localised in specific areas of the brain, but language comprehension also implicates whole-brain states (1) and network organisation (2). Whole-brain patterns of functional connectivity are crucial for language processing, and decompositions of intrinsic connectivity have identified the dimensions underlying these patterns (3). We investigated the effect of the two first connectivity dimensions on macroscale patterns of activity induced by different psycholinguistic variables during a sentence comprehension task using written and spoken words.

Methods: 204 right-handed Dutch participants (100 males, mean age=22) of the MOUS dataset (4) *read or listened* to sentences and scrambled word lists during fMRI. Data were pre-processed using FSL following a previous study (5). We considered the following parameters of interest: at the contextual level - sentence processing, semantic similarity and position in the sentence; at the word level - number of characters/phonemes, orthographic/phonological distance and word frequency. GLMs in FSL were used to estimate the effects of each parameter on brain activation, resulting in macroscale cortical maps. Similarities between visual and auditory maps were investigated by means of Pearson correlations, and each parameter's cortical map was related to the two dimensions of connectivity using linear and quadratic models in R, using spin permutations and FDR correction to assess statistical significance in both cases (6).

Results: Macroscale brain patterns of activity were significantly similar across modalities only for sentence-level ($r=.81$, $p_{\text{spin}}<.006$) and semantic variables ($r=.33$, $p_{\text{spin}}=.006$), consistent with evidence at the regional brain level suggesting that higher-order processing is heteromodal (7). Interestingly, effects of orthographic and phonological distance on brain activation were negatively correlated between modalities ($r=-.24$, $p_{\text{spin}}=.04$), indicating that these analogous auditory and visual variables produced an opposite macroscale pattern of activation. This was consistent with the effect that the first connectivity dimension had on brain activation, which was also opposite for the two modalities in orthographic/phonological distance ($t=4.77$, $p_{\text{spin}}<.005$, $t=-6.59$, $p_{\text{spin}}<.005$) and word length ($t=-3.95$, $p_{\text{spin}}<.005$; $t=6.76$, $p_{\text{spin}}<.005$). Specifically, processing of spoken words with frequent auditory forms was dependent on the unimodal end of the dimension, whereas for written stimuli, it was unique visual forms that recruited this unimodal end. Moreover, longer spoken words relied more on control regions, but longer written words recruited memory-based heteromodal processes. This suggests that auditory linguistic stimuli might fit better the ‘noisy channel model of communication’ (8,9). Finally, the second connectivity dimension revealed an asymmetry between primary processing systems when *listening* to long and semantically ambiguous words, involving more recruitment of primary auditory and somato-motor regions ($t=-6.15$, $p_{\text{spin}}=.009$; $t=5.65$, $p_{\text{spin}}=.017$).

Conclusion: The dimensions underlying whole-brain intrinsic connectivity modulate macroscale patterns of activity evoked by reading and listening to sentences in a different fashion depending on level of processing (sentence, context or word) and modality (visual or auditory). Our findings help understand both balances and asymmetries between functional brain systems when processing auditory

and visual linguistic stimuli, and highlight the relevance of investigating brain patterns at the macroscale level.

References:

1. Aliko S, Wang B, Small SL, Skipper JI (2023): The entire brain, more or less is at work: 'Language regions' are artefacts of averaging. *bioRxiv*:2023.09.01.555886.
2. Hagoort P, Indefrey P (2014): The neurobiology of language beyond single words. *Annu Rev Neurosci* 37:347–362.
3. Margulies DS, Ghosh SS, Goulas A, Falkiewicz M, Huntenburg JM, Langs G, Bezgin G, Eickhoff SB, Castellanos FX, Petrides M, Jefferies E, Smallwood J (2016): Situating the default-mode network along a principal gradient of macroscale cortical organization. *Proc Natl Acad Sci U S A* 113:12574–12579.
4. Schoffelen JM, Oostenveld R, Lam NHL, Uddén J, Hultén A, Hagoort P (2019): A 204-subject multimodal neuroimaging dataset to study language processing. *Sci Data* 6:1–14.
5. Eisenhauer S, Alam TR del JG, Cornelissen PL, Smallwood J, Jefferies E (2024): Individual word representations dissociate from linguistic context along a cortical unimodal to heteromodal gradient. *Hum Brain Mapp* 45:e26607.
6. Alexander-Bloch AF, Shou H, Liu S, Satterthwaite TD, Glahn DC, Shinohara RT, et al. On testing for spatial correspondence between maps of human brain structure and function. *Neuroimage*. 2018;178:540–51.
7. Price CJ (2012): A review and synthesis of the first 20 years of PET and fMRI studies of heard speech, spoken language and reading. *Neuroimage* 62:816.
8. Gibson, E., Bergen, L., & Piantadosi, S. T. (2013). Rational integration of noisy evidence and prior semantic expectations in sentence interpretation. *Proceedings of the National Academy of Sciences of the United States of America*, 110(20), 8051–8056.
9. Dautriche, I., Mahowald, K., Gibson, E., Christophe, A., & Piantadosi, S. T. (2017). Words cluster phonetically beyond phonotactic regularities. *Cognition*, 163, 128–145.

Mapping the effects of functional and structural network reorganization on the tau-cognition relationship in Alzheimer's disease

Authors: Julie Ottoy¹, Min Su Kang¹, Jazlynn Xiu Min Tan¹, Lyndon Boone¹, Reinder Vos de Wael², Bo-yong Park^{3,4}, Gleb Bezgin^{5,6}, Firoza Z. Lussier^{5,7}, Tharick A. Pascoal⁷, Nesrine Rahmouni⁵, Jenna Stevenson⁵, Jaime Fernandez Arias⁵, Joseph Therriault⁵, Seok-Jun Hong⁸, Bojana Stefanovic^{1,9}, JoAnne McLaurin^{1,10,11}, Jean-Paul Soucy², Serge Gauthier⁵, Boris C. Bernhardt², Sandra E. Black^{1,12}, Pedro Rosa-Neto^{2,5}, Maged Goubran^{1,9,13,*}

¹Sunnybrook Research Institute, University of Toronto, Toronto, ON, Canada

²McConnell Brain Imaging Centre, Montreal Neurological Institute and Hospital, McGill University, Montreal, Quebec, Canada

³Department of Data Science, Inha University, Incheon, Republic of Korea

⁴Center for Neuroscience Imaging Research, Institute for Basic Science, Suwon, Republic of Korea

⁵Translational Neuroimaging laboratory, McGill Centre for Studies in Aging, McGill University, Montreal, QC, Canada

⁶Neuroinformatics for Personalized Medicine lab, Montreal Neurological Institute, McGill University, Montréal, QC, Canada

⁷Department of Psychiatry, University of Pittsburgh, Pittsburgh, PA, USA.

⁸Department of Biomedical Engineering, Sungkyunkwan University, Suwon, Republic of Korea

⁹Department of Medical Biophysics, University of Toronto, Toronto, ON, Canada

¹⁰Department of Laboratory Medicine and Pathobiology, University of Toronto, Toronto, ON, Canada

¹¹Biological Sciences Platform, Sunnybrook Research Institute, University of Toronto, Toronto, ON, Canada

¹²Department of Medicine (Division of Neurology), University of Toronto, Toronto, ON, Canada

¹³Physical Sciences Platform, Sunnybrook Research Institute, University of Toronto, Toronto, ON, Canada

Background: Tau pathology can spread through connectivity-based networks, with certain regions (or epicenters) accumulating more tau than others. Such spatial vulnerabilities may be due to their unique apical position in the cortical hierarchy, which can be elucidated through ‘gradients of connectivity’ (Margulies 2016 PNAS). Prior work showed that the primary gradient of functional connectivity unveils a uni-to-transmodal topography of the healthy neocortex which highly correlates with a cognitive gradient of perception-to-abstraction. Here, we hypothesized that the gradients of functional/structural connectivity interact with tau to affect cognitive functions in Alzheimer’s disease (AD).

Method: We included 213 participants from TRIAD (103 CN A β -, 103 CN A β +, and 75 CI A β +) with diffusion-weighted MRI, resting-state functional MRI, ^{18}F -MK6240 tau-PET, and an extensive cognitive battery. We performed non-linear dimensionality reduction on the individual functional and structural connectomes, and extracted the first components ('gradients') -explaining most variance ($G1_{\text{FC}}$ and $G1_{\text{SC}}$). First, we compared $G1_{\text{FC_or_SC}}$ between diagnostic groups. Second, we investigated the interaction effect of $G1_{\text{FC_or_SC}} * \text{tau}_{\text{SUVR}}$ on cognition (across 9 cognitive domains). Last, we investigated whether the tau-cognition relationship changed in a topography-specific manner along the cortical hierarchy, within (equally-sized) gradient-derived meta-ROIs along $G1_{\text{FC_or_SC}}$. Results were compared to Braak-derived regional associations. Analyses were adjusted for age, sex, APOE, education, and multiple comparisons.

Result: We observed reduced segregation of functional networks in AD compared to controls, with unimodal (lower-order cognitive) and transmodal (higher-order cognitive) regions moving closer on $G1_{\text{FC}}$. This may indicate loss of network specialization in AD. Participants who had both higher tau and $G1_{\text{FC}}$ alterations had more cognitive impairment (**Fig.1A**; shown for MMSE/language). This interaction-effect was less pronounced with $G1_{\text{SC}}$ (**Fig.1B**). Last, tau correlated with cognition in a topography-specific *progressive* manner (i.e., along the transmodal-unimodal $G1_{\text{FC}}$ axis and anterior-posterior $G1_{\text{SC}}$ axis) (**Fig.1C**). Notably, tau correlated with delayed memory progressively along the posterior-anterior $G1_{\text{SC}}$ axis ($R^2=0.93$ in all and $R^2=0.95$ in A+) and BraakI-VI axis ($R^2=0.77$ in all and $R^2=0.28$ in A+).

Conclusion: Our work supports the contribution of connectome-driven tau distribution on cognitive impairment in AD. Connectome gradients may provide a spatial framework to study tau spreading along the major axes of brain organization underlying specific cognitive domains.

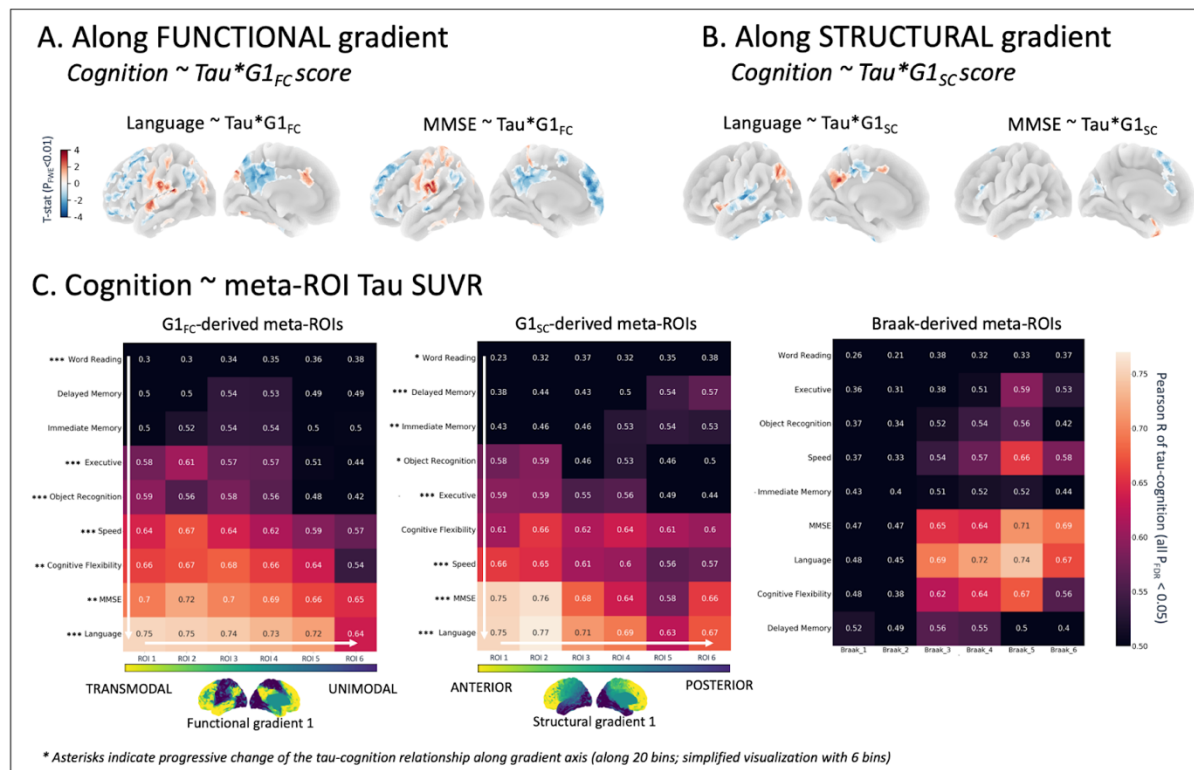


Figure 1. Interrelation between connectome gradients, tau, and cognition in the AD continuum. A) Interaction between regional tau SUVR and functional gradient score on cognition. A negative interaction effect (blue; transmodal regions) is reflective of higher tau together with higher gradient score -that is, moving inward on the gradient- leading to lower cognitive outcome. B) Interaction between regional tau SUVR and structural gradient score on cognition. C) Cognitive correlates (absolute Pearson's R) of tau SUVR averaged across G1_{FC}-derived (left panel) and G1_{SC}-derived (middle panel) meta-ROIs. The resultant correlation coefficients changed in a topographic-specific manner along G1_{FC} and G1_{SC}; asterisks (*P<0.01, **P<0.001, ***P<0.0001) indicated significance of a linear model between gradient bin ordering (20 bins; simplified visualization with 6 bins) and the correlation coefficient within each bin. Tau-cognition correlations within the Braak I to VI regions are shown in the right panel. All analyses (panels A-C) were adjusted for age, sex, education, and APOE-ε4, and multiple comparisons. Sample sizes varied across composite scores: word reading n=87, delayed memory n=76, immediate memory n=82, executive function n=86, object recognition n=86, processing speed n=84, cognitive flexibility n=81, MMSE n=107, and language n=90; all subjects were amyloid-positive. Analyses were repeated across the full cohort showing similar results.

1. Abstract

Title: Thalamic Functional Connectivity Gradients in Children with Temporal Lobe Epilepsy

Background

The thalamus participates in spread of seizures and is a target for therapeutic neuromodulation for epilepsy. Whilst thalamic functional connectivity alterations exist in adult with temporal lobe epilepsy and may affect post-surgical seizure freedom, thalamic connectivity alterations have rarely been examined in children. We identified functional topographic organisation (gradients) of thalamo-to-whole-brain connections in paediatric temporal lobe epilepsy and explored the seizure and cognitive associations.

Methods

64 children with temporal lobe epilepsy (5-18 years, 41 females) and 61 healthy controls (6-20 years, 29 females) underwent a covert verb generation task fMRI. We estimated thalamic functional gradients using connectomic mapping techniques: We generated within-thalamus FC similarity matrices for each hemisphere and applied non-linear manifold learning to this matrix, yielding gradients for each side of the thalamus. Projection maps were created to depict changes in thalamic-to-whole brain connectivity along this gradient. We assessed the projection maps of thalamic gradients in relations to thalamic anatomical structure, disease status and memory measures.

Results

The primary thalamic gradient followed an anterior-to-posterior axis across the thalamus for both children with temporal lobe epilepsy and controls (**Fig. 1**). The anterior thalamus displayed greater connectivity with prefrontal and orbitofrontal cortices, as well as the basal ganglia. The mid-thalamic gradient zone was preferentially connected to the somatosensory cortex and anterior hippocampus. The posterior thalamus was more connected with the visual cortex and posterior hippocampus. Under the framework of the primary gradient, children with TLE showed stronger connectivity of the anterior thalamus to the bilateral basal ganglia, amygdala and hippocampus compared to controls (**Fig. 2**, FDR-corrected $p<0.05$). The atypical thalamo-basal-ganglia connectivity was more heightened in those with focal to bilateral tonic-clonic seizures (**Fig. 2**, FDR-corrected $p<0.05$). The secondary gradients followed an a dorsal-to-ventral axis mirrored the cortical projection (**Fig. 1**), where thalamic connectivity to amygdala, hippocampus, pallidum, temporal and posterior cortical regions showed relations to the patient's memory performance (**Fig. 3**, FDR-corrected $p<0.05$).

Conclusions

Two principal functional organisations of thalamic connectivity across the entire brain were revealed for children with temporal lobe epilepsy: An anterior–posterior gradient may involve in seizure generalisation and a dorsal–ventral gradient may involve in memory processing.

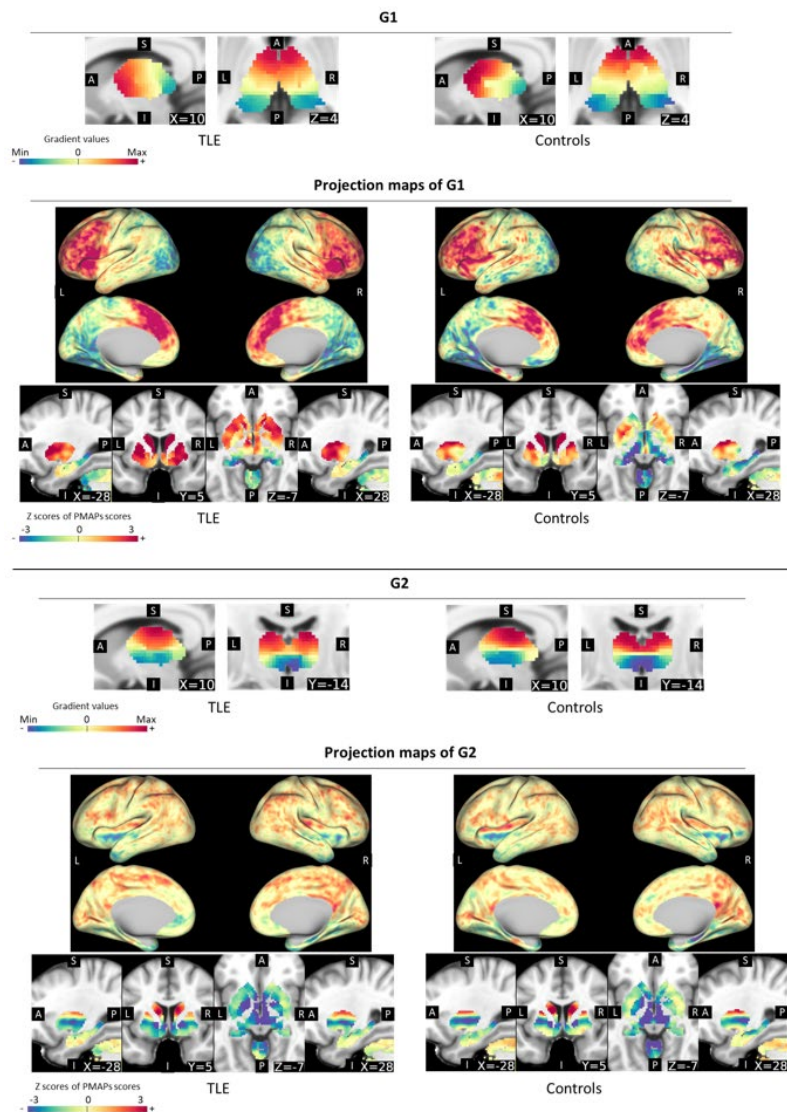


Fig. 1

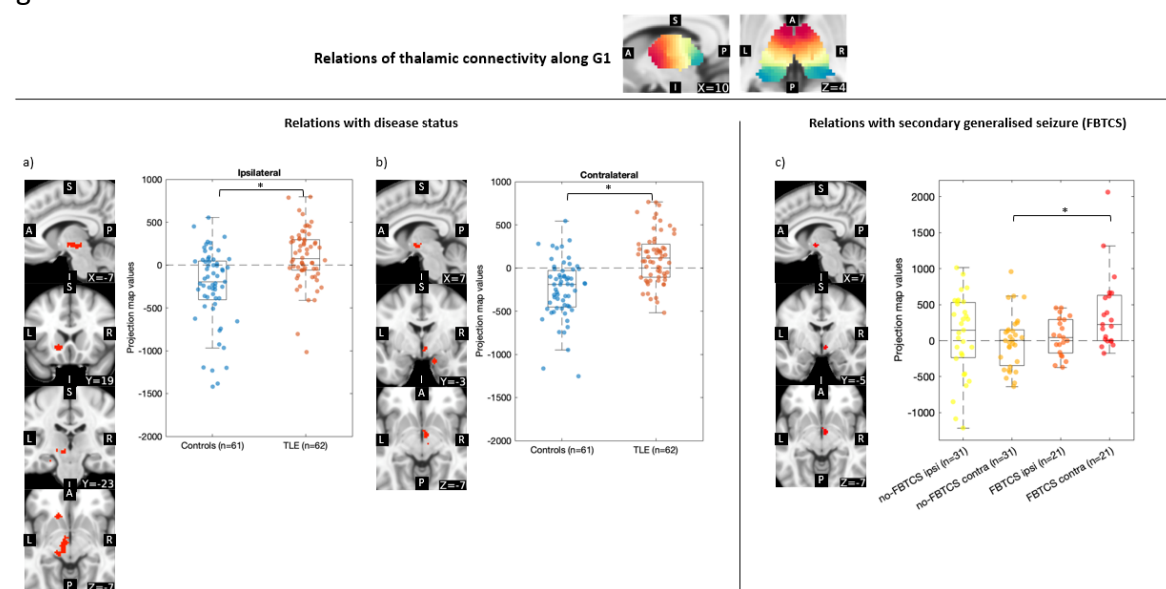


Fig. 2

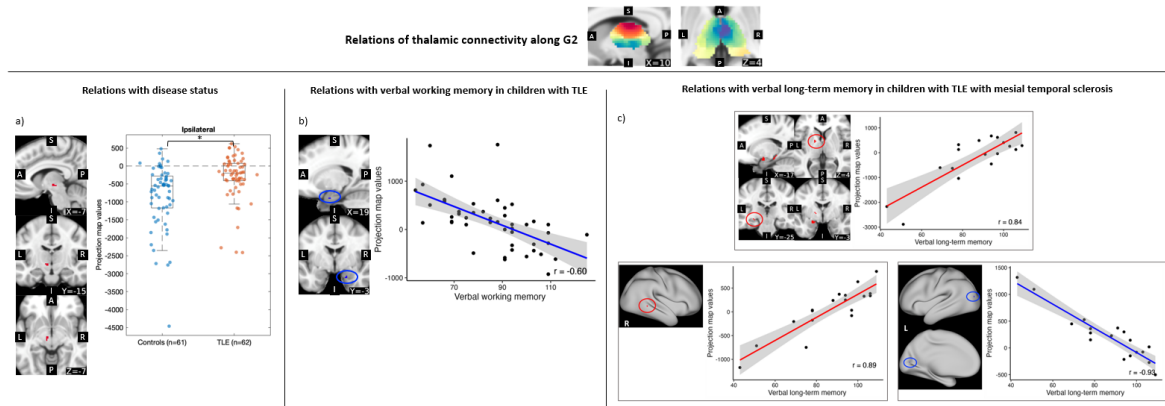


Fig. 3

2. Author List

Xiyu Feng¹, Hua Xie², Rory Piper^{1,3}, Freya Prentice¹, Priyanka Illapani², Lauren Reppert², Seok-Jun Hong⁴, Mohamad Koubeissi⁵, Torsten Baldeweg¹, Leigh Sepeta²

¹UCL Great Ormond Street Institute of Child Health, London, United Kingdom, ²Children's National Hospital, Washington, D.C., USA, ³Great Ormond Street Hospital, London, United Kingdom, ⁴Sungkyunkwan University, Seoul, South Korea, ⁵Epilepsy Centre, Washington, D.C., USA